Volume 44 | Number 14 | 21 July 2015 | Pages 4475–4974

Chem Soc Rev

Chemical Society Reviews

www.rsc.org/chemsocrev

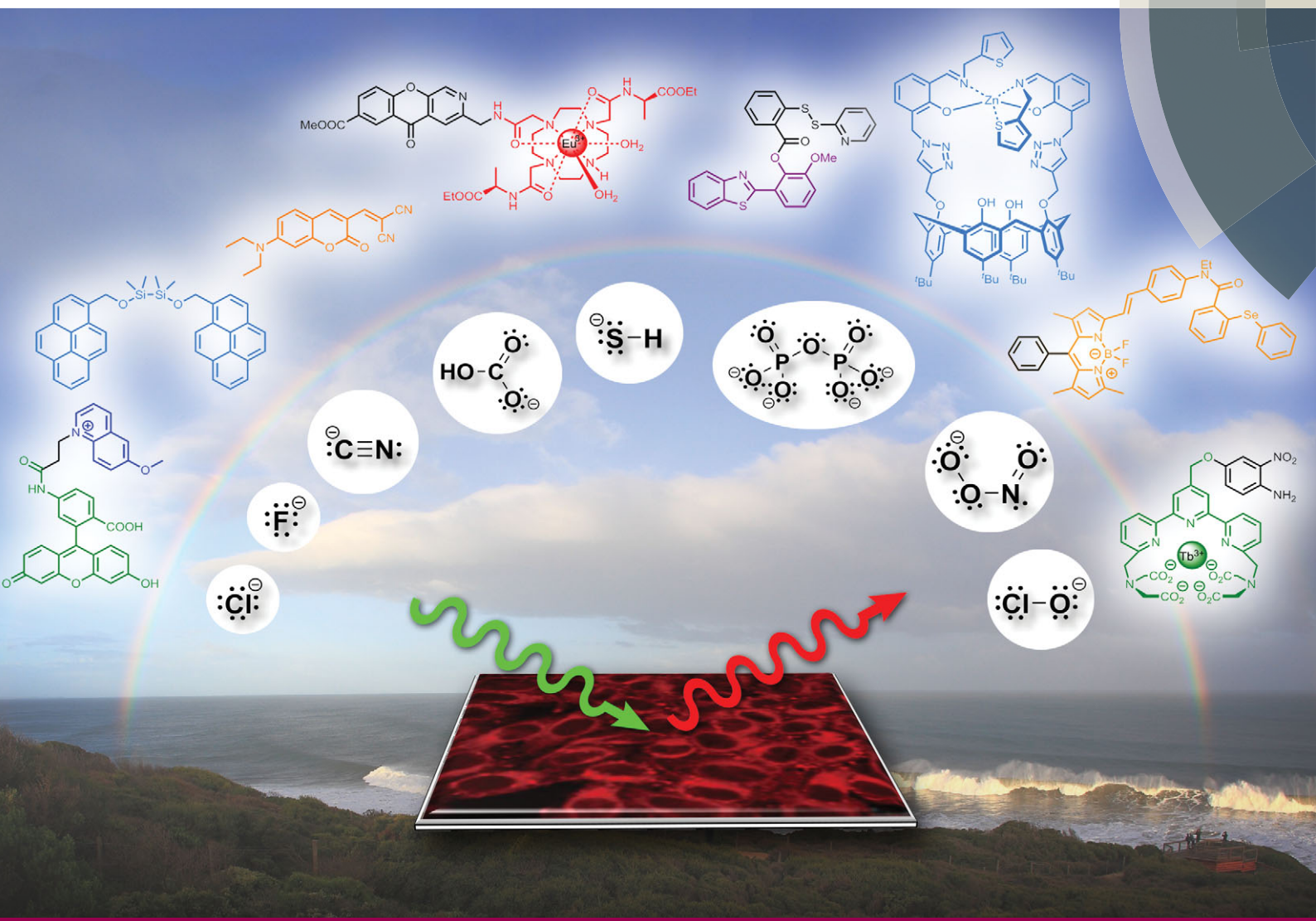

Themed issue: Imaging agents

ISSN 0306-0012

ROYAL SOCIETY OF CHEMISTRY

REVIEW ARTICLE

Frederick M. Pfeffer *et al.*

Luminescent probes for the bioimaging of small anionic species *in vitro* and *in vivo*

Chem Soc Rev

REVIEW ARTICLE

View Article Online
View Journal | View Issue

Cite this: *Chem. Soc. Rev.*, 2015, **44**, 4547

Luminescent probes for the bioimaging of small anionic species *in vitro* and *in vivo*

Trent D. Ashton,[a] Katrina A. Jolliffe[b] and Frederick M. Pfeffer*[a]

Received 3rd November 2014

DOI: 10.1039/c4cs00372a

www.rsc.org/csr

The ability to spatiotemporally identify the formation of specific anionic species, or track changes in their concentration inside living systems, is of critical importance in deciphering their exact biological roles and effects. The development of probes (also called bioimaging agents and intracellular sensors) to achieve this goal has become a rapidly growing branch of supramolecular chemistry. In this critical review the challenges specific to the task are identified and for a select range of small anions of environmental and biological relevance (fluoride, chloride, iodide, cyanide, pyrophosphate, bicarbonate, hydrosulphide, peroxynitrite, hypochlorite and hypobromite) a comprehensive overview of the currently available *in vitro* and *in vivo* probes is provided.

1. Introduction

1.1 Overview

The study of anion *recognition* is now a relatively mature science in line with the closely related field of cation recognition.[1–5] Over the last 10–15 years sustained effort from the supramolecular chemistry community has refined the fundamental principles relating to how a host interacts with a negatively charged guest.[1–17]

[a] *Centre for Chemistry and Biotechnology, School of Life and Environmental Sciences, Deakin University, Pigdons Rd, Waurn Ponds, Victoria, Australia. E-mail: fred.pfeffer@deakin.edu.au*
[b] *School of Chemistry, School of Chemistry (F11), The University of Sydney, Sydney, New South Wales, Australia*

Similarly anion *sensing* has matured and an array of effective molecular detectors, operating by means of well understood principles, are now available.[11,18–32] An excellent recent tutorial review by Gale (see also other articles in this special issue) neatly highlights the strategies that are now widely employed in the detection and/or quantification of anionic species.[33] While the field has matured, challenges still exist for the detection of anions in water; the heavily hydrated nature of these species in aqueous environments makes strong binding difficult and also hinders their reactivity.[7,12,26,34]

As the study of anion recognition and sensing has advanced supramolecular chemists have applied their fundamental knowledge to the detection of anions of biological significance.[14,21,35–46] Indeed the rise of anion recognition as a field of study was in no

Trent D. Ashton

Trent Ashton received his PhD in organic chemistry from Monash University's Victorian College of Pharmacy campus (now Monash Institute of Pharmaceutical Sciences) in 2008. After a year working for Prof. Michael Pollastri at Boston University he returned to Monash to work for Peter Scammells. He originally joined the Pfeffer lab at Deakin University in 2010 to work on small molecule agents for the treatment of type II diabetes in conjunction with Verva Pharmaceuticals. In addition to supramolecular anion recognition chemistry his current research interests include the development of class selective HDAC inhibitors to target metabolic disorders.

Katrina A. Jolliffe

Katrina (Kate) Jolliffe received her BSc (Hons 1) in 1993 and PhD in 1997 from the University of New South Wales. She then held positions at Twente University, The Netherlands; the University of Nottingham, UK and the Australian National University before taking up an ARC QEII research fellowship at The University of Sydney in 2002. In 2007 she became a Senior lecturer at the same institution and was promoted to Associate Professor in 2008 and to full Professor in 2009. She is currently Head of the School of Chemistry at The University of Sydney. Kate's research interests encompass elements of synthetic organic chemistry, supramolecular chemistry and peptide chemistry.

Table 1 Design criteria for anion sensors *versus* anion probes *in vitro* and *in vivo*

For recognition/sensing in water	For recognition/sensing *in vitro* and *in vivo*
Selective for the target in water	Selective for target in cells/small organisms
Strong binding/signalling and low detection limit	Sensitive at relevant biological concentrations (*e.g.* Cl^- *vs.* $ONOO^-$)
Water soluble	Water soluble yet amphiphilic for cell permeability.
	Localise in relevant compartment
	Non-toxic
''Switch on'' or ratiometric	''Switch on'' or ratiometric
Large extinction coefficient, quantum yield and Stokes shift.	Large extinction coefficient, quantum yield and Stokes shift.
	Red or NIR emissive
	Photostable and metabolically stable

small part due to the fact that the majority of intracellular operations involve anionic species.[47] A natural extension of such efforts is the detection or sensing of biologically relevant anions in a *biologically relevant setting* such as inside living cells or in living organisms.[30,35,43,45,48–60] Thus the field of anion *imaging* has emerged and supramolecular chemists now find themselves planning and executing the synthesis of reporters to *selectively detect* and *indicate* the presence of anions *inside* living cells and organisms. Probes capable of achieving this feat are amongst the most powerful resources available for elucidating the exact biological role of the target anion. While the number of probes capable of efficiently communicating an anion recognition event from such a venue is growing, it is still small when compared to the large number of intracellular sensors/probes for cationic species[61] (see also other articles in this special issue). As such the field provides fertile ground for both emerging and established researchers alike.

1.2 Challenges

The ideal anion sensor functioning *in vitro* or *in vivo* must satisfy a demanding set of criteria (outlined in brief in Table 1)[62–64] and it is clear from this list that an imaging agent must 'do more' than a sensor. Key challenges include (i) selecting a suitable fluorophore, (ii) choosing an effective switching mechanism and (iii) catering for the biological environment in which the probe must function (see additional discussion for these three points below). Few, if any, of the currently available probes satisfy all of these criteria and given that sensors that are truly selective for specific anions in water have only emerged in the last 10–15 years it is no surprise that the development of selective anion sensors for bioimaging applications is currently at the forefront of applied supramolecular chemistry.

1.2.1 The fluorophore. An extensive range of fluorophores are now available, however, for *in vivo* work those that are not just bright ($\varepsilon \times \Phi$) but have NIR emission are of considerable benefit.[54,65–67] A ''window'' of increased optical transparency exists in the range 650 to 950 nm and at these wavelengths tissue autofluorescence is minimised and the major interferents (haemoglobin, lipids and water) absorb to a less significant extent.[66] The use of NIR emission also minimises light scattering and is far less likely to damage the living system. The use of multiphoton excitation (or inverse Stokes) techniques is also of particular relevance for *in vivo* studies[68,69] and several multiphoton probes for anions are described herein. For *in vitro* studies which require little photon penetration the requirements are slightly more forgiving and probes with emission wavelengths ranging to 350 nm have been successfully used. In all cases a large Stokes shift is desirable to minimise light scattering. Emission wavelengths (and in turn Stokes shift) are known to be influenced by a number of factors including the structure of the excited state and solvent reorganisation upon excitation.[70–72] Recently, quantum chemical calculations have been employed in the design of fluorophores with *ca.* 200 nm Stokes shift.[73]

While well-known fluorophores (such as rhodamine, fluorescein, BODIPY and cyanine)[48,64,74–77] are common in anion imaging studies, several unconventional fluorophores (*e.g.* Si, Se, Ge and Te rhodamines[78,79] and squaraine-rotaxanes[54]) have successfully been used in recent years. An increasing number of effective probes also employ lanthanide based luminescence for signal transductance.[45,56,80–83]

1.2.2 The switch. The ideal probe must either ''switch on'' in the presence of the target analyte or if quantitation is required the probe should arrive with an ''internal standard'' present *i.e.* the active signalling luminophore should be coupled to a fluorophore that has a constant unwavering response in the biological environment. Such *ratiometric* sensing[84,85] allows exact quantification of

Frederick M. Pfeffer

Fred Pfeffer received his BSc (Hons 1) in 1996 and PhD in 2001 from Deakin University. He then worked for three years at Trinity College Dublin, first as a lecturer then as postdoctoral fellow in the group of Prof Thorfinnur Gunnlaugsson. In 2004 he returned to Australia as lecturer and in 2010 was appointed Senior lecturer. Research interests include many aspects of supramolecular chemistry including anion recognition and sensing. A research focus is the synthesis and use of fused [n]polynorbornane scaffolds as preorganising elements for further applications including host : guest chemistry and the construction of metallo-supramolecular cages.

the target as the response from the active signalling moiety can be measured against that of the "constant" fluorophore. Such requirements can also be met if both the unbound and bound probe are fluorescent at measurably distinct wavelengths. A recent article by Sessler highlights the use of ratiometric probes for bioimaging applications.[43] Unfortunately, for many anions (such as Cl^-, I^-, HCO_3^- and BrO^-) the current list of selective "switch on" and ratiometric probes is limited.

A probe can also be classified according to the *electronic* event by which fluorescence is "switched" or modulated (for example ICT/PET modulation, FRET, heavy ion effect, and excimer formation). Many sensors—known as chemodosimeters—have been designed such that a chemical reaction controls this modulation[30,33,35,49,86] and it is logical that these strategies have been adopted by those pursuing the goal of *in vitro* and *in vivo* imaging. While the chemodosimeter approach is by far the most popular (and is excellent for the selective detection of a specific species) the chemodosimeter is, in most instances, *irreversibly* transformed to the signalling moiety and as such true spatiotemporal information cannot be gleaned. Continued effort from the research community is required to achieve the goal of *tracking* rather than *trapping* the anionic species of interest. Another very popular approach to modulating fluorescence is the displacement approach.[27,46,87] The luminophore is quenched by a species that is non-covalently attached and the luminophore–quencher combination is chosen such that the target anion interacts with the quencher more strongly than it does with the luminophore. Hence the quencher is displaced, the luminophore is released and fluorescence is "switched on".

1.2.3 The biological environment. The solvent for life is water, hence the probe must possess a degree of water solubility and many hydrophobic probes have been made more biocompatible by attaching either a PEG[88] or a sugar.[89] Nevertheless, a hydrophilic/hydrophobic (amphipathic) balance must be struck such that the sensor can passively diffuse through cell membranes. In the wider field of cellular imaging a commonly employed manoeuvre to ensure uptake is to mask polar hydroxy groups and carboxylates as esters (especially acetoxymethyl (AM) esters[90]) that are subsequently hydrolysed by one of the myriad of intracellular esterases to release the desired probe. This approach has been adopted in the field of anion imaging agents and three peroxynitrite probes are shown in Fig. 1 as examples. The early (1997) dichlorodihydrofluorescein was used as the diacetate diester **DA-DCHF**[91] and the more recent (2010) **HKGreen3** employed a single acetate.[92] The tetra-acetoxymethyl ester **AM-DTTA** passively diffused into cells whereupon the tetracarboxylate ligand (**DTTA**) was liberated and in the presence of terbium and europium the desired lanthanide probes assembled *in cellulo*.[93] An added benefit of this approach is that the unmasked probe is typically retained inside the cell, nevertheless, even probes containing carboxylates can be expelled from the cell by active anion transport mechanisms.[94]

Ideally once the probe is inside the living entity it should localise in the most relevant sub-cellular compartment. Guidelines to predict the likely compartmentalisation of new probes

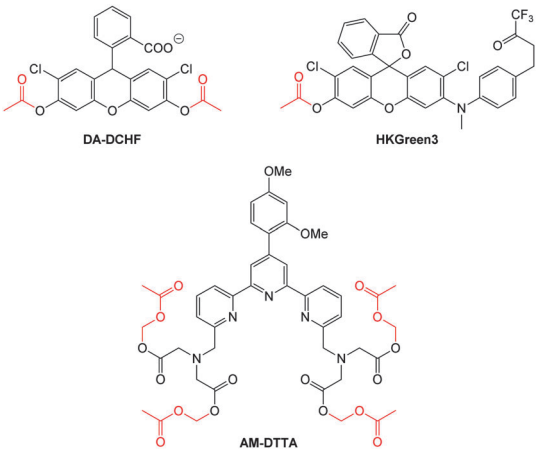

Fig. 1 Examples of peroxynitrite probes **DA-DCHF**, **HKGreen3** and **AM-DTTA** in which intracellular uptake and subsequent trapping was performed using a lipophilic ester (highlighted in red) that was cleaved *in vivo* by intracellular esterases.

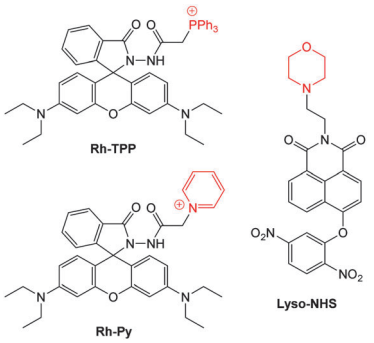

Fig. 2 Examples of probes that localise in the mitochondria (**Rh-TPP**, **Rh-Py**) and lysosome (**Lyso-NHS**).

are not unequivocally established[63,95] and colocalisation studies with well-established dyes are generally required. Nevertheless some general trends exist: (i) cationic probes gravitate to the mitochondria[96,97] as the mitochondrial membrane is negatively polarised and (ii) weakly basic probes accumulate within the more acidic lysosomes.[98] These general guidelines have also been adopted in the field of anion bioimaging, for example, the recently described probes for hypochlorite **Rh-TPP** and **Rh-Py** (Fig. 2)[99] employ a triphenylphosphonium and pyridinium appendage respectively for mitochondrial localisation. The intracellular sensor for hydrosulfide **Lyso-NHS** used a morpholine substituent for lysosomal localisation.[100]

1.3 Structure of this review

In conjunction with a comprehensive listing of recent examples (the majority of examples are from the last 5 years) the broad concept of this review is to provide both a "*why*" and "*how to*" target the specific anion of interest. For each of the anions covered herein a justification of the cellular relevance is first provided—even anions of obvious environmental importance (such as cyanide and fluoride) have considerable relevance and interest for intracellular studies (see Section 2). Also covered are

a number of anions that are of relevance *primarily* at a cellular level (see Section 3), for example bicarbonate plays a critical role in living systems as a measure of CO_2 uptake/respiration (hypercapnia/hypercapnia = CO_2/HCO_3^- poisoning respiratory acidosis). Similarly, reactive oxygen and nitrogen species (such as hypochlorite ClO^- and peroxynitrite $ONOO^-$) have critical *in vivo* roles and elevated levels of these species are associated with many disease states (see Section 4). Where possible, examples have been grouped by the means (mechanism) by which sensing is achieved and also whether the probes are: intensity modulated ("switch off" or "switch on") or ratiometric (wavelength modulation). The terms fluorescent probe, anion imaging agent and intracellular sensor are all used interchangeably.

2. Anions of environmental and biological relevance

There now exists a number of excellent sensors for anions such as fluoride and cyanide;[35,37,39,101] widely recognised as anions of environmental concern. While not commonly appreciated, these anions also have significant relevance in a biological setting and a number of intracellular probes have been developed for their detection. Chloride has a more passive, nonetheless important, role in the environment and, like iodide, plays an important physiological role.[102] Anions covered in this section are fluoride, chloride, iodide and cyanide.

2.1 Fluoride

Fluoride is a very well-known anion due to its use in drinking water and toothpaste to prevent dental caries and osteoporosis.[103] Nevertheless excess fluoride is responsible for a number of deleterious conditions including dental and skeletal fluorosis and is now linked to cancer and neurotoxicity.[104–106] Probes capable of selectively indicating fluoride *in vitro* and *in vivo* may assist in clarifying the exact biological roles of this anion.

Given its "Janus" behaviour the recognition and sensing of fluoride has been a focus of supramolecular chemists.[37,39,101,107,108] Two approaches that have been widely used in the design of both sensors and bioimaging agents are (i) deprotonation (Section 2.1.1) and (ii) desilylation (Section 2.1.2). *Deprotonation*, mediated by the strongly basic fluoride anion, leading to enhanced ICT of a luminophore, was one of the first means by which this anion was detected,[18,109–112] and while the approach has been used for imaging, this design is prone to interference from other basic anions (such as acetates). By far the most common approach employs the fluoride mediated *desilylation* reaction of chemodosimeters that have been designed with a silyl ether.

2.1.1 Fluoride mediated deprotonation. The phenolic naphthalimide probe **NIM** (Fig. 3) was reported in 2014.[113] The probe was both colourimetric (strong absorption band emerging at 641 nm in the presence of F^-) and fluorescence "switch off" (λ_{ex} = 490 nm, λ_{em} = 582 nm decreases). In solution, a similar, yet less pronounced, change was also recorded with acetate—a common interferent for probes operating by means of deprotonation.

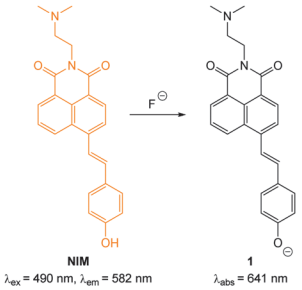

Fig. 3 Structure, and deprotonation, of **NIM** with fluoride.

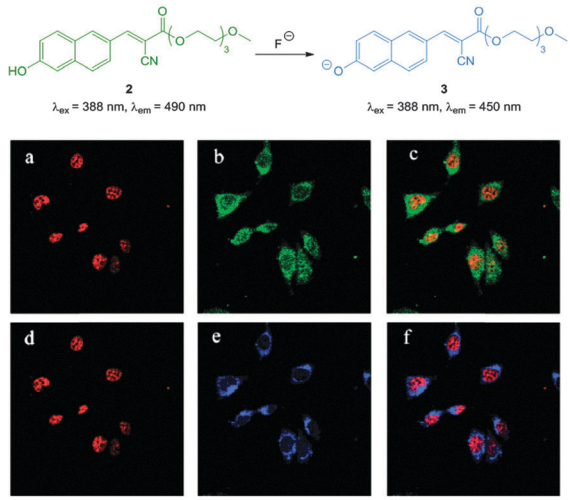

Fig. 4 Top: structure of hydroxynaphthalene **2**. Bottom: PC3 cells incubated with **2** (10 μM) and nucleus stain propidium iodide (a) red channel image; (b) green channel image of (a); (c) overlay of (a) and (b). PC3 cells incubated with **2**, NaF and propidium iodide (d) red channel image; (e) blue channel image of (d); (f) overlay of (d) and (e). Image reproduced with permission.[114]

Of interest, and hinting at an additional role for this probe, the fluorescence of the unreacted probe was considerably enhanced in the lysosomes of cancer cells as opposed to healthy cells. Preliminary experiments indicate that both a protein-rich and an *acidic* environment (such as in cell lysosomes) were required for the enhancement.

The ratiometric hydroxynaphthalene probe **2** (Fig. 4) was reported by Liu and Ke in 2014.[114] A PEG cyanoacrylate was included to enhance ICT and also balance solubility. The probe was selective to fluoride (no significant fluorescent changes were elicited by AcO^-) and the emission intensity ratio I_{490}/I_{450} nm could be used to quantitate fluoride up to 10 equivalents with a limit of detection (LOD) of 8.5 μM. The probe was cell permeable, non-toxic to prostate cancer (PC3) and epithelial cervical cancer (HeLa) cells and located in the cytoplasm of these cells (confirmed using the red nuclear stain propidium iodide—PI). In PC3 cells a clear change in emission colour was observed when cells pre-treated with **2** were exposed to fluoride.

A recent report by Mahapatra (2014) outlined the ratiometric BODIPY azaindole **4** (Fig. 5) which was synthesised in three steps.[115] In solution studies (7 : 3 $CH_3CN:H_2O$) the strong emission at 512 nm (λ_{ex} = 350 nm) decreased upon addition

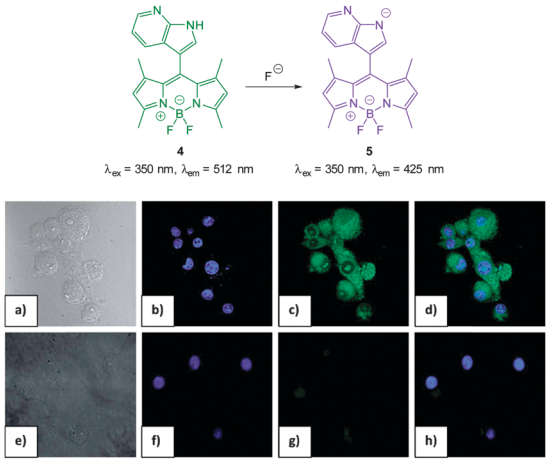

Fig. 5 Top: structure, and deprotonation, of probe **4** by F^-. Bottom: images of RAW264.7 cells. (a) Bright field image; (b) nuclei stained with 4′,6-diamidino-2-phenylindole (DAPI); (c) cells treated with probe **4**; (d) overlay image of (b) and (c); (e) bright field image of probe **4** and F^-; (f) probe **4** and F^- (g) nuclei with DAPI; (h) overlapping image of (f) and (g). Image reproduced with permission.[115]

of fluoride (and to a similar extent acetate) as weak emission at 425 nm increased and the ratio F_{425}/F_{512} was used to determine F^- concentration (<200 equivalents). The N–H of indole has been used previously for the recognition and sensing of fluoride anions[116,117] and for probe **4** deprotonation significantly enhanced ICT and a clear change in fluorescence emission was recorded in murine macrophages (RAW264.7) upon addition of fluoride.

In 2013 Chellappa reported the rhodamine based probe **RDF-1** (Fig. 6) that operates by means of deprotonation leading to spirocycle ring opening.[118] A strong "switch on" fluorescence response at 557 nm was observed in the presence of F^-. In HeLa cells **RDF-1**

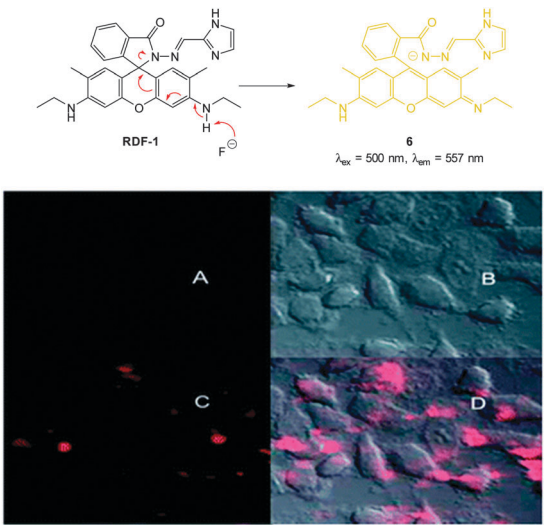

Fig. 6 Top: structure and reaction of rhodamine probe **RDF-1** with F^-. Bottom: (A) fluorescence image of HeLa cells incubated with **RDF-1**; (B) corresponding bright-field image; (C) fluorescence image of HeLa cells incubated with **RDF-1** and NaF; (D) overlaid images of HeLa cells (B and C). Image reproduced with permission.[118]

was non-toxic and within 10 minutes of NaF addition significant fluorescence enhancement was observed.

2.1.2 Fluoride mediated desilylation. Many chemodosimeter have been designed to use the selective reaction of fluoride with silicon (incorporated as a Si–O–C bond) to form the exceptionally strong Si–F bond (>800 kJ mol^{-1}). The approach is essentially identical to the fluoride mediated cleavage of silyl containing protecting groups.[119] For the probes shown herein the hydroxy fragment is released as a phenoxide anion which is a component of an ICT fluorophore; hence the desilylation reaction leads to a dramatic fluorescence "switch on".

One of the earliest "switch on" probes functioning by means of desilylation, a TBDPSO-coumarin (**TBPCA**, Fig. 7), was published by Park and Hong in 2009.[120] The probe readily entered cells and was retained with no toxicity. Images in human epithelial lung carcinoma A549 cells show clear blue fluorescence upon exposure to NaF.

The "switch on", red emitting probe **8** (Fig. 8) was recently published by Zhu (2014).[121] Synthesis of the masked ICT fluorophore involved aldol type reaction of the potential electron donor 4-OTBPS-benzaldehyde with the electron withdrawn 2-dicyanomethylene-3-cyano-4,5,5-trimethyl-2,5-dihydrofuran (TCF). For probe **8** a linear emission "switch on" at 612 nm was observed upon reaction with fluoride and a LOD = 0.07 mM was determined. The *absorption* spectra could be used to quantify

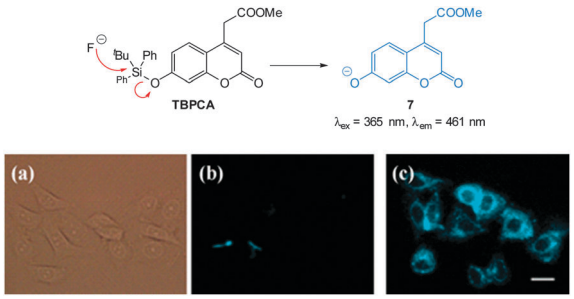

Fig. 7 Structure and reaction of coumarin **TBPCA** with fluoride. (a) Bright-field image of A549 cells with **TBPCA** (b) fluorescence image with **TBPCA** without NaF (c) fluorescence image with **TBPCA** and NaF. Scale = 20 μm. Reproduced with permission.[120]

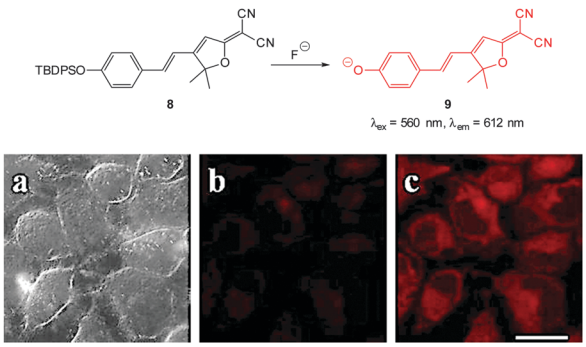

Fig. 8 Top: structure and reaction of "switch on" fluoride probe **8**. Bottom: fluorescence images of HeLa cells incubated with probe **8** (a) bright-field transmission (b) red channel with no NaF (c) red channel with NaF. Scale = 20 μm. Image reproduced with permission.[121]

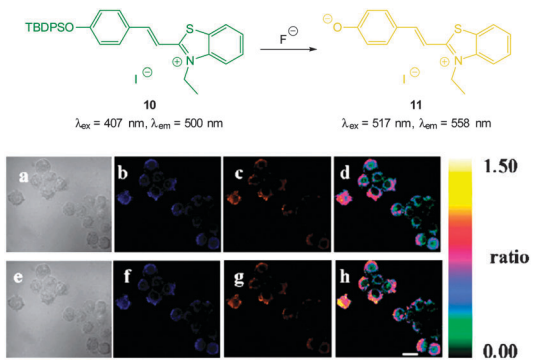

Fig. 9 Top: structure and reaction of benzothiazolium hemicyanine **10** with F^-. Bottom: images of RAW264.7 macrophages incubated with **10** and no added F^- (a) bright-field, (b) blue channel at 490 ± 20 nm, (c) orange channel at 560 ± 20 nm, and (d) ratio image from (c) and (b). Images of RAW264.7 macrophages incubated with **6** after addition of NaF (e) bright-field, (f) blue channel at 490 ± 20 nm, (g) orange channel at 560 ± 20 nm, and (h) ratio image from (g) and (f). Scale = 20 μm. Image reproduced with permission.[122]

the amount of fluoride present in solution due to the linear relationship between the increase at 596 nm and the decrease at 438 nm. Imaging was performed in live HeLa cells and 10 μM NaF was readily visualised using fluorescence microscopy.

The highly selective, ratiometric, benzothiazolium hemicyanine **10** (Fig. 9) developed by Ma, Du and Zhang (2011)[122] could monitor fluoride concentration using the ratio F_{500}/F_{558}. A limit of detection (0.08 nM) was identified and in live RAW264.7 macrophages a distinct ratiometric fluorescence response was observed upon addition of buffered NaF. The probe was also shown to penetrate rapidly (<5 minutes) and was non-toxic.

A variation on the desilylation probe was reported by Zhang in 2013.[123] In the presence of fluoride, desilylation of the functionalised naphthalimide chemodosimeter **12** (Fig. 10) was immediately followed by fragmentation to give the conjugate base of 4-hydroxynaphthalimide **13**. In solution studies a linear fluorescence

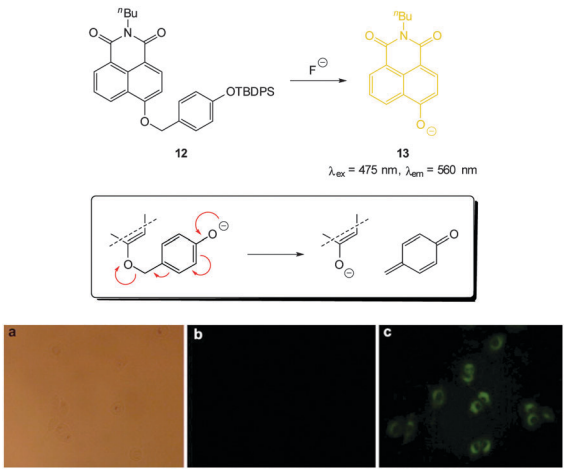

Fig. 10 Top: functionalised naphthalimide probe **12** and its reaction with F^-; inset shows fragmentation mechanism. Bottom: (a) bright-field image of A549 cells incubated with **12** (20 μM) for 24 h (a) bright field (b) without NaF (c) with NaF (50 mM). Image reproduced with permission.[123]

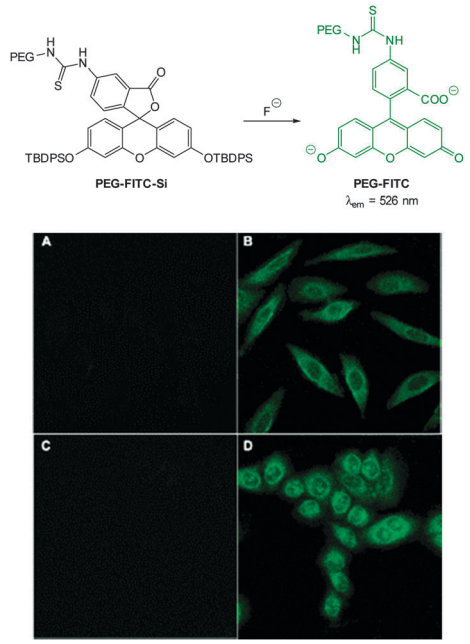

Fig. 11 Top: structure of fluoride chemodosimeter **PEG-FITC-Si**. Bottom: fluorescence imaging of L929 (top) and HeLa (bottom) cells incubated with the sensor before (A and C) and after (B and D) treatment with NaF. Image reproduced with permission.[88]

"switch on" (λ_{em} = 560 nm) was realised (20-fold increase in one hour with only 1.0 equivalent of F^-; LOD = 0.35 μg L^{-1}). After incubation of probe **12** with human epithelial carcinoma cells (A549) addition of a solution of NaF elicited a distinct green fluorescent response.

With an eye to enhanced solubility the PEG-thiourea-fluorescein probe **PEG-FITC-Si** (Fig. 11) was synthesised by Zeng and Wu (2013)[88] in two steps from the corresponding fluorescein isocyanate. Again in the presence of fluoride a dramatic increase in fluorescence (λ_{ex} = 490 nm, λ_{em} = 526 nm) was observed (LOD = 19 ppb). Imaging was successfully achieved in HeLa and murine fibroblasts (L929) only 15 minutes following addition of fluoride (100 μM) with perinuclear probe localisation.

The TBSO-benzothiazole **BBTGA** (Fig. 12), also deliberately designed for biocompatibility by conjugating glucosamine to improve solubility, was reported by Wang in 2013.[89] A linear

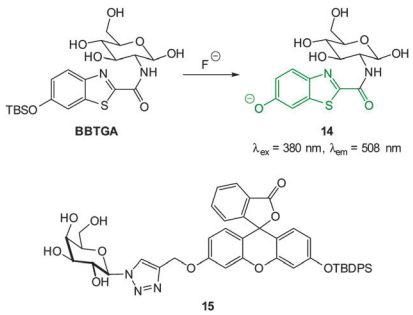

Fig. 12 Structure of **BBTGA** and **15**, showing reaction of **BBTGA** with F^-.

30-fold fluorescence enhancement (λ_{em} = 508 nm) was noted 5 minutes after the addition of NaF in PBS buffer. The probe was water soluble, non-toxic and when a buffered solution of NaF (0.1 mM) was added to human nasopharyngeal epidermal carcinoma (KB) cells that had been pre-treated with a dilute solution of **BBTGA** strong fluorescence was observed.

Again with solubility and biocompatibility in mind the carbohydrate conjugate probe **15** (Fig. 12) was synthesised by Du (2011) using the well-known copper assisted azide alkyne cycloaddition (CuAAC).[124] A very strong (160 fold), linear, fluorescence "switch on" response (λ_{em} = 520 nm) was observed with increasing NaF (from 0 to 1.4 mM, probe concentration 50 μM) and a limit of detection of 10.5 μM was identified. A strong fluorescence response was observed upon addition of NaF solution to Hep2G cells that had been incubated with **15** (Fig. 13).

The pyrene dimer **16** (Fig. 14) containing a disilane (Si–Si) bond was designed and constructed by Li and Shen (2012).[125] Ratiometric measurement in solution (THF : H_2O) was possible as the well-known pyrene excimer fluorescence at 470 nm ceased upon reaction of the probe with fluoride and only monomer emission at 378 nm was present. Up to 6 equivalents of F^- could be measured using F_{378}/F_{470}. Loading of **16** into HeLa cells was performed using polylactic acid nanoparticles and upon exposure to fluoride a clear change in emission was detected.

In 2012 Lee, Kim and Ahn published an interesting variant on the desilylation probe.[126] Upon desilylation the carefully functionalised aminonaphthalene **P1** (Fig. 15) reacts in an additional intramolecular process to give the extended aminocoumarin **20**. A fluorescence "switch on" (λ_{em} = 595 nm) was observed in both murine metastatic melanoma (B16F10) cells and also in live zebrafish. Imaging was accomplished using two photon microscopy (TPM) and the lower excitation energy associated with this technique is perfect for *in vivo* research to understand how fluoride is distributed in a whole body context. In the zebrafish, increased concentrations of F^- in the tail and abdomen were observed at t = 2 h *versus* t = 30 min.

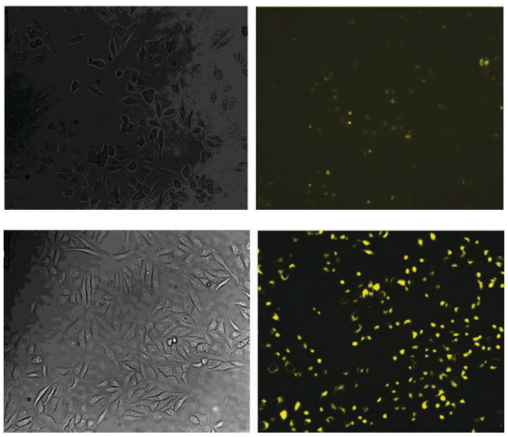

Fig. 13 Images of HepG2 cells (left) brightfield and (right) fluorescence with (above) only probe **15**, (below) probe **15**, and NaF. Image reproduced with permission.[89]

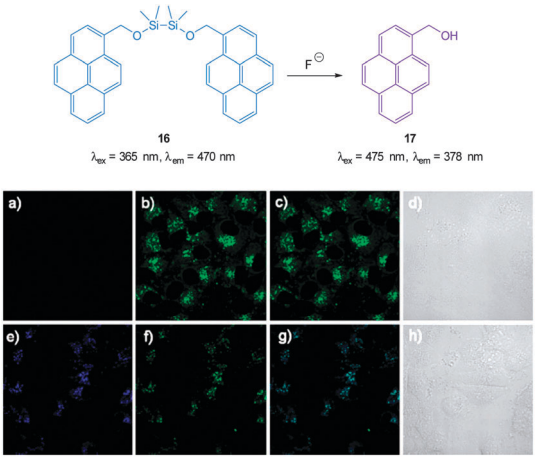

Fig. 14 Top: structure and reaction of pyrene dimer **16** with F^-. Bottom: images of live HeLa cells incubated with probe **16**; (a) emission 410–440 nm (blue channel) (b) emission 440–600 nm (green channel), (c) overlaid a and b, (d) bright-field transmission image. The above cells after addition of 100 μM F^- (e) emission 410–440 nm, (f) 440–600 nm, (g) overlaid e and f, (h) bright-field transmission image. Image reproduced with permission.[125]

A recent report (2014) by Song also outlined a dicyanoacrylate "switch on" probe (**21**, Fig. 15) in which a desilylation cascade approach was used to create a red fluorescent iminocoumarin.[127] The probe itself was non-fluorescent and for the product a Stokes shift of more than 140 nm was recorded. Using fluorescence microscopy the probe was shown to be readily internalised and was capable of indicating the presence of fluoride in living human keratinocyte (HaCaT) cells (*not shown*).

The related probe **FP** (Fig. 15) from the group of Peng (2014),[128] also relies on an additional reaction occurring post Si cleaving. The probe was synthesised from the corresponding quinolinecarbaldehyde and the final product of the reaction sequence is a highly fluorescent (ϕ_F = 0.84, λ_{ex} = 441 nm, λ_{em} = 485 nm) aminobenzopyranimine. The probe was shown to be relatively non-toxic, localised in the mitochondria of both breast cancer (MCF-7) and fibroblast-like (COS-7) cells and fluorescence was dramatically "switched on" when the cells were treated with dilute solutions of NaF (Fig. 16).

2.1.3 Miscellaneous. A Se–B bond can be selectively cleaved by fluoride and the unusual red emitting BODIPY probe **22** (Fig. 17) reported by Tang (2011) was designed on this principle.[129] The presence of Se quenched fluorescence but upon reaction with fluoride the "usual" F–B bond was formed (**23**) and red fluorescence (λ_{ex} = 640 nm, λ_{em} = 690 nm) was "switched on" (*ca.* three-fold enhancement). The chemodosimeter was selective for fluoride and the increased fluorescent response was readily observed in human hepatoma cells (HepG2) pre-treated with F^-.

2.2 Chloride

Chloride is the most abundant anion in living organisms and its transport across cellular membranes is essential for a number of physiological processes including the maintenance

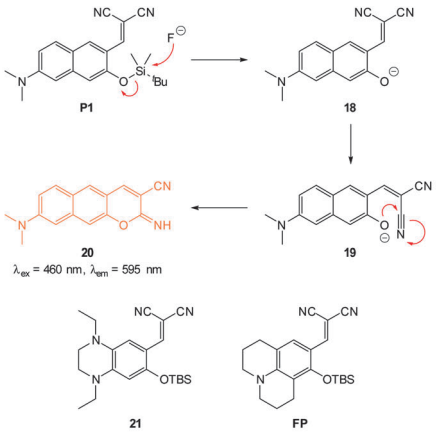

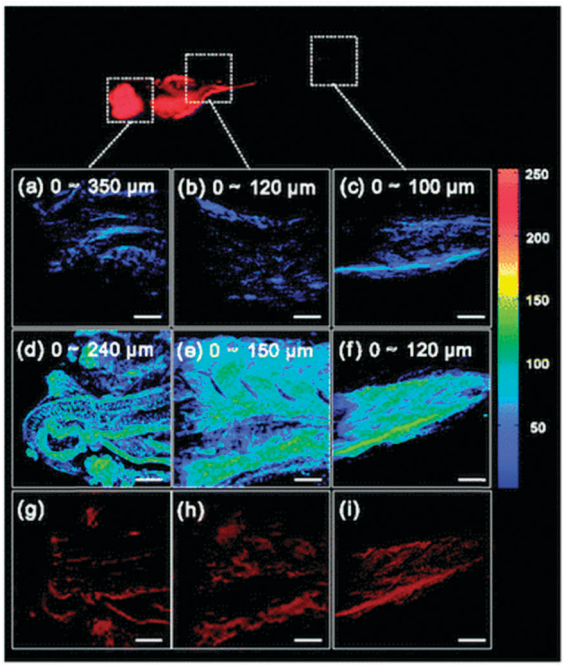

Fig. 15 Top: structure and reaction of aminonaphthalene probe **P1** with F^- to form extended coumarin **20**. Bottom: accumulated TPM images for three zebrafish parts: (a–c) probe **P1** alone (d–i) probe **P1** followed by F^- (a–f) intensity data; (g–i) fluorescence images constructed by image stacking for 0–350 μm depth, with a 2 μm imaging depth step. Scale = 50 μm. View area: 300 μm^2. Image reproduced with permission.[126]

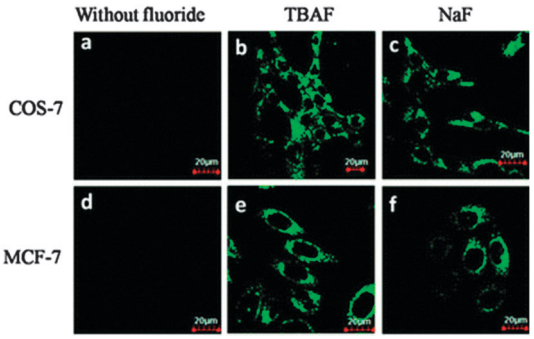

Fig. 16 Images of COS-7 and MCF-7 cells incubated with **FP** before (a and d) and after (b, c, e, and f) treatment with TBAF or NaF. Image reproduced with permission.[128]

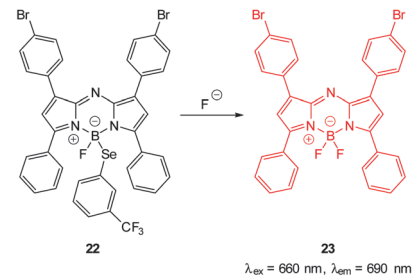

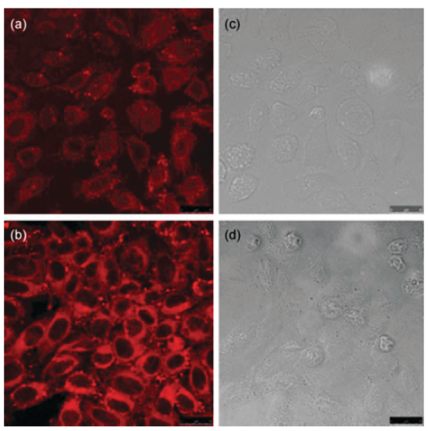

Fig. 17 Top: structure and reaction of Se BODIPY **22** with F^-. Bottom: images of living HepG2 cells Incubated with (a) probe **22** for 1 h; (b) F^- for 1 h then probe **22** for 1 h. Images (c) and (d) are bright field images of (a) and (b), respectively. Image reproduced with permission.[129]

of cell volume, acidification of internal compartments and even electrical excitability. Impaired transport of this anion due to a of genetic mutation in a cAMP-regulated Cl^- channel defines the condition known as cystic fibrosis (CF).[130] Indeed, the pursuit of biologically active chloride transporters to remedy this condition is an important current goal for supramolecular chemists.[131–138]

Other than some recent developments (Section 2.2.3) the strategy employed in the design of chloride imaging agents relies on halide mediated collisional quenching (Section 2.2.1) and as such the majority of Cl^- probes are "switch off". Nevertheless by attaching such probes to "constant" fluorophores several ratiometric probes have been successfully designed and used (Section 2.2.2).

2.2.1 Chloride mediated collisional quenching. Due to its recognised physiological importance the development of functionalised quinolones (such as **SPQ** and **MEQ**, Fig. 18)[102,139–141] as chloride imaging agents was accomplished long before other anions were targeted and several are commercially available.[142] Nevertheless, these quinolone based probes are "switch off"; they are not selective for chloride amongst other halides and they also suffer from photobleaching.[143,144] Furthermore, unless invasive techniques are used to deliver the probe into cells, probes such as **MEQ** must be reduced (using $NaBH_4$) to the charge neutral, cell permeable dihydro form (**diHMEQ**) first which following uptake is oxidised back to the Cl^- responsive form.[145] Despite their limitations, functionalised quinolone

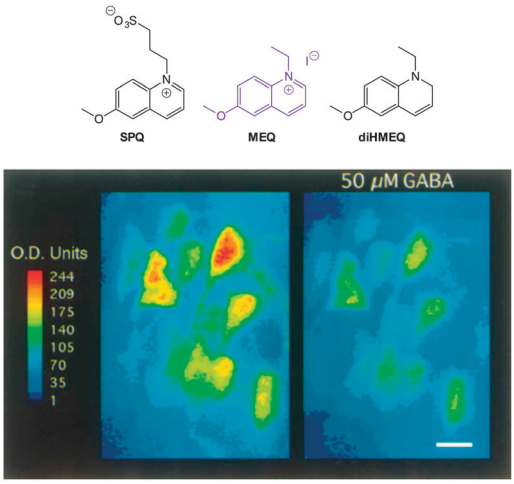

Fig. 18 Top: structure of **SPQ**, **MEQ** and the cell permeable **diHMEQ** probes for Cl^-. Bottom: images of **MEQ**-loaded neurons (left) before and (right) 20 min after GABA application. Scale = 15 μm. Image reproduced with permission.[146]

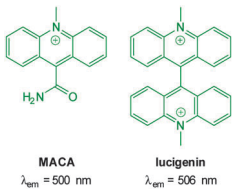

Fig. 19 Acridine and quinolinium "switch off" probes **MACA** and **lucigenin**.

probes have proven very useful. Clear images were obtained by Inglefield who used **MEQ** (λ_{em} = 320 nm) to confirm Cl^- transport (mediated by manipulating the $GABA_A$ ion channel, Fig. 18) into neuronal cells obtained from a rat brain slice,[146] and Durack employed **SPQ** to measure intracellular chloride in porcine lymphocytes using flow cytometry.[147] Recently this style of probe has also been shown to be compatible with two-photon excitation.[148]

The identification of *N*-methylacridinium-9-carboxamide **MACA** (λ_{em} = 500 nm, Fig. 19) and also the bisacridinium lucigenin (λ_{em} = 506 nm, Fig. 19) as longer wavelength variants was a welcome development.[149] However, while these compounds have been used successfully in vesicle/liposome based studies[150] they were shown to be unstable in cell based studies.[149]

2.2.2 "Switch on" and ratiometric probes. Ratiometric measurement of intracellular chloride has been achieved by conjugating the chloride sensitive methoxyquinoline to the "constant" dimethylaminoquinoline fluorophore to give **bis-DMXPQ** (λ_{em} = 450 for **MQ** *vs.* λ_{em} = 565 nm for **DMQ**, Fig. 20).[151] This dimer distributed uniformly in the cytoplasm and was reported to be stable and non-toxic. Related compounds could be reduced (in a similar process to that for **MEQ**) for non-invasive cell loading.[151] While not classed as a small molecule the bisacridinium tetramethylrhodamine conjugate **BAC-TMR-dextran** (Fig. 20) was constructed from the carbohydrate aminodextran.[152]

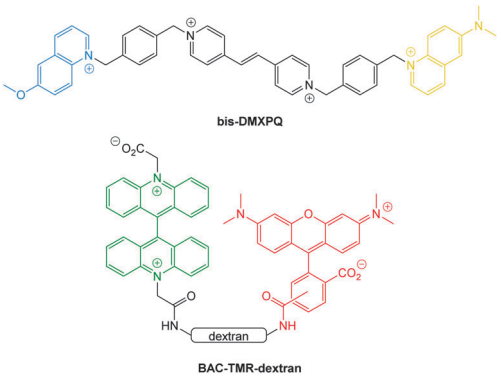

Fig. 20 Ratiometric probes **bis-DMXPQ** and **BAC-TMR-dextran** used for chloride imaging.

Green emission from the biasacridinium (λ_{em} = 505 nm) was quenched on addition of Cl^- while red rhodamine emission remained constant. The ratiometric probe was successfully used for intracellular imaging to link chloride concentration to endosomal acidification.

More recently, the ratiometric probe **MQAF** (Fig. 21) was reported by Tang (2012).[153] The structure consisted of the "switch off" methoxyquinolium combined with aminofluorescein and monitoring at two channels [chloride sensitive emission λ_{ex} = 318 nm, λ_{em} = 436 nm and insensitive λ_{ex} = 494 nm, λ_{em} = 519 nm] gave accurate measurements of Cl^- concentration. This probe was successfully used in ventricular myocytes to illustrate that induced ischemia results in increased Cl^- concentration. In 2014 the same group published the ratiometric methoxyquinolium dansyl combination (**MQDS**, Fig. 19) and the ratio λ_{em} = 440 nm against λ_{em} = 560 nm was used to monitor chloride concentration.[154] Imaging of liver cancer cells (HepG2) was performed and intracellular chloride concentration was successfully monitored as the extracellular levels in the surrounding media were deliberately increased (Fig. 21).

2.2.3 Recent developments. A "switch on" probe selective for *in vitro* or *in vivo* chloride has yet to be reported however the groups of Fusi and also Smith are getting close. Fusi reported that both the Cd(II) complex with nitrobenzooxadiazole-tetraazacyclododecane **24** (λ_{ex} = 410 nm, λ_{em} = 520 nm) and also the bis Zn(II) complex of **25** (λ_{ex} = 325 nm λ_{em} = 543 nm) act as "switch on" sensors for halides (Cl^- and F^-) (Fig. 22).[155,156] It was postulated that for both complexes the metal to nitrogen (nitrobenzooxadiazole) distance and M to N (cyclam) distances change upon binding of chloride and it is the balance between fluorescence enhancement (ICT to nitrobenzooxadiazole) from freeing the *N*-nitrobenzooxadiazole nitrogen and quenching (PET) of nitrobenzooxadiazole fluorescence by the cyclam that leads to the fluorescence modulation. The *ligands* have been internalised in human neuroblastoma (HeLa) cells to give fluorescence signals, however, images of the halogen sensitive metal complexes functioning in cells have not yet been published.

Another new, and very interesting, class of chloride probes are the squaraine-rotaxanes developed by Smith (Fig. 23).[157,158]

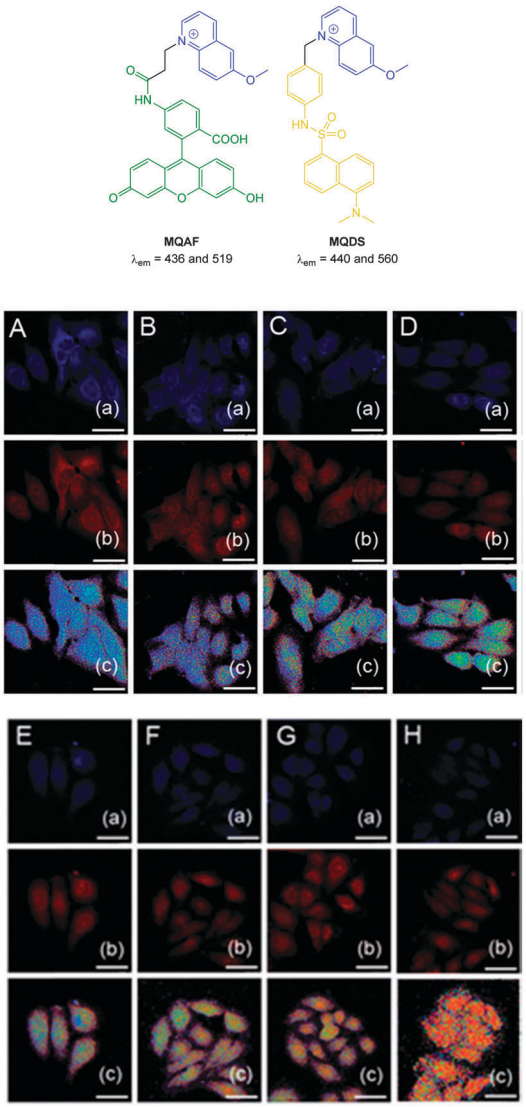

Fig. 21 Top: structures of ratiometric quinolium conjugates **MQAF** and **MQDS**. Bottom: images of HepG2 cells loaded with **MQDS** exposed to: A–H, 0–140 mM chloride. Top in each row is blue channel, middle is red channel and the bottom is a ratio image (F_{red}/F_{blue}). Scale = 25 μm. Image reproduced with permission.[154]

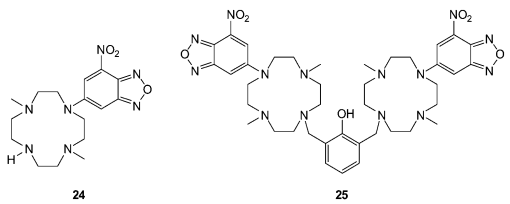

Fig. 22 NBD-cyclam ligand **24** and related ditopic **25**.

The squaraines have been somewhat overlooked as a biologically compatible fluorophore due to their susceptibility to hydrolysis. In contrast, hydroxysquaraines have been found to be much more stable and for rotaxane **26** (Fig. 23) interaction with chloride shifts the surrounding macrocycle slightly along the squaraine "axle" which in turn leads to fluorescence

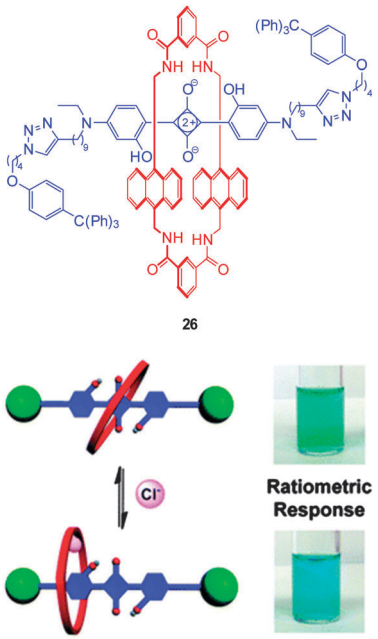

Fig. 23 Fluorescent Cl^- sensor **26** based on a squaraine-rotaxane shuttle. Image reproduced with permission.[166]

modulation. While not yet demonstrated in an intracellular setting squaraine-rotaxane probes are red emissive, ratiometric (in acetone λ_{em} = 698 nm decreases and λ_{em} = 665 nm increases) and, unlike the first generation of probes they are selective for chloride (I^- is not bound; Br^- binding is 10 fold weaker than that of Cl^-) and thus have tremendous potential for further development in an intracellular setting.

2.3 Iodide

In the environment iodide occurs naturally in minerals (alutarite and iodargyrite) and it is interesting that AgI is used by humans as a as a nucleation agent in "cloud seeding" programs due a similarity in crystal structure to that of water ice.[159] Iodide is also a common additive to table salt as deficiencies can lead to the condition known as goitre. Indeed the consumption of trace amounts of iodide is essential for human health—the anion is transported to, and accumulated in, the thyroid gland for incorporation into the iodine containing hormones.[160,161]

Selective probes for iodide bioimaging are rare. It is interesting to note that the early probes for chloride such as **SPQ** and **MEQ** (see Fig. 18) were actually more sensitive to iodide than chloride,[102,140,141] nevertheless the far greater concentration of chloride resulted in minimal interference from iodide.

2.3.1 Recent developments. A recent publication from Mahapatra (2012) outlines a successful displacement approach for the detection of iodide in *Candida albicans* (IMTECH3018) cells.[162] The complexation of Hg(II) by the thiosemicarbazole ligand **27** (Fig. 24) quenches the inherent fluorescence of the carbazole fluorophore (heavy metal effect). Iodide is capable of displacing Hg(II), liberating the highly fluorescent carbazole (λ_{em} = 425 nm) and a four-fold fluorescence "switch on" (λ_{em} = 425 nm)

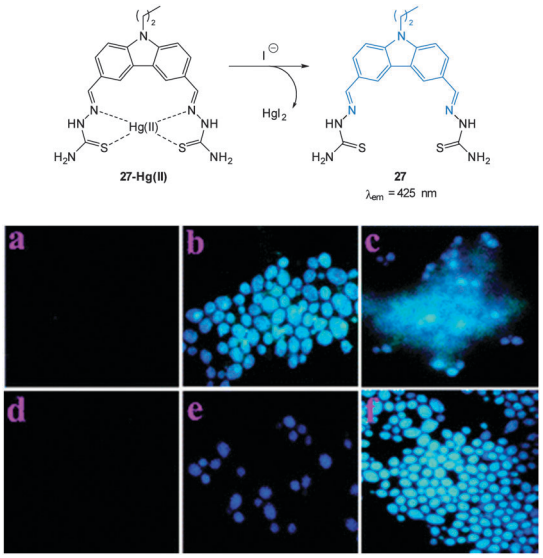

Fig. 24 Top: structure and reaction of iodide probe **27-Hg(II)**; bottom: fluorescence images of *Candida albicans* (a) cells only, (b) cells with **27**, (c) cells with **27** after addition of Hg(II) (5 μM), (d) cells with **27** and Hg(II) (25 μM), (e) cells with the preformed **27-Hg(II)** complex and KI, (f) same as (e) after 10 min. Image used with permission.[162]

was observed. Importantly, selectivity for iodide over other halides was excellent.

2.4 Cyanide

Cyanide has a long history of use in industry and is also well known as an environmental poison but for cystic fibrosis (CF) sufferers $^{-}$CN has a particularly sinister role. Infection with *Pseudomonas aeruginosa* (PA) is common amongst patients with CF and PA is a cyanogenic bacteria (synthesises $^{-}$CN)[163] and *in vivo* cyanide functions as a potent inhibitor of cellular respiration.[164] Indeed PA-mediated cyanogenesis has an acknowledged role in the pathogenesis of CF lung disease.[165] Less common, but more problematic is infection with *Burkholderia cepacia* complex (Bcc) which is typically multidrug resistant and is also cyanogenic.[165,166] Hence diagnostics for $^{-}$CN *in vivo* would be welcome for rapid identification of these problematic lung infections. Other sources of *in vivo* cyanide come from cyanogenic glycosides produced by some plants as part of their innate defence system (for example in almond seeds) and these glycosides can be enzymatically hydrolysed to produce free $^{-}$CN in living tissues.[167]

A number of strategies exist for the detection of cyanide but the most common approaches for imaging $^{-}$CN rely on its (i) nucleophilicity or (ii) affinity for copper ions.[40,168] The *nucleophilicity* of cyanide has been exploited in the design of chemodosimeters (see Section 2.4.1). Typically, nucleophilic attack of $^{-}$CN at a chemodosimeter incorporating a C=O (aldehyde), C=NR, C=C–CN or related functionality results in a product in which conjugation at some point of the probe is broken and in turn the fluorescence response is modulated. The other successfully used approach involves the *displacement* of copper (Section 2.4.2). These probes are functionalised with copper chelating groups

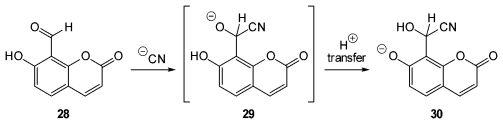

Fig. 25 Coumarin based ESIPT sensor **28** for the detection of cyanide.

such that when Cu(II) is introduced the resultant assembly exists in quenched form (heavy/transition metal ion induced quenching). Cyanide has a very high affinity for copper and is capable of selectively displacing the fluorophore. A very stable $Cu(CN)_2$ species is formed and the fluorophore is liberated—"switched on".

2.4.1 Cyanide as a nucleophile. A relatively early example (2007) was the coumarin aldehyde **28** (Fig. 25) by Kim and Hong.[169] This probe incorporated a structure known to function by means of the excited state intramolecular proton transfer (ESIPT) principle.[170] Attack at the aldehyde occurs in the vicinity of an acidic OH (phenol) which ultimately leads to formation of a cyanohydrin and a phenoxide anion. As the phenoxide is part of an ICT fluorophore, its formation leads to a dramatic enhancement of fluorescence (λ_{em} = 450 nm). Proton transfer to form **30** was confirmed by the significant upfield shift in the ^{1}H NMR spectrum as the phenolic proton (δ_H = 10.1 ppm) was "transferred" to the cyanohydrin (δ_H = 6.1 ppm). While microscopy was not performed a fluorescent plate reader was used to confirm selective "switch-on" (λ_{ex} = 350 nm, λ_{em} = 450 nm) cyanide sensing in murine embryonal carcinoma (P19) cells.

Yoon, designed the ESIPT hydroxyfluorescein aldehyde probes (both mono and di were synthesised; dialdehyde **31** shown in Fig. 26) for microfluidic sensing of cyanide as well as both *in vitro* and *in vivo* probes for cyanide.[171,172] Formation of the phenoxide in this instance leads to spirocyclic ring opening and strong fluorescence "switch on" (λ_{em} = 520 nm). Using dialdehyde **31** the imaging of cyanide in BALB/c nude mouse model was accomplished (Fig. 26) *in vivo*.[172] This probe was

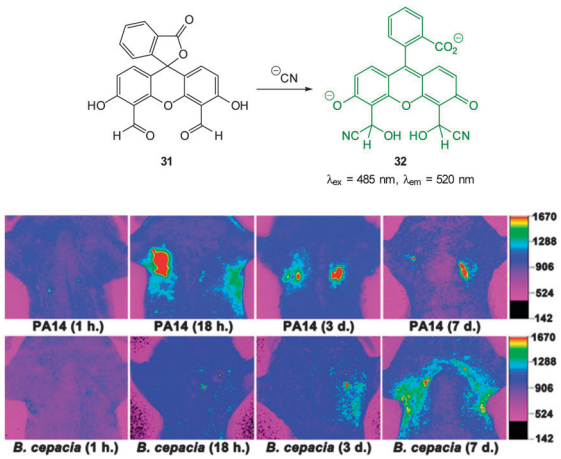

Fig. 26 Top: fluorescein dialdehyde chemodosimeter **31** for $^{-}$CN. Bottom: *in vivo* images of $^{-}$CN in the lungs after various incubation times after infection with PA and Bcc. Colour images were reconstructed from inverted fluorescence images. Image reproduced with permission.[172]

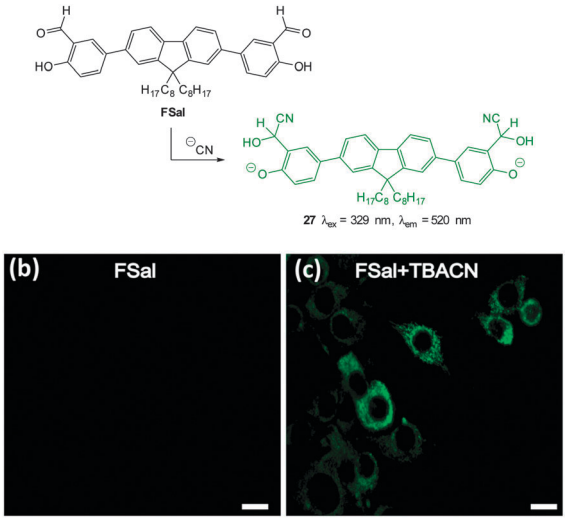

Fig. 27 Top: structure and reaction of fluorene based **FSal** with $^{-}$CN. Bottom: images of SH-SY5Y neuronal cells which were incubated with (left) **FSal** alone and (right) **FSal** then TBACN. Image reproduced with permission.[173]

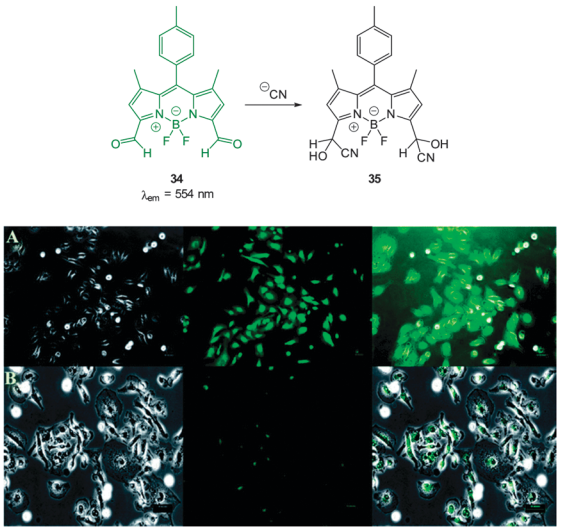

Fig. 28 Top: structure and reaction of BODIPY dialdehyde **34** with $^{-}$CN. Bottom: images of MDA-MB-231 cells (A) treated with **34** only and (B) after incubation with **34** and $^{-}$CN. Left is bright field, centre is fluorescence and right is overlay image. Scale = 50 μm. Image reproduced with permission.[174]

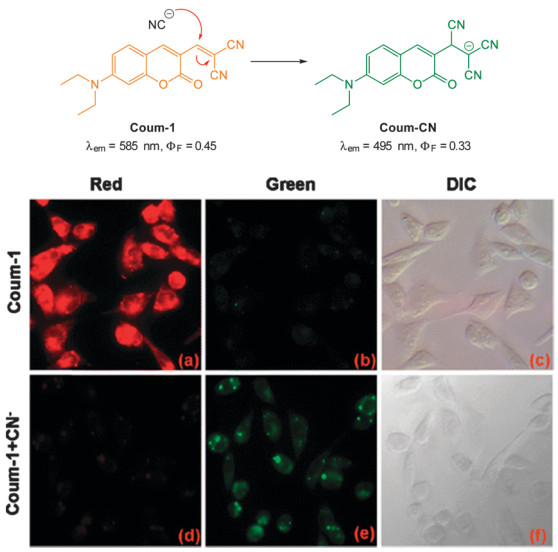

Fig. 29 Top: structure and chemodosimetric reaction of **Coum-1** with $^{-}$CN. Bottom: images of HeLa cells incubated with **Coum-1** with and without $^{-}$CN; (a, d) red channel (b, e) green channel and (c, f) brightfield differential interference contrast (DIC). Image reproduced with permission.[175]

able to detect, in the lungs of the mice, increased levels of cyanide due to infection caused by PA and Bcc. The probe itself did not cause adverse effects when injected as a DMSO solution directly into the lungs of the mice.

The salicylaldehyde functionalised fluorene ESIPT probe **FSal** (Fig. 27) was reported by Malik in 2014.[173] The sensor could detect cyanide in solution at very low concentration (<0.1 ppb) by reaction to form the corresponding cyanohydrin leading to a strong fluorescence 'switch-on' (λ_{ex} = 329 nm, λ_{em} = 520 nm). The probe was capable of imaging cyanide (as tetrabutylammonium cyanide, TBACN) in human neuroblasts (SH-SY5Y) and the probe was both highly selective and non-toxic.

The "switch off" BODIPY dialdehyde **34** (Fig. 28) was reported by Ravikanth in 2013.[174] Using NMR spectroscopy the probe was clearly shown to react with two equivalents of $^{-}$CN and fluorescence (λ_{em} = 554 nm) was quenched with the addition of 2.2 equivalents of the anion. In human breast adenocarcinoma cells (MDA-MB-231) the probe was non-toxic and the intense green fluorescence of the probe was quenched upon treatment of the cells with $^{-}$CN.

The ratiometric aminocoumarin probe **Coum-1** (Fig. 29) reported by Li (2012)[175] possesses a reactive dicyanoacrylate appendage (readily installed using the reaction of malononitrile with the corresponding coumarin aldehyde). A distinct response (both colourimetric and fluorescent) was observed following the conjugate addition reaction of cyanide to the alkene. The diminished length of the ICT system leads to a shift in both absorption and emission maxima and using excitation at λ = 447 nm ratiometric measurement of cyanide could be performed [initial coumarin (ϕ_F = 0.45, λ_{em} = 585 nm), product **Coum-CN** (ϕ_F = 0.33, λ_{em} = 495 nm)]. An impressive 470 fold increase in F_{495}/F_{585} was realised with the addition of only 1.0 equivalent of $^{-}$CN. The probe was successfully used for the detection of cyanide in HeLa cells by comparing emission from the red and green channels.

Also relying on the conjugate addition of $^{-}$CN the BODIPY chemodosimeter **36** (Fig. 30) was developed by Jang (2012).[176] The reaction of cyanide with the dicyanoethylene appendage interrupts the ICT and as a consequence both visible and fluorescent properties were modulated. Interference from fluoride was noted in CH_2Cl_2 but in water the strong solvation of fluoride rendered it less competitive. A clear "switch on" response (λ_{ex} = 480 nm, λ_{em} = 520 nm) was observed in the cytoplasm of HeLa cells that had been incubated with the probe for 20 min then treated with NaCN.

A "switch-on" phenothiazine–hemicyanine probe **Phc** (Fig. 31) was reported by Yang and Li (2014).[177] The cyanide anion readily

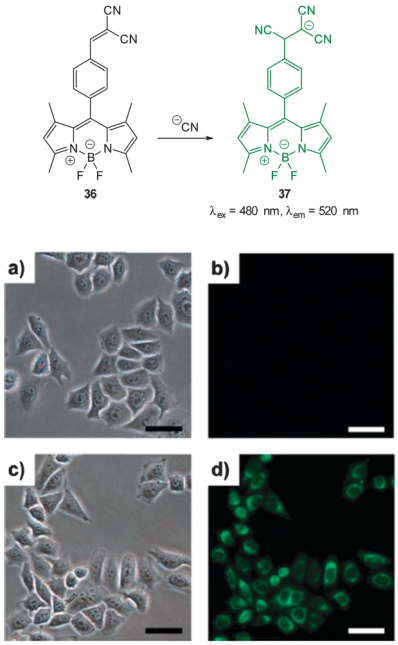

Fig. 30 Top: reaction of dicyanoethylene BODIPY **36** with $^{-}$CN. Bottom: brightfield (a, c) and fluorescence (b, d) images of HeLa cells with only **36** (a, b) then 20 min after treatment with NaCN (c, d). Scale = 50 μm. Image reproduced with permission.[176]

attacked the C=N bond of the indolium and a 20 fold enhancement in fluorescence (λ_{em} = 488 nm) was observed when solutions of the probe were exposed to only 3.0 equivalents of $^{-}$CN. The probe was selective amongst other anions tested and was used in both human breast cancer (GES) and HeLa cells to demonstrate a quick (15 min) "switch on" effect in the presence of *in vitro* cyanide. Furthermore in adult zebra fish exposed to **Phc** and cyanide (30 μM) a strong fluorescent response was observed, particularly in the gills and abdomen.

The related red-emitting phenazine(di)cyanine-based chemodosimeters **PMI** and **PDMI** (Fig. 32) were reported by Hua (2014)[178] and again these probes rely on nucleophilic attack of cyanide on a indolium cation. As **PDMI** has two indolium appendages an excess of $^{-}$CN was required before the fluorescence "switch on" (λ_{ex} = 425 nm, λ_{em} = 580 nm) occurred.

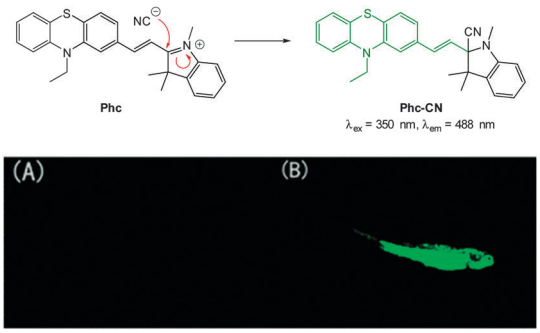

Fig. 31 Top: reaction of $^{-}$CN with indolium **Phc**. Bottom: images of adult zebrafish under 390 nm light: (A) fish incubated with **Phc**; (B) fish incubated with **Phc** and $^{-}$CN. Image reproduced with permission.[177]

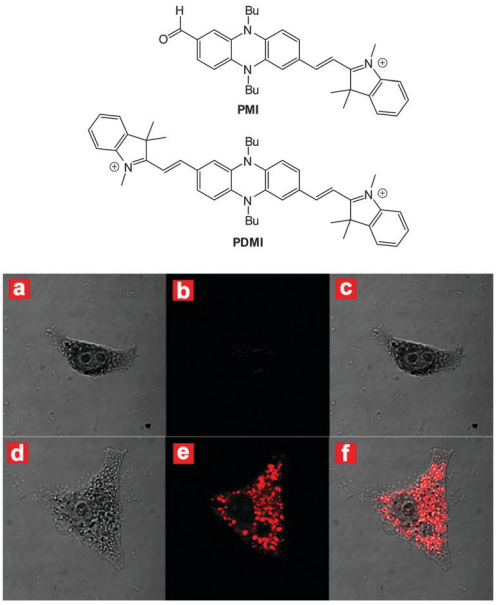

Fig. 32 Top: structures of **PMI** and **PDMI**. Bottom: images of HeLa cells incubated with **PMI**: bright-field (a), dark-field (b) and merged (c). Images of HeLa cells incubated with **PMI** then $^{-}$CN: bright-field (d), dark-field (e) and merged (f). Image reproduced with permission.[178]

In contrast, for **PMI** an instantaneous response was observed (λ_{ex} = 530 nm, λ_{em} = 620 nm). Of interest, given that aldehydes are also used as a reactive group for $^{-}$CN, ^{1}H NMR spectroscopy was used to monitor the intact C*H*O even as an excess of cyanide was added. The probe located in the cytoplasm In HeLa cells (confirmed using co staining) and a clear "switch on" response to cyanide was noted within 30 minutes of exposure.

2.4.2 Cyanide mediated displacement. Several papers from the group of Yoon describe probes for cyanide bioimaging based on Cu(II) displacement (shown schematically in Fig. 33—the probe is introduced to the cells in the Cu(II) complexed quenched state (heavy metal effect) and upon cyanide mediated displacement of the Cu(II) from the complex fluorescence is restored). The fluorescein tetracarboxylate "switch-on" probe **38-Cu(II)** was published in 2009[179] and was one of the first to prove that the copper displacement method could be used both *in vitro* and *in vivo*. When **38-Cu(II)** was trialled in solution studies, the addition of 100 equivalents of $^{-}$CN increased the quantum yield from 0.057 to 0.53 (λ_{ex} = 505 nm, λ_{em} = 522 nm). When *Caenorhabditis elegans* nematodes (a model host for studying microbial pathogenesis and innate immunity)[180] that were initially incubated with **38** and Cu(II) were subsequently incubated with $^{-}$CN a strong fluorescence "switch on" was observed. Of interest when these fluorescent nematodes were again incubated with Cu(II), fluorescence was quenched.

In additional work from the group of Yoon, the NIR emissive cyanine fluorophore (λ_{ex} = 680 nm, λ_{em} = 748 nm) functionalised with picolylamino groups **39** (Fig. 34) was synthesised in a short overall sequence from commercially available cyanine IR-780.[181] In the presence of Cu(II) no significant fluorescence was observed ($\phi_F < 0.01$) and initial solution based studies confirmed selective, "switch on" sensing (ϕ_F = 0.65, λ_{em} = 748 nm)

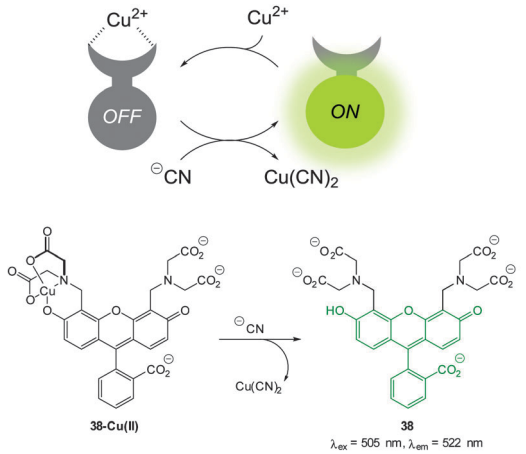

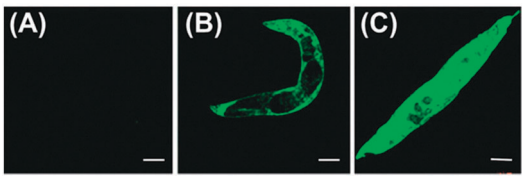

Fig. 33 Top: schematic representation of the Cu(II) displacement approach to sensing cyanide. Middle: structure and displacement reaction of **38-Cu(II)**. Bottom: fluorescence images of (A) young adult nematodes previously incubated with **38** then incubated with Cu(II), (B) nematodes previously incubated with **38** and Cu(II) then incubated with one equiv. of $^{-}$CN or (C) with ten equiv. of $^{-}$CN. Scale = 50 mm. Image reproduced with permission.[179]

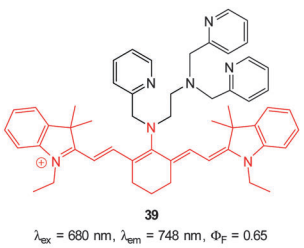

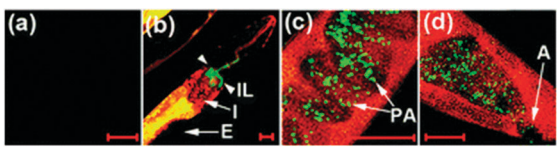

Fig. 34 Top: cyanine based ligand **39**. Bottom: imaging of cyanide in *C. elegans* infected with *P. aeruginosa* (GFP). Prior to incubation with **39-Cu(II)** *C. elegans* nematodes were fed for 2 d on non-infectious *E. coli* OP50 (a) or GFP-labelled PA14 (b–d). (b) the anterior end, (c) the medial part, (d) the posterior. (I = intestine; IL = intestinal lumen; I = intestine; E = eggs; PA = PA14-GFP; A = anus). Scale = 20 μm. Image reproduced with permission.[181]

of cyanide. Again using the *C. elegans* nematode as a model organism, aqueous NaCN was readily detected *in vivo*. Of significant interest when the nematodes were infected with *P. aeruginosa* (PA14) labeled with green fluorescent protein, the $^{-}$CN that the bacteria are known to produce was also detected *in vivo*. Such a result neatly conveys the significance of such small fluorescent probes for medically relevant assays.

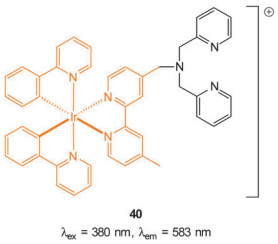

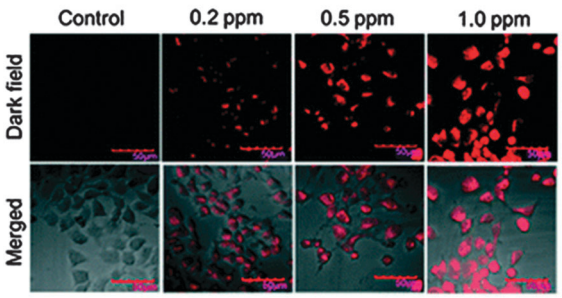

Fig. 35 Structure of DPA functionalised Ir complex **40**. Bottom: images of live HeLa cells in the presence of **40-Cu(II)** acquired after treatment with increasing concentrations of NaCN. Image reproduced with permission.[182]

The Cu(II) displacement approach has also been used by Ghosh and Das to develop a "switch on" probe for cyanide, however, in this instance the emitting species (λ_{ex} = 380 nm, λ_{em} = 583 nm) was a phosphorescent DPA-functionalised iridium complex **40** (Fig. 35).[182] Detection of cyanide was achieved inside live HeLa cells within 2 minutes using cells pre-incubated with **40-Cu(II)** then exposed to a 0.2 ppm aqueous solution of $^{-}$CN.

A Cu(II) displacement probe operating by both a colour change and also fluorescent enhancement was reported by Kim.[183] Coumarin imine **41** (Fig. 36) was synthesised in four steps from *m*-anisidine with the last step involving condensation with 2-aminophenol. A crystal structure of the stable non-fluorescent **41-Cu(II)** (ϕ_F = 0.02) confirmed that the metal was complexed by both oxygen atoms and the imine nitrogen atom as shown in Fig. 36. Similar to the previous examples the probe operates by means of Cu(II) displacement, however, unlike the Cu(II) complex, the free coumarin imine **41** is prone to hydrolysis (cyanide actually enhances the rate of hydrolysis) and ultimately it is the coumarin aldehyde **42** (λ_{ex} = 479 nm, λ_{em} = 514 nm, ϕ_F = 0.65) that functions as the reporting species. Again, excellent selectivity for cyanide amongst a selection of anions was reported ($^{-}$CN detected at 10^{-8} M). No adverse effects were noted when human hepatoma cell line HepG2 cells were treated with the complex and a strong intracellular fluorescence response was detected when cells were treated with solutions of KCN.

An interesting copper displacement probe for cyanide was devised by Zheng (2014).[184] The *non-fluorescent* Cu(II) schiff base complex of benzimidazole hydroxynaphthalene **43** (Fig. 37) was itself formed by displacing Zn(II) from the corresponding, *highly fluorescent* Zn complex (both the Cu and the Zn complexes were characterised by means of X-ray diffraction). Displacement of copper from the **43-Cu(II)** complex was effected by cyanide to give the fluorescent free **43** (λ_{ex} = 366 nm, λ_{em} = 425 nm).

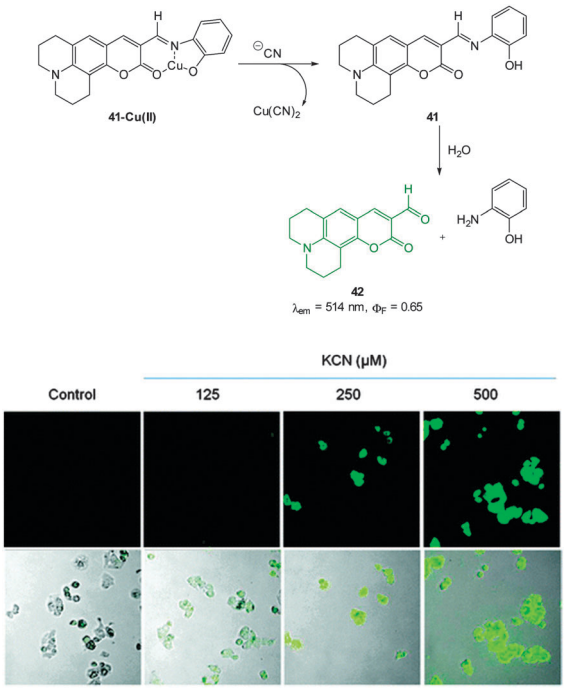

Fig. 36 Top: structure, CN mediated displacement, and hydrolysis of **41-Cu(II)**. Bottom: images of human HepG2 cells pre-treated with **41-Cu(II)** (1.0 μM) acquired 1 min after addition of KCN (125, 250, and 500 μM). Image reproduced with permission.[183]

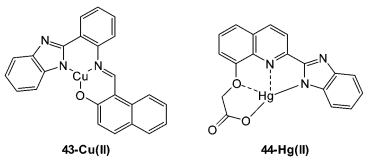

Fig. 37 Structure of the naphthalene–benzimidazole complex **43-Cu(II)** developed by Zheng[184] and the **44-Hg(II)** complex from Zhang and Liu.[185]

Displacement of Cu(II) was also effected by S^{2-} and it should be noted that this anion (known to have an affinity for Cu) is often omitted from the standard suite of anions used to evaluate the selectivity of many Cu based probes. In HeLa cells incubated with the Zn(II) complex addition of Cu(II) quenched the fluorescence, however, the corresponding addition of $^{-}$CN to restore fluorescence was not performed.

The Hg(II) complex of benzimidazole **44** (Fig. 37) was described by Zhang and Liu (2013)[185] for the intracellular sensing of $^{-}$CN. The complex is non-fluorescent (heavy metal effect) and in the presence of cyanide a strong fluorescence "switch on" (λ_{ex} = 345 nm, λ_{em} = 467 nm) was observed due to displacement of Hg(II). Unfortunately both sulphide and also iodide displaced the cation to give an equivalent response. While these competitors might ultimately limit *in vivo* applications (toxicity was also not evaluated), successful *in vitro* sensing of cyanide was demonstrated when HeLa cells that had been incubated with **44-Hg(II)** were treated with cyanide.

2.4.3 Miscellaneous. Very few *in vitro* or *in vivo* probes that function by means of H-bonding exist—a testament to the lack

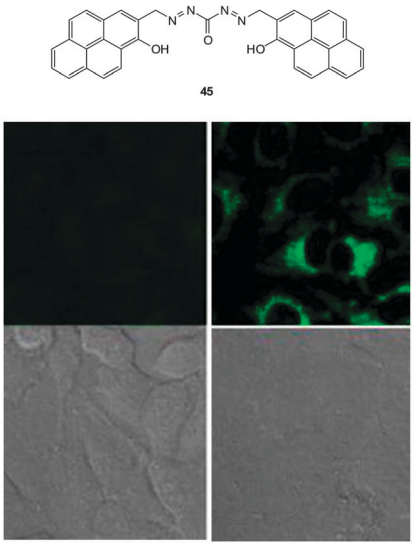

Fig. 38 Top: structure of $^{-}$CN probe **45**. Bottom: images of **45** in HeLa cells with (left) 30 μM **45** and (right) 30 μM **45** and 30 μM NaCN. Upper images: fluorescence. Lower images: bright-field. Image reproduced with permission.[186]

of truly selective anion sensors that function by H-bonding in highly competitive media. The bispyrenecarbohydrazide **45** (Fig. 38) reported by Yoon (2014)[186] bound cyanide such that excimer emission (λ_{ex} = 500 nm, λ_{em} = 550 nm) was "switched on". A proposed "clamshell" H:G complex of **45** with cyanide was proposed leading to close proximity of both pyrene moieties. In aprotic solvents fluoride also elicited a "turn on" response, however, when small amounts of protic solvents were present $^{-}$CN was targeted more selectively. Again HeLa cells were used for imaging and, in addition to rapid uptake, a distinct fluorescence "switch on" was observed when $^{-}$CN was added.

3. Anions of biological relevance

Many crucial intracellular processes involve anionic species[47] and the dysregulation of these species is known to accompany a number disease states. Indeed, the dysregulation of intracellular pyrophosphate (PPi) levels is associated with many conditions including cancer (see Section 3.1). Imaging agents for specific anionic targets *in vitro* and *in vivo* can be used to confirm the exact biological role of these anions and importantly they can also function as diagnostics for specific medical conditions. Anions covered in this section are: pyrophosphate, bicarbonate and hydrosulfide.

3.1 Pyrophosphate

Pyrophosphate (PPi) is produced or used in many cellular metabolic processes, such as ATP hydrolysis and DNA/RNA polymerisation reactions. Intracellular PPi concentrations can provide information on important cellular processes and have recently been suggested as a means of cancer diagnosis.[187] The concentration of PPi in other physiological fluids, such as

synovial fluid and urine, can also be used to identify diseases such as chondrocalcinosis or calcium pyrophosphate dihydrate (CPPD) crystal deposition disease.[188]

This knowledge has led to the recent development of numerous colourimetric and fluorescent sensors for PPi (see also the review by Yoon in this special issue).[14,36,189] However, significant challenges remain in the development of such probes, due to the difficulties associated with binding PPi in water and distinguishing it from related polyphosphates such as ATP. As many of the fluorescent sensors developed for PPi to date are "switch-off" or only exhibit weak fluorescence they are of only limited use in bioimaging applications. Nevertheless, there are several examples where such compounds have been successfully used to image the presence of cellular PPi and there are a handful of recent examples where "switch on" sensors have been developed and effectively used in imaging applications.

3.1.1 PPi binding to metal complexes. One of the earliest examples of the use of a PPi sensor in cellular imaging was reported by Kim.[190] The 1,8-naphthalimide–DPA–Zn(II) complex **46-2Zn(II)** (Fig. 39) was prepared in good overall yield over five steps and in CH_3CN:HEPES buffer, ligand **46** exhibited weak emission at 476 nm (λ_{ex} = 360 nm), characteristic of the 4-amino-1,8-naphthalimide fluorophore. Formation of the **46-2Zn(II)** complex resulted in a 59-fold fluorescence enhancement together with a 29 nm bathochromic shift to 505 nm, attributed to suppression of PET from the DPA amine. The addition of PPi to **46-2Zn(II)** resulted in a hypsochromic shift (23 nm) and *ca.* 50% quenching of fluorescence (10 equivalents of PPi). Calculations indicated that PPi bound to only one Zn(II)DPA centre and PET quenching was mediated by PPi. Imaging was performed using mouse myoblasts (C2C12) and cells were first incubated with 5 μM $Zn(OAc)_2$, then with 1 μM **46**. Subsequent addition of PPi lead to a dose-dependent decrease in cellular fluorescence (Fig. 39).

Hong and co-workers reported the three step synthesis of the NIR emissive benzothiazolium hemicyanine ligand **47** (Fig. 40), which readily forms a bis Zn(II) complex as a PPi binding site.[191] In aqueous buffer (pH 7.4) Probe **47-2Zn(II)** showed weak emission at 548 nm (λ_{ex} = 500 nm, Φ_F = 0.08) and addition of PPi (1.0 equivalent) "switched on" emission (Φ_F = 0.10) with a bathochromic shift to 558 nm. While ATP also gave a measurable response, **47-2Zn(II)** was used to image PPi uptake in a C2C12 myoblast cell line with a clear increase in intracellular fluorescence observed 30 minutes following addition of 2.5 equivalents of PPi. Importantly, the cells remained viable as determined using Hoechst nuclear stain and the probe had good cell permeability.

3.1.2 PPi mediated displacement. The **[DCCA]$_2$Cu** complex, comprising both a dicyanomethylene-4*H*-chromene fluorophore and a copper(II) complex of iminodiacetic acid group for PPi binding, has been reported as a NIR emissive "switch on" sensor for PPi.[192] In aqueous buffer **DCCA** (Fig. 41) is highly fluorescent (λ_{ex} = 500 nm; λ_{em} = 675 nm; Φ_F = 0.79), but upon addition of Cu(II) the fluorescence intensity decreased and complete quenching was observed with five equivalents of Cu(II). On addition of

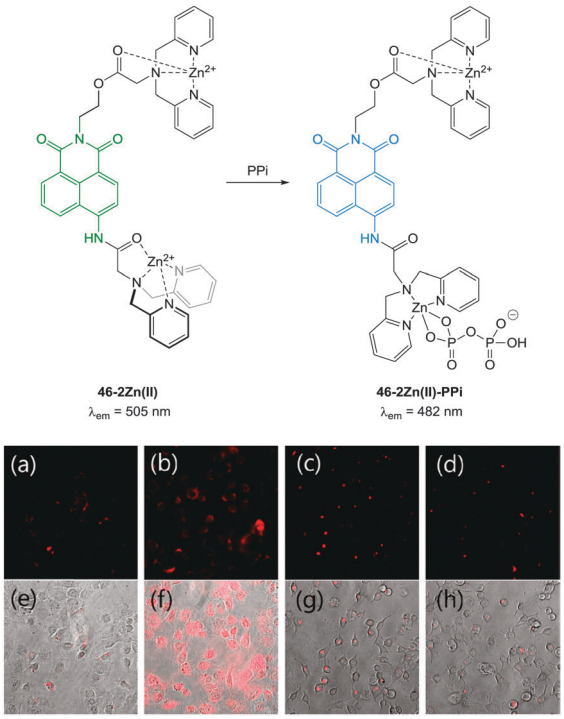

Fig. 39 (a) Fluorescence image of C2C12 cells treated with **46-2Zn(II)** (1.0 μM). (b) Fluorescence images of C2C12 cells treated with **46** (1.0 μM) and Zn(II) (5.0 μM). (c) Fluorescence images of C2C12 cells treated with **46** (1.0 μM), Zn(II) (5.0 μM) and PPi (0.5 mM). (d) Fluorescence images of C2C12 cells treated with **46** (1.0 μM), Zn(II) (5.0 μM) and PPi (1.0 mM). (e–h) Bright field images of (a–c) respectively. Image reproduced with permission.[190]

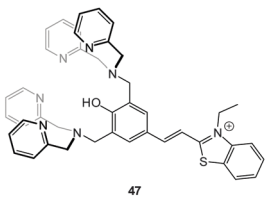

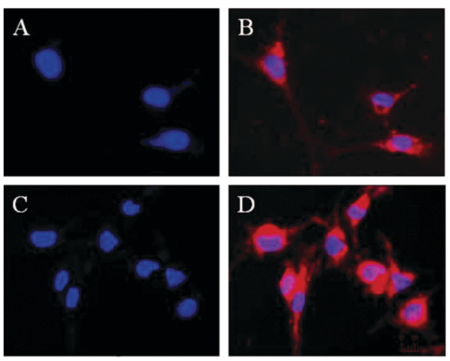

Fig. 40 Fluorescence live-cell pseudo-color images of C2C12 myoblast cells. (A and C) Cells stained by Hoechst nuclear dye. (B) Cells incubated with Hoechst nuclear dye and then with **47-2Zn(II)**. (D) Cells incubated with Hoechst nuclear dye followed by **47-2Zn(II)**, then $Na_4P_2O_7$. Emission collected at (A, C) blue channel and (B, D) Cy3 channel upon excitation at (A, C) 350 ± 25 nm and (B, D) 543 ± 11 nm. Image reproduced with permission.[191]

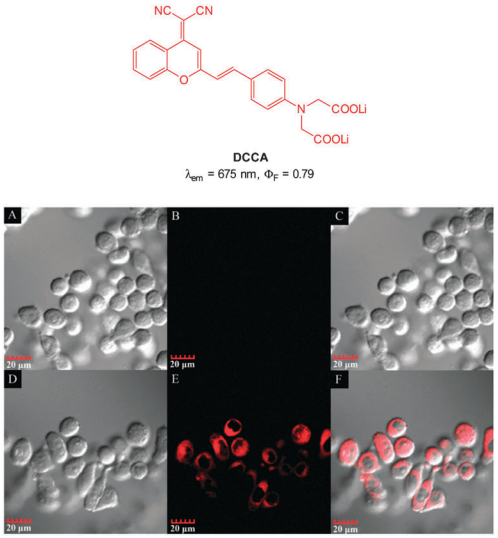

Fig. 41 Top: structure of copper ligand **DCCA**. Bottom: confocal fluorescence images in KB cells: (A–C) cells incubated with **$DCCA_2$–Cu(II)** alone. (D–F) Cells incubated with **$DCCA_2$–Cu(II)**, then $K_4P_2O_7$. Emission collected at 630–730 nm, excitation at 405 nm. Bright field (A and D), fluorescence (B and E) and overlap field (C and F). Image reproduced with permission.[192]

PPi to a 1 : 5 mixture of **DCCA** and $Cu(ClO_4)_2$ fluorescence "switch on" was observed, and peaked after 15 equivalents PPi (Φ_F = 0.48). The enhancement was attributed to the displacement of one of the ligands from the Cu(II) complex. This probe was evaluated in KB cells and almost no intracellular fluorescence was observed for the **$[DCCA]_2Cu$** complex alone. After incubation with PPi, a significant increase in cellular fluorescence was observed within 30 minutes with signals localized in the perinuclear area of the cytosol, indicating a subcellular localisation of PPi and good cell membrane permeability of the **$[DCCA]_2Cu$** complex.

The imino-thiophenyl calix[4]arene derivative **48** (Fig. 42) has been used to image both Zn(II) and PPi in HeLa cells.[193] Ligand **48** was prepared in three steps from *p-tert*-butylcalix[4]arene and upon addition of Zn(II) in a fluorescence turn-on response (λ_{ex} = 390 nm, λ_{em} ~ 450 nm) was observed. Subsequent addition of PPi resulted in complete quenching of the emission, attributed to the displacement of Zn(II) from the **48-Zn(II)** complex as a result of the higher binding affinity of PPi for Zn(II). In HeLa cells incubated with 10 μM **48**, very low fluorescence intensity was observed. After subsequent incubation with $ZnSO_4$/pyrithione for 20 minutes, the cells exhibited highly intense blue fluorescence (4 times higher than with **48** alone). Further treatment with PPi resulted in a decrease in fluorescence intensity (1.5 times higher than **48** alone).

The bis Zn(II) complex of the pyridine-naphthalene based **SPHN** (Fig. 43) has been reported as a PPi selective fluorescent chemosensor.[194] Compound **SPHN** was readily prepared by condensation of the bis-glycine adduct of 2,6-diaminopyridine and 2-hydroxy-1-naphthaldehyde. In 7 : 3 CH_3CN : aqueous HEPES buffer the addition of $ZnCl_2$ to **SPHN** resulted in a "switch-on" of fluorescence (λ_{ex} = 400 nm; λ_{em} = 450 nm, Φ_F = 0.940) which was suggested to be a result of the formation of a 1 : 2 L : Zn(II) complex. The addition of PPi to **SPHN-2Zn(II)** led to

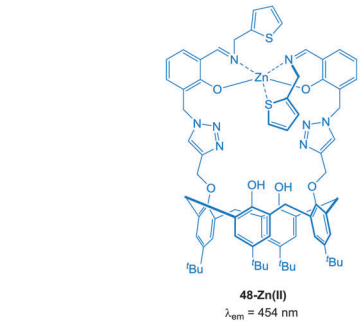

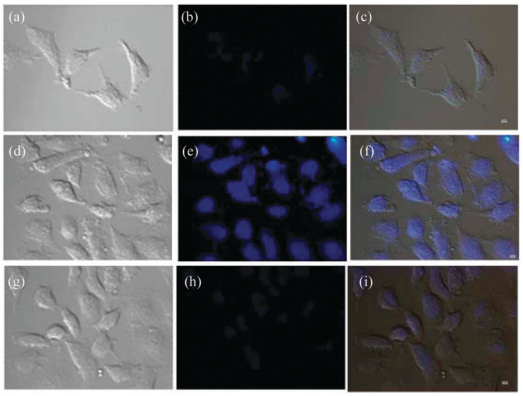

Fig. 42 Fluorescence images in HeLa cells (λ_{ex} ~ 358 nm and λ_{em} ~ 461 nm); (a) DIC image of cells treated with **48** (10 μM); (b) fluorescence image of (a); (c) merged image of (a) and (b). (d) DIC image of cells treated with **48** then Zn(II)/pyrithione (1 : 1) solution; (e) fluorescence image of (d); (f) merged image of (d) and (e). (g) DIC image of cells treated with [**48** + Zn(II)] followed by PPi; (h) fluorescence image of (g); (i) merged image of (g) and (h). Scale = 10 μm. Image reproduced with permission.[193]

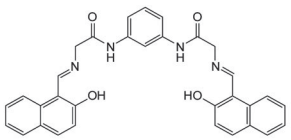

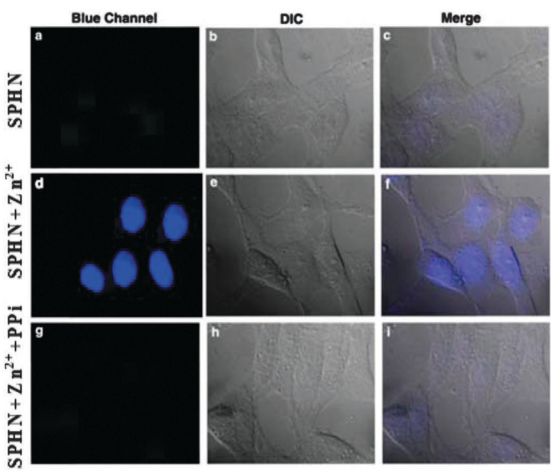

Fig. 43 HeLa cells showed intense blue fluorescence in the presence of both **SPHN** and Zn^{2+} (d) and did not show any fluorescence in the absence of Zn^{2+} (a) and in the presence of PPi (g). Corresponding differential interference contrast (DIC) images (e, b and h) and merge images (f, c and i) of the cells are shown. Image reproduced with permission.[194]

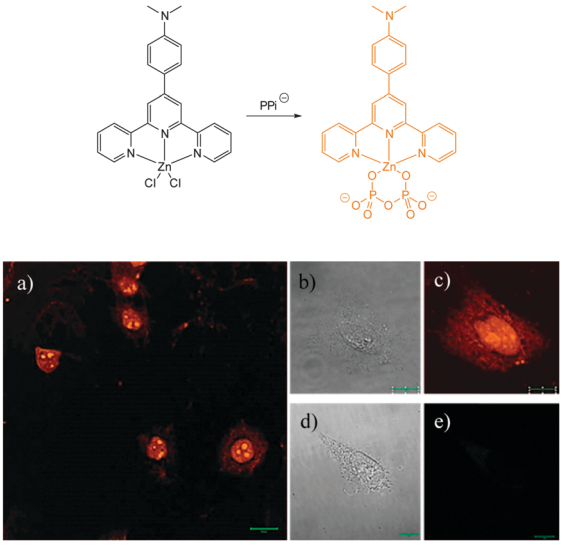

Fig. 44 Confocal fluorescence microscopy images of (a) HeLa cells incubated with probe **49-ZnCl$_2$** (50 μM), (c) single HeLa cell, and (e) single HeLa cell without staining (control). Differential interference contrast images of (b) single HeLa cell incubated with probe **49-ZnCl$_2$** (50 μM) and (d) single HeLa cell without staining (control). Image reproduced with permission.[195]

quenching of this fluorescence as a result of displacement of Zn(II) from **SPHN** and importantly, a selective response for PPi was observed in the presence of ATP. In HeLa cells preincubated with exogenous Zn(II) the addition of **SPHN** elicited a fluorescence response, however, when PPi was added at the same time as **SPHN**, significantly lower levels of fluorescence were observed.

More recently, Rissanen and co-workers have reported a terpyridine–Zn(II) complex **49-ZnCl$_2$** (Fig. 44) capable of the detection of nanomolar PPi concentrations in water, together with the first example of a small molecule probe to image native PPi concentrations in cells (*i.e.* without the addition of exogenous PPi).[195] The complex was prepared by mixing 4′-(4-*N*,*N*′-dimethylaminophenyl)-2,2′:6′,2″-terpyridine in a 1 : 1 ratio with $ZnCl_2$ and an X-ray crystallographic structure, confirmed the formation of a 1 : 1 complex. While **49-ZnCl$_2$** is fluorescent in the solid state, in water the fluorescence is quenched. The addition of PPi to a solution of **49-ZnCl$_2$** in 0.01 M HEPES buffer resulted in an approximately 500 fold increase in fluorescence (λ_{ex} = 440 nm; λ_{em} = 591 nm), attributed to the formation of a 1 : 3 complex between PPi and **49**. Cellular imaging was performed in HeLa cells. Cells were treated with 10 μM **49-ZnCl$_2$** for 30 min and bright orange-yellow emission was observed that allowed mapping of PPi concentration in different parts of the cells with the maximum emission observed in the nuclei as well as the cytoplasmic membranes.

3.2 Bicarbonate

The bicarbonate anion is the primary species responsible for maintaining cellular acid–base homeostasis. The enzyme carbonic anhydrase (CA) produces HCO_3^- inside cells from dissolved CO_2 and dysregulation of CA is associated with a number of tumour types.[196] The bicarbonate anion also plays a role in physiological processes such as cyclic AMP regulation, osteoporosis and kidney disease.[197] Unfortunately only indirect methods have been available for measuring bicarbonate in cells including total $H^{14}CO_3^-$ concentration or estimates based on pH; each of these are prone to significant error and do not provide spatiotemporal information. As such a more direct means for the bioimaging of this anion using fluorescent probes would be a welcome advance.

3.2.1 Recent developments. Very few small molecule probes exist for the cellular imaging of bicarbonate and these can be divided into two classes: dipyridylalkylbenzenes and luminescent lanthanide complexes.

The dialkynylbenzene probe **50** for the imaging of bicarbonate *in vitro* was reported by Murphy, Wong and Lee in 2011 (Fig. 45).[198] A NIR multiphoton approach was used for excitation and probe emission also tailed into the NIR region. Solution studies identified strong binding of bicarbonate ($\log K$ = 7.13) and a four-fold enhancement in fluorescence intensity (λ_{em} = 450 nm) was observed as well as a redshift of 30 nm. Binding was tentatively assigned to the δ^+ of the amide N leading to enhanced electron transfer (1 : 2 H : G binding stoichiometry supported this theory). In solution, binding of citrate was also observed ($\log K$ = 7.83), nevertheless, *in vitro* imaging of HCO_3^- was performed in both HeLa and A549 cells (λ_{ex} = 900 nm and λ_{em} = 400–650 nm) and after 3 h the probes had localised in the cytoplasm and the emission profiled matched the 30 nm red shift observed in solution indicating binding of the target anion.

With the aim of sensing bicarbonate and other oxyanions (such as malate and citrate) "*in cellulo*" a large body of research

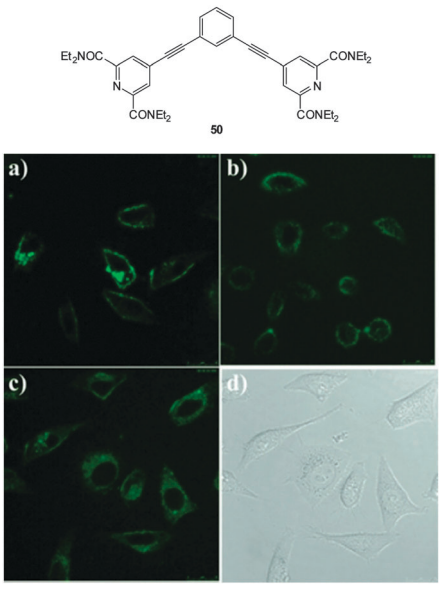

Fig. 45 Top: structure of dialkynylbenzene probe **50**. Bottom: *in vitro* cytoplasmic staining microscopy with **50** (λ_{ex} = 900 nm, λ_{em} = 450–750 nm) in A549 cells after (a) 1 h, (b) 6 h, and (c) 12 h. (d) Bright-field image of panel (c). Image reproduced with permission.[198]

effort has been undertaken by the group of Parker using luminescent lanthanide probes.[83,199] The cellular uptake, localisation, stability and toxicity of these probes have all been studied in detail.[45,81,200–202] These sensors have sharp emission bands (ΔJ = 1, 2, 3 and 4) and as they rely on energy transfer from a chromophore/sensitiser (normally incorporated as part of the ligand) to the metal the emission can be modulated by the target anion disturbing either the metal excited state or the ligand singlet or triplet states (for excellent overviews of the photophysical properties of lanthanides and how they can be manipulated for sensing and imaging see the excellent recent reviews by Meade,[82] Parker,[83] and Pierre[203]). Lanthanide complexes are capable of *selectively* binding anions if both the ligand and metal are judiciously selected. Typically, but not always, the mode of action involves displacement of a bound water (q) by the target anion leading to a modulated emission profile in which the ΔJ = 2 band (*e.g.* Eu at *ca.* 620 nm) is considerably altered whereas other bands such as ΔJ = 1 (*e.g.* Eu at *ca.* 590 nm) are not. Changes in these two distinct outputs allows the probe to function in a very useful ratiometric fashion.[82,83,203] Combinations of individual Tb and Eu complexes (one complex is responsive, the other is not) can also function in a ratiometric manner.[204]

The detection of bicarbonate by the lanthanide complexes **51-Eu(III)** and **52-Eu(III)** containing the 1-azaxanthone-4-carboxyl sensitiser was reported by Parker in 2011 and in a follow up study in 2012 (Fig. 46).[205,206] The probes were non-toxic and indicated the presence of bicarbonate (HCO_3^- formed by exposing the cells to a CO_2 atmosphere) in the mitochondria of a number of cell lines including A549, MCF-7 and HeLa cells. While solution based binding studies indicated little selectivity of the probes over the common carboxylate interferents citrate and lactate, in cells the concentration of bicarbonate is typically 10 fold greater than lactate and 100 times greater than citrate. Of additional interest the same ligands with terbium were unresponsive and could serve as in internal control for ratiometric imaging. Direct detection in A549 cells and selectivity for bicarbonate was confirmed as when the known carbonic anhydrase inhibitor acetazolamide was introduced to the cells little fluorescence was observed. Binding of the bicarbonate anion modulates either triplet sensitiser to metal energy transfer or the lanthanide excited state directly and ultimately leads to significant enhancement of the ΔJ = 2 band at ~620 nm (λ_{ex} = 340 nm).

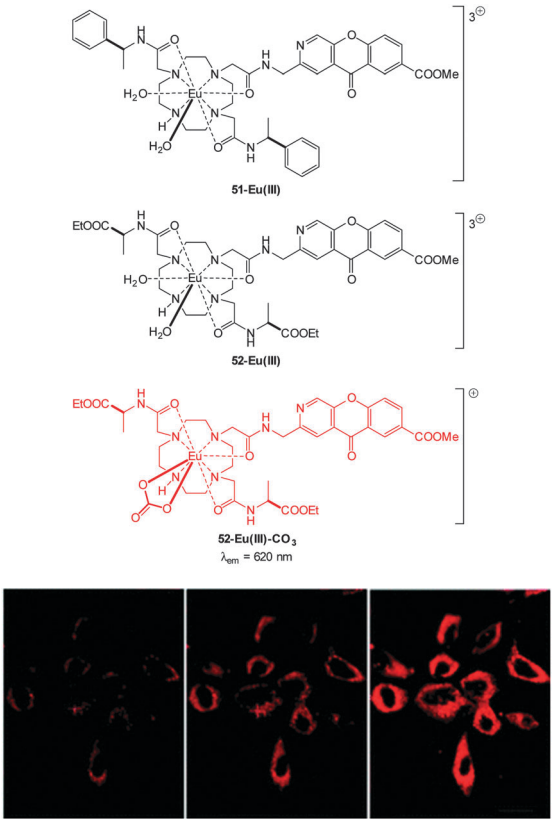

Fig. 46 Top: structure of HCO_3^- sensitive probes **51-Eu(III)**, **52-Eu(III)** and the bound **51-Eu(III)-CO3**. Bottom: images of HeLa cells incubated with **52-Eu(III)**, localised in the mitochondrial region under 3, 4 and 5% CO_2 atmosphere. Image reproduced with permission.[211]

3.3 Hydrosulphide

Hydrogen sulphide (H_2S), along with NO and CO, is considered to be the third gaseous signalling agent, or gasotransmitter.[207] Endogenous hydrogen sulphide is produced from homocysteine (Hcy) by the cytosolic enzymes; cystathionine-β-synthase (CBS) and cystathionine-γ-lyase (CGL).[208] In addition hydrogen sulphide is also produced from cysteine (Cys) by 3-mercaptopyrate sulfurtransferase (3MST) mediated metabolism; 3MST is present in both the cytosol and mitochondria.[208] Considering the first and second pK_a values for H_2S are 7.05 and 15 respectively (at 25 °C and pH 7.4 the ratio of $H_2S/HS^-/S^{2-}$ can be calculated as 30 : 70 : 0.00002 respectively).[207] As such, for the purpose of this review we can assume that appreciable quantities of HS^- are present. Nevertheless the challenge of targeting HS^- is complicated as pH varies between subcellular compartments and as such the H_2S/HS^- ratio will also vary accordingly.

Hydrogen sulphide has been linked to a number of physiological processes such as inflammation, angiogenesis, respiration, ischaemic reperfusion injury as well as oxidative stress.[208,209] As such the development of HS^- releasing drugs is an active area of research.[210]

Due to the rapid catabolism of HS^- by sulphide quinone oxidoreductase (SQR), persulfide dioxygenase (SDO), thiosulfate reductase (TR) and sulphite oxidase (SO),[208,211,212] any probe must react quickly and emit brightly (high quantum yield (ϕ_F) and molar absorptivity (ε)). This formidable challenge is made more difficult by the fact that the typical concentration of HS^- in blood are in the order of 10^{-6} M to 10^{-9} M and 30–300 μM in tissues have been reported.[207,212] There is still debate over the physiologically active form of hydrogen sulphide,[212] therefore a selective means to detect low concentrations of the anionic form could unlock some of the secrets of its remarkable biology.

The development of fluorescent indicators to sense HS^- in living systems is a rapidly developing field.[52,213–216] Given the large number of examples this review will highlight bioimaging agents that either (i) present significant advances in sensitivity, (ii) target particular cellular locations, (iii) emit in the NIR range

and (iv) have been demonstrated to be applicable to *in vivo* studies.

For probes that target hydrosulphide, three strategies are commonly employed to modulate fluorescence. The first two are chemodosimeter approaches that rely on HS^- as a *nucleophile* or HS^- mediated *reduction*. The third strategy is sulphide mediated metal *displacement*. *Nucleophilic* reactions (typically S_NAr or nucleophilic addition) are used to restore ICT or remove a group involved in a PET process, displace a trigger or interrupt a conjugated system. Anionic HS^- is a superior nucleophile compared to thiols ($pK_a > 8.5$) at physiological pH. When two proximal electrophiles are present interference from endogenous sulphur species such as cysteine (Cys), homocysteine (Hcy) and glutathione (GSH) is further circumvented. *Reduction* of an azide is an often utilised approach as the azide can be introduced directly to a fluorophore bearing an arylamine as a component of an ICT system, or as a sulfonylazide. Reduction of nitro groups, hydroxyl amines, and N-oxides are related examples of this strategy, however the reduction of the nitro-group invariably suffers from poor reaction kinetics. The *displacement* of a metal, typically Cu(II) or Zn(II), from a chelating ligand has also been widely used for bioimaging HS^-. There are obvious parallels between this approach and the probe design for ^-CN selective probes (see Section 2.4).

3.3.1 Hydrosulfide as a nucleophile. Lin *et al.* made use of both the donor photoelectron transfer (d-PET) properties and HS^- reactivity of the 2,5-dinitrophenylether in their hybrid cyanine–BODIPY probe, **NIR-H_2S** (Fig. 47).[217] **NIR-H_2S** is essentially non-fluorescent due to the d-PET process, however, upon treatment with HS^- the fluorescent phenol **53** (λ_{ex} = 650 nm, λ_{em} = 708 nm,) is revealed. **NIR-H_2S** has a detection limit of 50 nM although this value was determined at pH 7.0. Using probe **NIR-H_2S** visualisation of varying concentrations of exogenous HS^- in MCF-7 cells was achieved. Notably higher fluorescent intensity at the mitochondria was observed which was confirmed by colocalisation studies using Hoechst 33342.

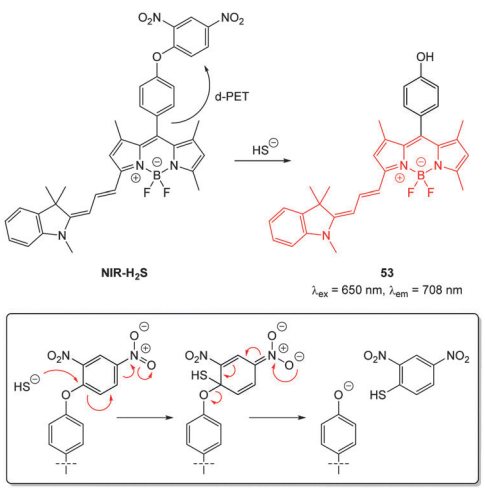

Fig. 47 Structure and reaction of cyanine–BODIPY hybrid probe **NIR-H_2S** with HS^-; INSET shows fragmentation mechanism.

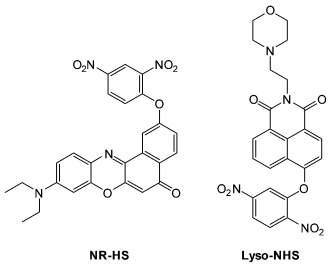

Fig. 48 Structures of **NR-HS** and **Lyso-NHS**.

Zheng and Cui (2014) functionalised nile red with this trigger to give a NIR-emissive (λ_{ex} = 488 nm, λ_{em} = 655 nm) HS^- responsive probe **NR-HS** (Fig. 48).[218] Upon reaction with HS^- the quantum yield of **NR-HS** (Φ_F = 0.05 in simulated physiological conditions) increased to 0.32 as nile red was regenerated. Maximum fluorescence was obtained after 20 minutes with a limit of detection of 270 nM. Fluorescence microscopy experiments were carried out using MCF-7 cells and **NR-HS** responded to exogenous HS^-.

The 2,5-dinitrophenylether trigger was incorporated onto a 4-hydroxynaphthalimide fluorophore by Liu *et al.* to give **Lyso-NHS** (Fig. 48). The probe also contained a basic morpholine substituent (**Lyso-NHS** pK_a = 3.12) which was responsible for compartmentalisation of the sensor into the lysosome (Fig. 49).[100] The reaction of HS^- with **Lyso-NHS** led to a significant increase in fluorescent intensity (λ_{ex} = 450 nm, λ_{em} = 555 nm) with a maximal response after 20 minutes. The probe had a nanomolar (480 nM) detection limit and was used to visualise exogenous HS^- in MCF-7 cell lysosomes (confirmed by co-staining with neutral red (NR) a known lysosomal stain) and was not toxic (MTT assay) at the concentrations used.

Also using the 2,5-dinitrophenylether trigger, the group of Govindaraju synthesised the HS^- probe **DNOPCy** (Fig. 50).[219] Dislodging the 2,5-dinitrophenyl group of **DNOPCy** (λ_{em} = 555 nm) gave **Cy-quinone** which has a red-shifted emission maximum

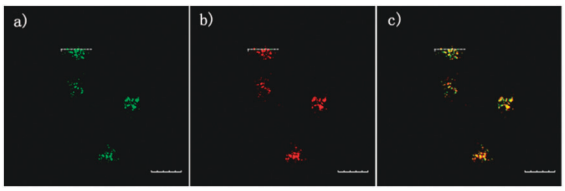

Fig. 49 Colocalisation images of **Lyso-NHS** in MCF-7 cells. (a) **Lyso-NHS** with HS^- (green channel. (b) Neutral red (red channel). (c) Merged images of (a) and (b). Image reproduced with permission.[100]

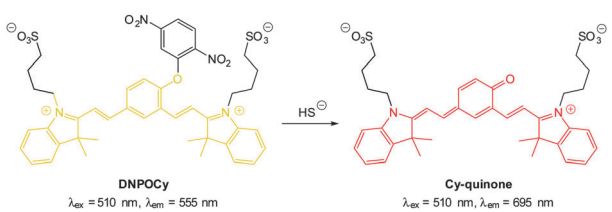

Fig. 50 NIR emissive HS^- probe **DNOPCy**.

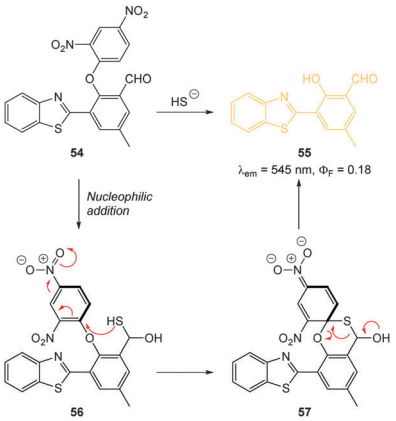

Fig. 51 Structure and reaction mechanism of benzothiazole probe **54** with HS^-.

at λ = 695 nm. This change in fluorescence emission was ideal for ratiometric detection and visualisation of exogenous NaSH in human embryonic kidney cells (HEK293T) was successfully accomplished.

Through the judicious placement of a proximal aldehyde, Feng (2014) developed the dinitrophenyl ether probe **54** (Fig. 51) that reacted fully within two minutes of exposure to HS^- to give maximum fluorescence.[220] The reaction generates the modified HMBT ESIPT fluorophore **55** (λ_{ex} = 450 nm, λ_{em} = 555 nm, Φ_F = 0.18) and HS^- at concentrations as low as 48 nM were detected in simulated physiological conditions. This probe was successfully used for the visualisation of exogenous HS^- in HeLa cells.

In 2012 Qian and co-workers reported a rapidly reacting **HBMT** based HS^- activated fluorescent probe (Scheme 1).[221] Probe **E1** can undergo thiol exchange with both HS^- and thiols, however only the persulfide generated from HS^- can cyclise to release the fluorescent **HBMT** (λ_{ex} = 295 nm, λ_{em} = 487 nm). Probe **E1** was weakly fluorescent due to PET from the pendant dithiol and reacted rapidly (2 min) with HS^- with an detection limit of *ca.* 120 nM. Once again this probe readily detected exogenous HS^- in HeLa cell.

In 2013 the Tang group reported the HS^- responsive ratiometric probe **HS-Cy** (Fig. 52) which incorporates a proximal electrophile.[222] Nucleophilic addition of HS^- at the aldehyde of **HS-Cy** leads to a rapid (within 3 min) loss of fluorescence

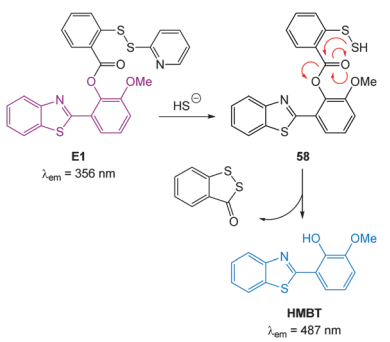

Scheme 1 Structure and reaction mechanism of **E1** with HS^-.

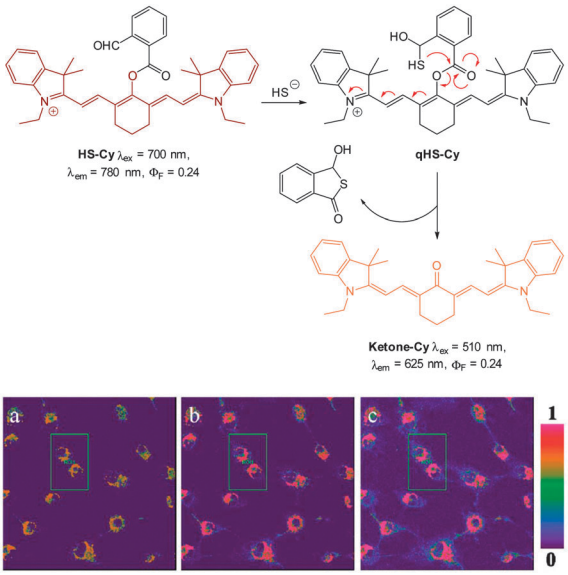

Fig. 52 Top: structure and reaction of **HS-Cy** with HS^-. Bottom: confocal fluorescence ratiometric images of endogenous HS^- in living A549 cells. A549 cells loaded with 5 mM **HS-Cy** for 30 min (a). Cells were pre-stimulated with SNP, then incubated with **HS-Cy** for 10 min (b) and 20 min (c). Scale = 50 mm. Image reproduced with permission.[222]

emission (λ_{em} = 780 nm, Φ_F = 0.24). This decrease in fluorescence was speculated to be caused by a PET process from the free hydroxyl or sulfhydryl groups of the intermediate **qHS-Cy**. The intramolecular cyclisation between the free sulfhydryl and the ester the releases the ketone cyanine (**ketone-Cy**) resulting in a 155 nm blue-shifted emission (λ_{em} = 625 nm). The cyclisation step is a much slower process, with the emission at 625 nm increasing slowly over 35 min. In the mitochondria of HepG2 cells (pH 8.0) the nucleophilic addition and substitution occurred within 30 s and 5 min respectively. The fluorescence intensity ratio F_{625}/F_{780} rises from 0.01 to 24.8 following the addition HS^-. Probe **HS-Cy** was used to image exogenous HS^- in HepG2 cells and could detect endogenous HS^- in A549 cells stimulated with sodium nitroprusside (SNP). A decrease in the F_{625}/F_{780} ratio was observed when an inhibitor (DL-propargylglycine, PPG) of the HS^- producing enzymes (CBS and CES) was added to the cells, confirming HS^- as the analyte responsible for the response.

Guo and co-workers reported a fast reacting flavylium derived ratiometric HS^- probe **59** (Fig. 53).[223] Nucleophilic attack of HS^- on this NIR emissive probe (λ_{ex} = 450 nm, λ_{ex} = 690 nm) disrupts conjugation and the fluorescent product is essentially a substituted aminocoumarin (λ_{ex} = 485 nm). In pure PBS buffer, the reaction was complete in 20 s, making probe **59** one of the fastest probes yet reported. Upon treatment with HS^- a 694-fold increase in the ratio F_{485}/F_{690} (0.07–83.90) was noted allowing a detection limit of 140 nM. While this probe did react with mercaptoethanol, selectivity for HS^- over cysteine and GSH was apparent. It was suggested that electrostatic repulsion between the benzopyrylium ion and the protonated amines of Cys and GSH prevents addition. Probe **59** was found to be non-toxic (MTT assay) and was subsequently used for the ratiometric imaging of exogenous HS^- in HeLa cells.

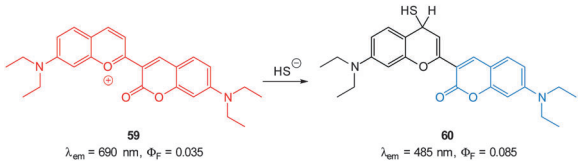

Fig. 53 Structure and reaction of **59** with HS^-.

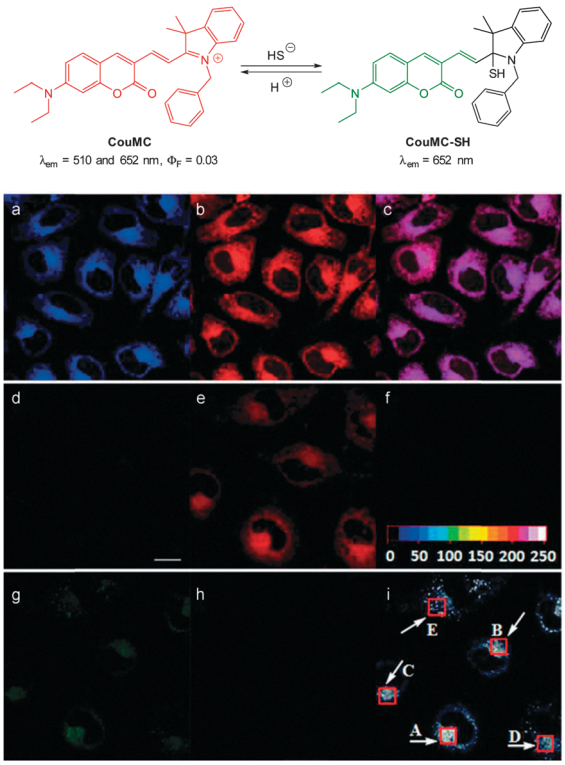

Fig. 54 Top: structure and reversible reaction of **CouMC** with HS^-. Bottom: (a–c) fluorescence images of MCF-7 cells co-stained by **CouMC** and Mito marker Deep Red 633. (a) Pseudocoloured image obtained with band path of 660–750 nm (λ_{ex} = 488 nm); (b) image from band path of 665–750 nm upon excitation of Deep Red (λ_{ex} = 633 nm); (c) overlay of (a) and (b). (d–i) Fluorescence imaging of MCF-7 cells (λ_{ex} = 488 nm). (d–f) Images of cells stained by **CouMC**; (g–i) images of cells preincubated with **CouMC** followed by NaSH. (d, g) Green-channel images collected with band path of 500–560 nm; (e, h) red-channel images collected with band path of 640–700 nm; (f, i) ratiometric image scale bar in (d): 20 mm. Image reproduced with permission.[224]

The mitochondria selective HS^- probe **CouMC** (Fig. 54) was reported by the groups of He and Guo in 2013.[224] The coumarin-hemicyanine probe **CouMC** has two fluorescent emissions (λ_{em} = 510 and 652 nm) with the red emission, which corresponds to the full conjugated system, being the more intense. Nucleophilic attack of HS^- at the indolium C=N interrupts the conjugated system of **CouMC** and the resultant truncated π-system of **CouMC-SH** exhibits coumarin-like fluorescence (λ_{em} = 510 nm). Maximum fluorescence emission was achieved in 30 s in simulated physiological conditions. The red fluorescence could be reinstated when the media containing **CouMC-SH** was acidified to pH 2.5; **CouMC** itself, was stable over the pH range of 2.5 to 8.0. *In vitro* ratiometric

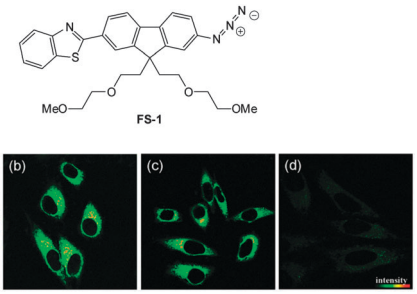

Fig. 55 Top: structure of hydrosulphide probe **FS-1**. Bottom: (a) two-photon microscopy images of HeLa cells labelled with **FS-1**. (b–d) Cells pre-treated with cysteine (b), GSH (c), or PMA (d) before labelling with **FS-1**. The TPEF was collected at 400–680 nm upon excitation at 750 nm. Scale = 30 mm. Image reproduced with permission.[225]

imagining studies with **CouMC** in MCF-7 cells revealed high localisation in the mitochondria (colocalisation with Deep Red 633). The intracellular reaction of the probe with HS^- occurred rapidly (<80 s) and as such this probe may find utility in the spatiotemporal tracking of this anion.

3.3.2 Hydrosulfide mediated reduction. In 2012 Cho reported **FS-1** (Fig. 55), the earliest example of a two-photon probe for HS^-.[225] The sensor employed the azide "trigger", which was pioneered by the Chang group for bioimaging.[226] When treated with HS^-, a 21-fold increase in fluorescent enhancement (λ_{em} = 548 nm, Φ_F = 0.46) was observed.[225] The probe also displayed an increase in two-photon cross section under the same conditions (HEPES buffer, $\Phi\delta$ = 15–302 GM). Endogenous HS^- was visualised in live HeLa cells using **FS-1**, pre-treatment with cysteine and GSH both led to enhanced two-photon excited fluorescence (TPEF) (λ_{ex} = 750 nm, λ_{em} = 520 nm). Phorbol 12-myristate 13-acetate (PMA) induced oxidative stress led to a decrease in observed emission intensity.

In 2012 Han and co-workers reported the NIR-emitting ratiometric cyanine-azide probe **Cy-N_3** (Fig. 56).[227] Upon treatment with NaSH the azide probe (λ_{ex} = 625 nm, λ_{em} = 710 nm Φ_F = 0.11) is reduced to give **Cy-NH_2** (λ_{em} = 750 nm, Φ_F = 0.12) with a concomitant increase in molar absorptivity (ε_{660} = 130 000 M^{-1} cm^{-1}). The maximum fluorescence response was achieved in 20 min which was superior to related examples at that time. The ratio of emission intensities (F_{750}/F_{710}) increased from 0.6–2.0 with the addition of 10 equivalents of NaSH, and a detection limit of 80 nM was established. The probe was successfully used to detect endogenous HS^- in live RAW264.7 macrophages (stimulated using PMA). The fluorescence emission intensity also increased in cells treated with NaSH and **Cy-N_3** was also used to study the time dependent decomposition of the HS^- releasing agent 5-(4-hydroxyphenyl)-3*H*-1,2-dithiole-3-thione (ADT-OH) in fetal bovine serum.

In 2013 the groups of Xu and Peng independently reported the red emitting dicyanomethylenebenzopyran probe **DCMC-N_3** (Fig. 57).[228,229] Probe **DCMC-N_3** is essentially non-fluorescent, however, upon reaction with HS^- fluorescence was "switched on" (λ_{em} = 670 nm in 1 : 1 PBS buffer : DMSO or λ_{em} = 655 nm in 1 : 1 phosphate buffer : MeCN). The Xu group showed that

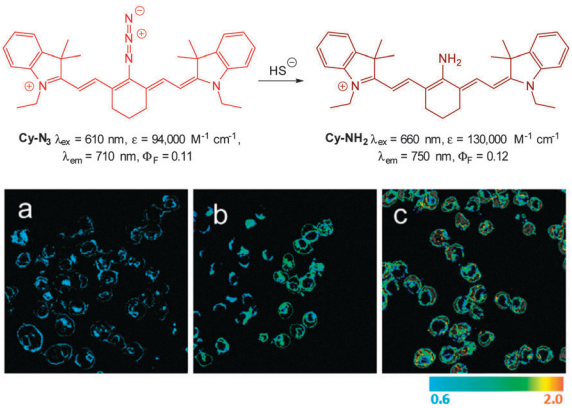

Fig. 56 Top: structure and reaction of **Cy-N$_3$** with HS$^-$. Bottom: ratiometric fluorescence images (F_{750}/F_{710}) of living RAW264.7 macrophage cells with **Cy-N$_3$**. Images displayed in pseudo colour represent the ratio of emission intensities. (a) Cells were pretreated with PMA before loading **Cy-N$_3$**. (b) Cells incubated with **Cy-N$_3$**. (c) RAW264.7 cells incubated with NaSH and **Cy-N$_3$** was added. Image reproduced with permission.[227]

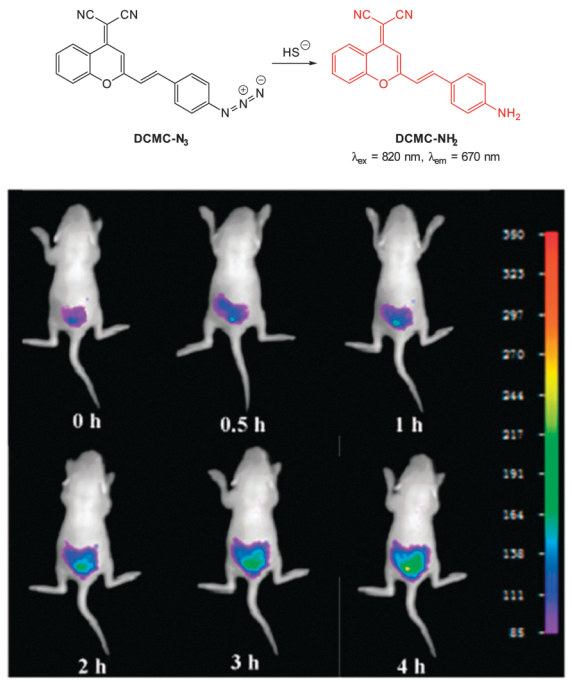

Fig. 57 Top: structure and reaction of probe **DCMC-N$_3$** with sulphide. Bottom: representative fluorescence images of mice (pseudo-colour) given a skin popping injection of probe **DCMC-N$_3$** and then injected with NaSH. Images were taken after incubation of NaSH for different times (0, 0.5, 1, 2, 3 and 4 h). Image reproduced with permission.[229]

DBMC-N$_3$ could be used to indicate the presence of exogenously administered HS$^-$ in human umbilical vein endothelial cells (HUVEC). Similarly, preliminary experiments by the Peng group used **DBMC-N$_3$** to image exogenous HS$^-$ in HeLa cells. The Peng group also utilised the favourable properties of **DCMC-N$_3$** (NIR, large Stokes shift and good $\Phi\delta_{max}$ = 50 GM at 820 nm in DMSO) to visualise the presence of HS$^-$ in MCF-7 cells using two photon microscopy. Furthermore, a skin-pop injection of probe **DCMC-N$_3$** and NaSH (25 equiv.) into ICR

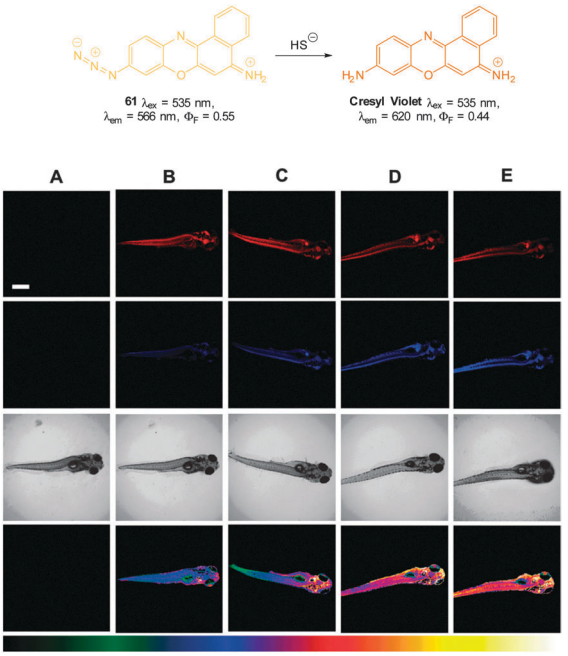

Fig. 58 Top: structure and reaction of **61** with HS$^-$. Bottom: fluorescent images of HS$^-$ in living 5-day-old zebrafish. (A) Zebrafish only (control). The zebrafish were treated with **61** and then with various concentrations of NaSH: (B) 0 mM, (C) 10 mM, (D) 100 mM, and (E) 500 mM. First row (570–600 nm), second row (640–670 nm) and third row (corresponding DIC images). The images of the fourth row are the ratio channel. The bottom color strip represents pseudocolor correlation with HS$^-$ concentration. Scale = 500 mm. Image reproduced with permission.[230]

mice revealed that the probe could be used *in vivo* as an enhanced fluorescent response (λ_{ex} = 530 nm, λ_{em} = 655 ± 20 nm) was observed. The development of the fluorescent response over 4 h is shown in Fig. 57.

Through a simple two-step azidation procedure Ma (2012) converted cresyl violet to the ratiometric azide probe **61** (Fig. 58).[230] Both **61** (λ_{em} = 566 nm, Φ_F = 0.54) and cresyl violet (λ_{em} = 620 nm, Φ_F = 0.44) were strongly fluorescent (λ_{em} = 620 nm). The emission ratio (F_{620}/F_{566}) ranged from 0.34–10.5 upon addition of HS$^-$ and a detection limit of 100 nM was determined. Probe **61** was used to visualise exogenous HS$^-$ added to MCF-7 cells, and the emission could be quenched with addition of $ZnCl_2$ to the cells, confirming that switching is a result of azide reduction. The utility of **61** to visualise HS$^-$ *in vivo* was demonstrated in live zebrafish. As the concentration of HS$^-$ was increased (10–500 μM) fluorescence emission ratio (F_{620}/F_{566}) of the probe (10 μM) ranged from 0.73–1.64 with no visible fluorescence decrease on standing for elongated times, indicating that probe **61** was stable *in vivo*.

Chang in 2013 reported probe **SF7-AM**; which incorporated AM-esters to facilitate passive diffusion into cells. Intracellular ester hydrolysis gave the free carboxylates and the probe was subsequently retained within the cells (Fig. 59).[231] The inclusion of two azide triggers to the rhodamine-based fluorophore gave enhanced sensitivity and **SF7-AM** was used as a tool to study vascular endothelial growth factor (VEGF) stimulated HUVEC HS$^-$ production as a model for angiogenesis.

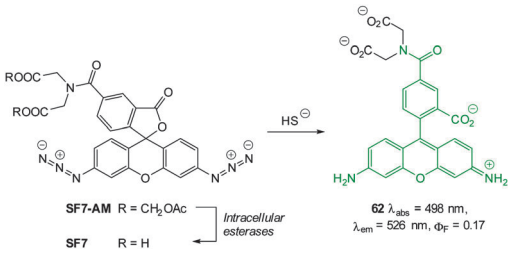

Fig. 59 Structure, intracellular esterase and sulphide reactions of **SF7-AM**.

As an advancement on their **Lyso-NHS** probe (Fig. 48) Cui and Xu developed the lysosome targeting probe **Lyso-AFP** (Fig. 60).[232] When HS^- mediated reduction of the essentially non-fluorescent azide (Φ_F = 0.012) occurred an increase in fluorescence response (Φ_F = 0.263, λ_{ex} = 426 nm, λ_{em} = 535 nm) was observed over 20 min. As with **Lyso-NHS** the pendant morpholine of **Lyso-AFP** lead to lysosomal localisation.

Another lysosome specific probe; rhodamine-based **SulpHensor** (Fig. 61) was described by Yang (2014).[233] No fluorescent response at physiological pH was observed for this probe upon treatment with HS^-. The acidic lysosome environment is required to open the spirocycle which results in a weakly fluorescent species (λ_{ex} = 540 nm, λ_{em} = 550 nm, Φ_F = 0.05). Subsequent azide reduction by HS^- greatly enhances the ICT fluorescent emission at 550 nm (Φ_F = 0.05) and a limit of detection of 500 nM for HS^- was determined. The HS^-/H^+ induced fluorescent response of

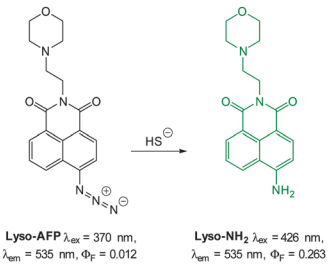

Fig. 60 Structure and reaction of **Lyso-AFP**.

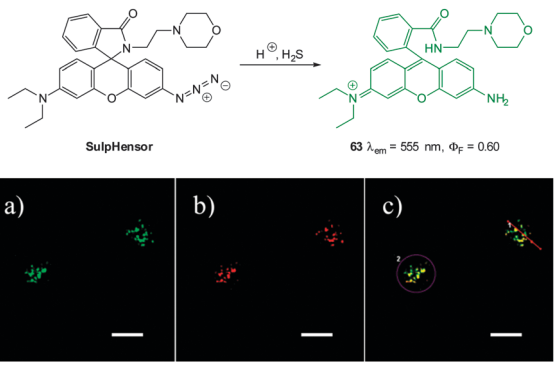

Fig. 61 Top: structure and reaction of **SulpHensor**. Bottom: HeLa cells stained with (a) LysoTracker Green (Ch1, green) and (b) **SulpHensor** (Ch2, red) with NaSH solution (c) overlay of (a) and (b). Scale = 10 μm. Image reproduced with permission.[233]

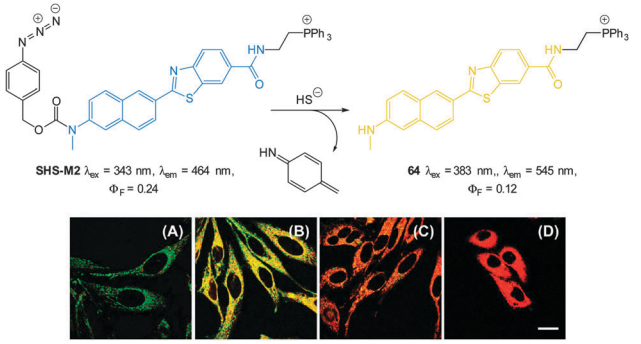

Fig. 62 Top: two-photon fluorescent probe **SHS-M2** developed by Kim. Bottom: (A–D) Pseudocoloured ratiometric TPM images F_{545}/F_{464} of (A, D) HeLa cells with (A) **SHS-M2** or (D) **SHS-M2** and (B, C) HeLa cells pretreated with (B) GSH or (C) cysteine prior to **SHS-M2**. Image reproduced with permission.[234]

SulpHensor was demonstrated *in vitro* using HeLa cells. Lysosomal accumulation was confirmed by co-staining with LysoTracker green and comparing the intensity profiles (Fig. 61) from the red (**SulpHensor**) and green channels (LysoTracker) over a selected region.

Bae *et al.* employed the 4-azidobenzylcarbamate trigger in their two photon fluorescent probe **SHS-M2** (Fig. 62). Hydrosulphide mediated reduction initially yields the aminobenzylcarbamate which subsequently fragments to give the observed products. In addition, the attachment of a pendant triphenylphosphonium moiety lead to mitochondrial accumulation in astrocytes.[234] Upon reduction with HS^- the emission wavelength of **SHS-M2** (λ_{em} = 464, Φ_F = 0.24) was red-shifted by 81 nm (λ_{em} = 545 nm, Φ_F = 0.12) and despite a decrease in quantum yield the two photon cross section was improved ($\Phi\delta_{max}$ = 17–55 GM). The probe was successfully used to detect mitochondrial HS^- in HeLa cells; metabolic precursors (GSH or Cys) of HS^- were added prior to the **SHS-M2** and an increase in the F_{545}/F_{464} ratio was recorded. The probe was also used to demonstrate the relationship between the DJ-1 gene and CBS mediated HS^- production in astrocytes as a model of Parkinson's disease.

The 4-aminonaphthalimide-based HS^- probes **NAP-1** and **AcSH-2** also bearing the 4-azidobenzylcarbamate trigger were independently reported by Zhao and Song in 2014.[235,236] Reaction of **NAP-1** (**AcSH-1**) with HS^- gives the fluorescent aminonaphthalimide and a corresponding red-shift in emission (from λ_{em} = 474 nm to λ_{em} = 540 nm).[235] A low limit of detection for HS^- was determined (50 nM at pH 7.0 and 110 nM at pH 7.4) and the probe was used by Song for monitoring endogenous HS^- production in sodium nitroprusside stimulated MCF-7 cells (Fig. 63) as well as quantifying HS^- levels in murine hippocampus. Zhao used **AcSH-2** to visualise exogenous HS^- in MCF-7 cells using TPM (λ_{ex} = 800 nm, F_{530}/F_{468} = 0.38–2.90). It was also evident that the *N*-(2-hydroxylethyl)-imide of **AcSH-2** promoted mitochondrial localisation.[236]

Chen and co-workers built the *m*-nitrophenyloxycyanine **Cy-NO$_2$** (Fig. 64) as a d-PET based probe for HS^-.[237] The 3-nitrophenylether attached to the cyanine framework could accept an

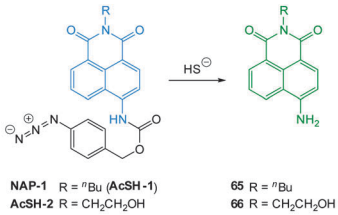

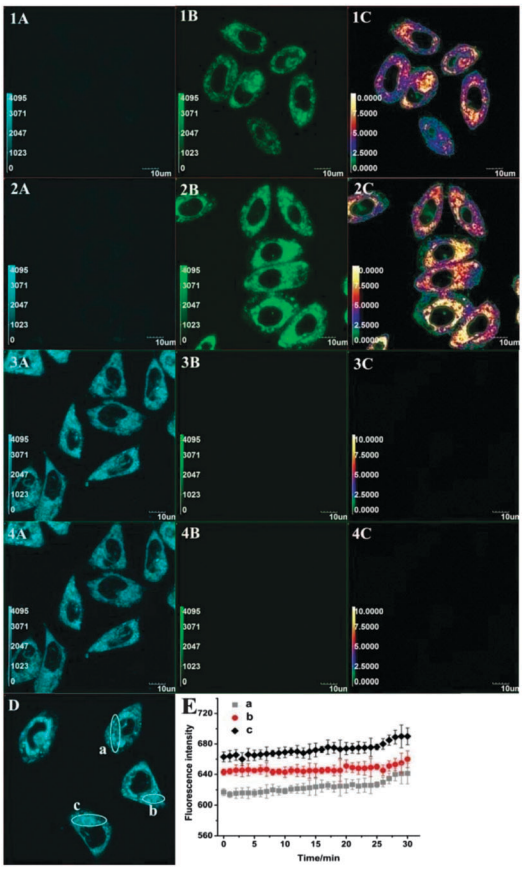

Fig. 63 Confocal fluorescence images of endogenous HS^- in living MCF-7 cells with **NAP-1**. Cells were pre-stimulated with SNP, then with **NAP-1** (1A, 1B, 1C). Cells were pre-stimulated with SNP, and then with **NAP-1** (2A, 2B, 2C). Cells were pre-treated with DL-propargylglycine (PPG), and then with **NAP-1** (3A, 3B, 3C). Cells in (3A, 3B, 3C) were thereafter treated with SNP (4A, 4B, 4C). Cells were incubated with **NAP-1** alone (D). The average fluorescence intensity from the regions of interest a, b and c in (D) was recorded with 60 s intervals (E) (n = 3). Ratiometric images (F_{530}/F_{468}) generated by the Olympus software (1C, 2C, 3C, 4C). Scale bars = 10 μm. Image reproduced with permission.[235]

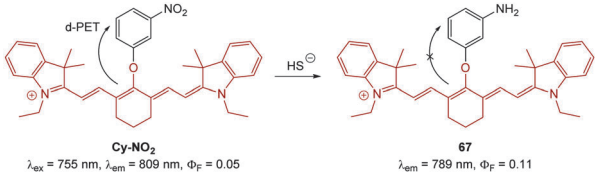

Fig. 64 Structure and reaction of hydrosulphide probe **Cy-NO$_2$**.

electron from the excited state of the cyanine fluorophore. Reduction of the nitro group with HS^- disrupts the d-PET process resulting in significantly enhanced emission (from Φ_F = 0.05 to Φ_F = 0.11, λ_{ex} = 755 nm, λ_{em} = 789 nm). The probe localised in the cytosol of RAW264.7 macrophages and was used to detect exogenous HS^-. A significant drawback associated with unassisted nitro group reduction is that it is a kinetically slow process, and in this instance fluorescence intensity peaked only after 60 min, even at 37 °C.

3.3.3 Hydrosulfide mediated metal displacement. In 2014 Huang and Deng reported a NIR emitting probe based on Cu(II) displacement from the Cu(II)–cyclen complex **68-Cu(II)** (Fig. 65).[238] The probe was originally designed to function by means of HS^- mediated NO_2 reduction, but no reaction occurred at ambient temperatures. The probe was redesigned and the nitro group was reduced to an amine and functionalised with the cyclen-macrocycle. Complexation of **68** with Cu(II) gave the non-fluorescent probe which, when treated with HS^- in buffered solution studies gave a significant fluorescence "switch on" response (λ_{ex} = 716 nm, λ_{em} = 765 nm). Visualisation of exogenous HS^- in RAW264.7 macrophages was successfully demonstrated as was the detection of endogenous HS^- which was produced by the overexpression of wild-type (WT) cystathionine-γ lyase (CSE) in human embryonic kidney (HEK293). *In vivo* studies were then performed by injecting imprinting control region (ICR) mice with **68-Cu(II)** by skin-pop injection. One **68-Cu(II)** treated mouse was then injected with Na_2S (as source of HS^-) and the fluorescence images were recorded (λ_{ex} = 670 nm, λ_{em} = 790 nm). The fluorescence signal increased seven-fold 1 h after treatment with HS^- (compared to the control) and continued to rise gradually over 5 h.

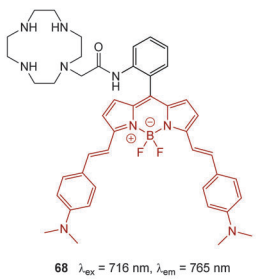

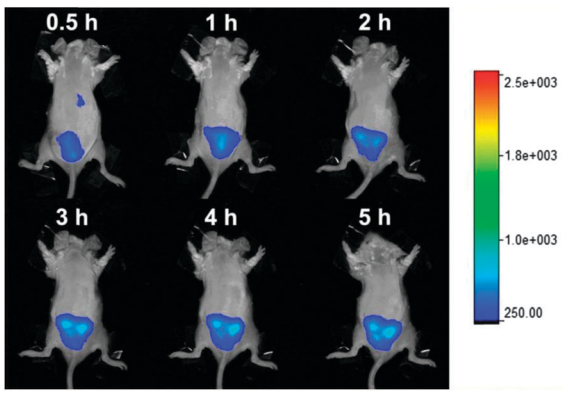

Fig. 65 Top: NIR emissive cyclen dosimeter **68** by Deng and Huang. Bottom: representative fluorescence images of mice (pseudocolour) that were injected with **68-Cu(II)** (40 mm), followed by Na_2S. The images were recorded after the injection of Na_2S within 5 h. Image reproduced with permission.[238]

In order to keep this section to a reasonable length and highlight the most relevant recent examples it was not possible to include all recent examples of probes functioning by way of (i) nucleophilicity[100,218,219,223,224,239–247] (ii) reduction (aryl-azides,[226–228,231–235,248–258] sulfonylazides,[259–261] nitro groups,[262,263] hydroxyl amines,[264] and N-oxides[265]) as well as (iii) displacement[53,266–269] and readers are referred to these citations for additional information.

4. Reactive anions

In addition to the well-known oxidative stress caused by reactive oxygen and nitrogen species, it is becoming increasingly apparent that these moieties are involved in a wide range of physiologically essential processes (such as cellular migration and circadian rhythm).[270] Reactive oxygen/nitrogen species can be neutral, anionic, radicals or even radical anions (Table 2) and as many of these species exist only fleetingly they are exceptionally challenging targets for small molecular probes.[50,271]

At physiological pH (*ca.* 7.4) several of these species exist to a considerable extent as an anion (peroxynitrite, hypochlorite and hypobromite) and can therefore be considered biologically relevant anionic targets. Given their diverse roles interest in detecting these species *in vitro* and *in vivo* has been strong and several reviews on the topic are available.[34,60,271,272]

4.1 Peroxynitrite

Peroxynitrite is formed from the rapid reaction of two other RO/N species: superoxide $O_2^{\bullet -}$ and nitric oxide NO$^\bullet$ (Fig. 66) and its detection in living systems is hampered by a number of factors including (i) its reactivity (it is a potent nucleophile and is a more powerful oxidant than superoxide) with a number of *in vivo* targets such as proteins, nucleic acids and lipids (especially those containing thiols) and (ii) degradation to other highly reactive species (including both the hydroxyl radical and the nitrogen dioxide radical).[57,273] The pK_a of ONOOH is 6.8 and as a result ~80% of the species is found in the anionic form at pH 7.4. Typically the anion adopts a cisoid structure that is responsible for its 'relative' stability compared to the parent acid.[274]

Elevated levels of this species are associated with cardiovascular and neurodegenerative disorders, metabolic diseases, inflammation, pain, and cancer.[275,276] Hence the development of probes for its detection *in vivo* is an important task *en route* to fully understanding its diverse physiological roles.[57]

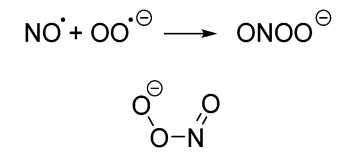

Fig. 66 Formation and cisoid structure of peroxynitrite.

Peroxynitrite has long been known as a cellular oxidant and hence sensors to monitor this anion emerged last century.[272] Probes for peroxynitrite rely on the same reactivity that the anion exhibits *in vivo*; $ONOO^-$ is both nucleophilic (reacts with CO_2 *in vivo* to form carbonate[277]) and highly oxidative (by one and two electron processes) and is a known nitrating agent.[273] All three of these reaction types has been employed in the design of imaging agents for the species however probes that employ the oxidation power of $ONOO^-$ are by far the most prominent (Section 4.1.1). Amongst these, probes based on the oxidation of B, Se, and Te form an interesting subset (Section 4.2.2). Common interferents with the detection of $ONOO^-$ are typically other ROS in particular hypochlorite (ClO^-) and nitroxide radical (•NO).

Early anion sensors for peroxynitrite inside cells include the "switch on" probes dichlorodihydrofluorescein **DCHF** and dihydrorhodamine **DHR-123** (Fig. 67).[278–280] While many imaging studies, and even flow cytometry assays,[281] were performed using these, (and similar) probes they are somewhat non-selective and in some instances light sensitive.[272]

4.1.1 Peroxynitrite mediated oxidation/fragmentation. A recent report by Shivanna (2013) detailed the use of rhodamine B phenyl hydrazide **RBPH** (Fig. 68).[282] The probe was readily oxidised by $ONOO^-$ to give the highly fluorescent (λ_{em} = 580 nm) ring open **rhodamine–B**; the product confirmed by ^{1}H NMR spectroscopy ESMS. Interferents such as H_2O_2 did not elicit the same reaction (ClO^- was not tested) and as such some selectivity was noted. Live MCF-7 cells incubated with the probe gave a clear "switch on" response within 30 min when exogenous $ONOO^-$ was added.

A strategy developed by Yang involves $ONOO^-$ nucleophilic attack on a reactive trifluoromethyl ketone group followed by

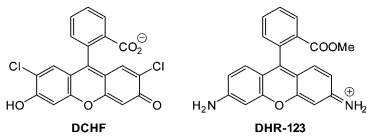

Fig. 67 Early chemodosimeter based agents for peroxynitrite; dihydrodichlorofluorescein (**DCHF**) and dihydrorhodamine (**DHR-123**).

Table 2 Reactive oxygen/nitrogen species

Neutral	Anionic	Radical anion	Radical
Hydrogen peroxide HOOH	Peroxynitrite $ONOO^-$	Superoxide $O_2^{\bullet -}$	Nitric oxide NO$^\bullet$
Singlet oxygen $^1O_2$	Hypochlorite ClO^-		Hydroxyl HO$^\bullet$
	Hypobromite BrO^- [a]		Nitrogen dioxide $NO_2^\bullet$
			Peroxy radicals ROO$^\bullet$

[a] A percentage of this species can also be found in neutral form (HOBr pK_a = 8.7).

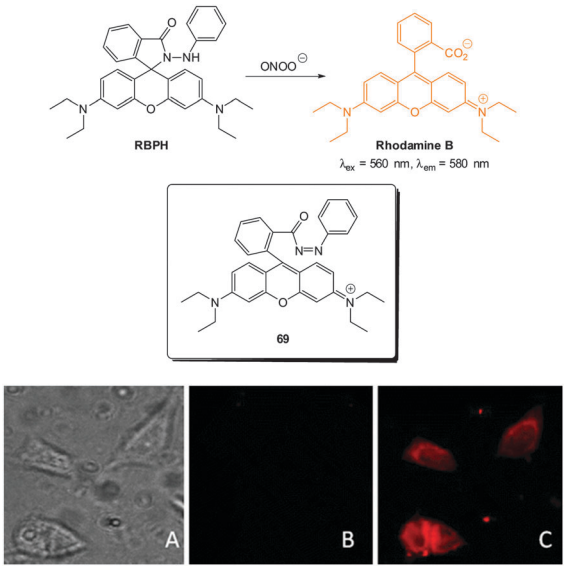

Fig. 68 Top: structure and reaction of **RBHP** with $ONOO^-$; inset shows the diazo intermediate **69** that forms prior to fragmentation. Bottom: (A) bright-field image of MCF-7 cells incubated with **RBPH**. (B) Corresponding fluorescence image (C) fluorescence image of MCF-7 cells incubated with **RBPH** then peroxynitrite. Image reproduced with permission.[282]

formation of a spirohemiacetal *via* a dioxirane intermediate.[283] Three separate probes have been developed: employing dichlorofluorescein **HKGreen1**,,[284] BODIPY **HKGreen2**,[285] and rhodol **HKGreen3**[92] fluorophores (Fig. 69). For these chemodosimeters fluorescence is quenched in the ketone form but following spirohemiacetal formation (and for **HK1** and **HK3** fragmentation) fluorescence is "switched on". For **HKGreen2** a 21-fold enhancement of fluorescence (λ_{em} = 539 nm) was observed upon reaction with just one equivalent of $ONOO^-$. The probes react to a small extent with $HO^\bullet$ but not the common ClO^- interferent. Evaluation in cells was performed for all probes (Results for **HKGreen3** in RAW264.7 macrophages shown in Fig. 69). This cell line is known to produce ROS/RNS, including $ONOO^-$, in response to immunological and inflammatory stress and after stimulation of endogenous $ONOO^-$ production using bacterial endotoxin lipopolysaccharide (LPS), interferon-γ (IFN-γ) and phorbol 12-myristate 13-acetate (PMA) strong fluorescence was noted. No fluorescence enhancement was noted when $ONOO^-$ production was inhibited by (2,2,6,6-tetramethylpiperidin-1-yl)oxy (TEMPO) a superoxide scavenger or aminoguanidine (AG) an inhibitor of NO synthase[286] confirming that endogenous production of $ONOO^-$ was being detected.

In a more recent article from the Yang group a functionalised rhodol chemodosimeter **HKGreen-4** (Fig. 70) was described in which the oxidation of electron rich aromatics was exploited.[287] The "switch on" probe (290-fold increase in λ_{em} = 535 nm) was capable of discriminating between peroxynitrite and other reactive oxygen species including hydroxyl radical and hypochlorite. **HKGreen4** also performed in the presence of CO_2, a molecule known to react quickly with $ONOO^-$. The probe was water soluble and was successfully used with either conventional or two photon microscopy to image endogenous $ONOO^-$ production in *E. coli*

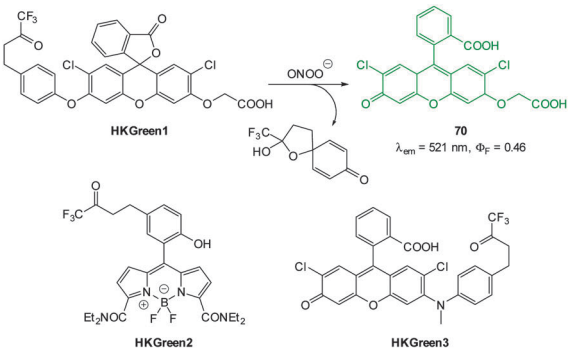

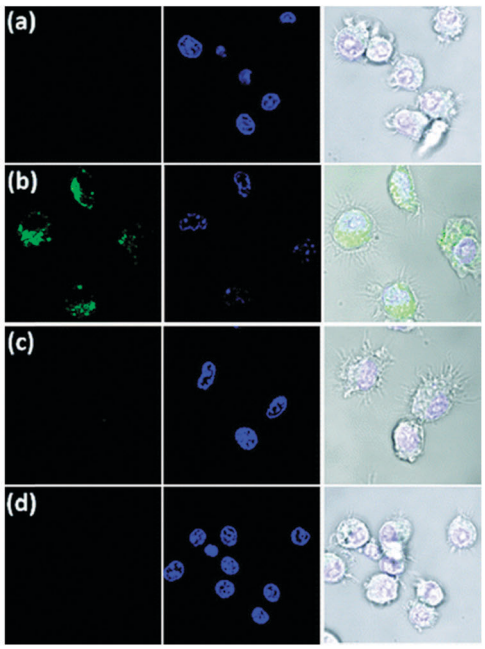

Fig. 69 Top: structure of **HKGreen1**, **2** and **3** and reactivity of BODIPY based chemodosimeters **HKGreen1** with peroxynitrite to form **70**. Bottom: images of live RAW264.7 cells were treated with stimulants to elicit endogenous $ONOO^-$ production then stained with **HKGreen-3** (green channel) and Hoechst 33342 (blue channel). (a) Cells without stimulation. (b) Cells stimulated with LPS, IFN-γ, and PMA. (c) Cells pre-treated with TEMPO, and then stimulated with LPS, IFN-γ, and PMA. (d) Cells pre-treated with AG, then stimulated with LPS, IFN-γ, and PMA. Image reproduced with permission.[92]

challenged RAW264.7 cells. In conjunction with a number of enzymatic inhibitors the probe was used to further confirm the generation of endogenous $ONOO^-$ production in response to the presence of *E. coli*. Generation of $ONOO^-$ is thought to be an immune effector for bacterial clearance, and the results of this study suggest that the $ONOO^-$ formation in *E. coli* challenged macrophages is enzymatically regulated.

The "switch on" coumarin pyridinium probe **C-Py-1** was reported by Yu in 2014 (Fig. 71).[288] The probe was selective for peroxynitrite amongst other reactive oxygen/nitrogen species with a 25-fold enhancement of emission at λ_{em} = 493 nm. The emitting species was identified (^{1}H NMR spectroscopy and ESI-MS) to be the coumarin aldehyde **72** formed from oxidative cleavage of the alkene in the presence of $ONOO^-$. Excellent cell

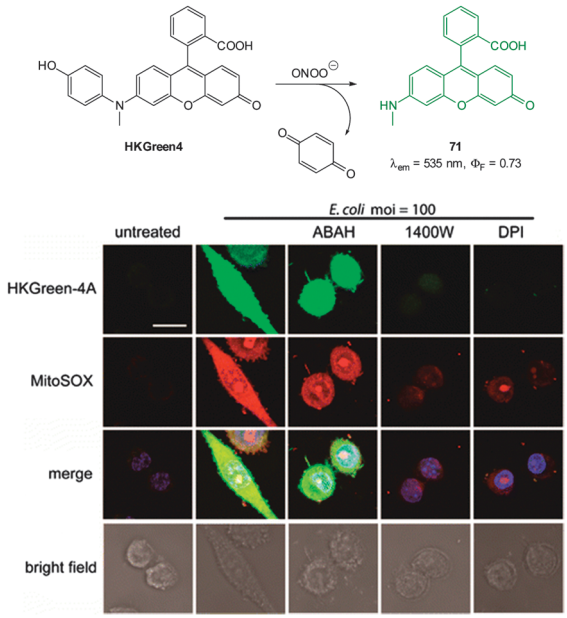

Fig. 70 Top: structure and reaction of **HKGreen4** with $ONOO^-$. Bottom: images of RAW264.7 macrophages. Cells were co-treated with heat-killed *E. coli* and various enzyme inhibitors then stained with **HKGreen4A**, MitoSOX, and Hoechst 33342 before imaging. Aminobenzoic acid hydrazide (ABAH) is an inhibitor of myeloperoxidase that produces ClO^-; 1400 W and DPI are inhibitors for iNOS and NOX, respectively. The merged images are overlays of all fluorescence channels. Scale = 10 μm. Image reproduced with permission.[287]

membrane permeation and low cytotoxicity were noted and the probe was successfully applied to the imaging of endogenous $ONOO^-$ in RAW264.7 cells. *In vitro* fluorescence was "switched on" within 30 min of the addition of lipopolysaccharide (LPS) to the cells to stimulate endogenous production of $ONOO^-$.

The related hemicyanine probe **CHCN** (Fig. 72) has recently been published by Yoon (2015).[289] Oxidative cleavage of the alkene gives coumarin aldehyde **73** and 1,3,3-trimethyloxindole; both products confirmed using ESMS and ^1H NMR spectroscopy. This probe indicated $ONOO^-$ in a linear ratiometric fashion (F_{515}/F_{635} increase), had a low LOD (49.7 nM) and displayed excellent

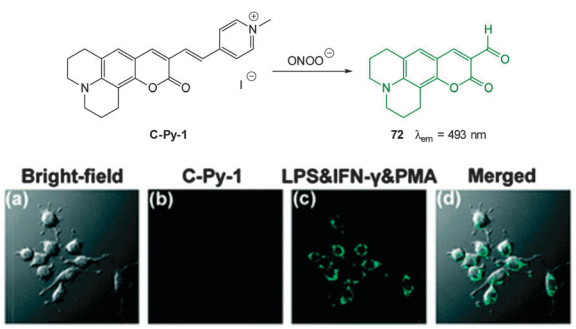

Fig. 71 Top: structure and reaction of $ONOO^-$ probe **C-Py-1**. Bottom: images of RAW264.7 cells. (a) Bright-field image; (b) cells stained with **C-Py-1**; (c) cells were stained with LPS and IFN-γ then PMA and finally with **C-Py-1**; (d) merged image of (a) and (c). Scale = 10 μm. Image reproduced with permission.[288]

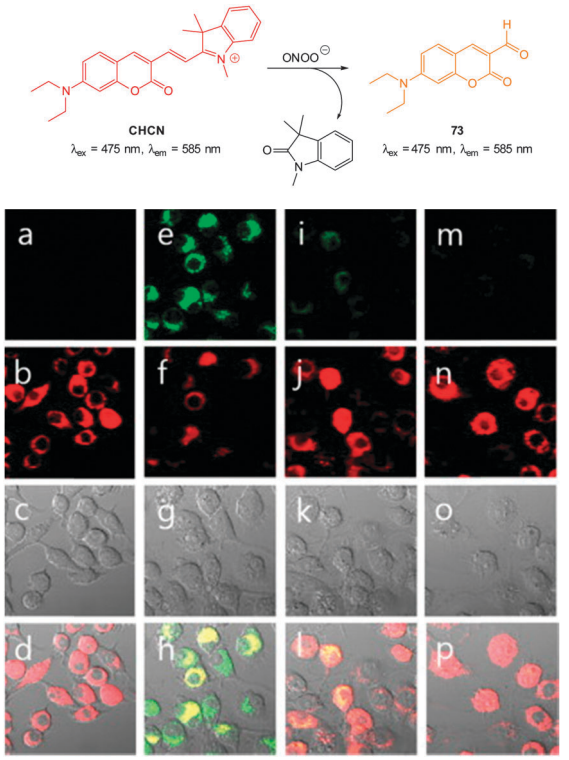

Fig. 72 Top: structure and reaction of coumarinindolium probe **CHCN**. Bottom: images of RAW264.7 cells for endogenous $ONOO^-$ during phagocytic immune response. The cells were stained with **CHCN**. (a) Control; (e) LPS, IFN-γ and PMA; (i) LPS, IFN-γ and PMA then AG; (m) LPS, IFN-γ and PMA then TEMPO. Green channel (a, e, i, m); red channel (b, f, j, n); images (c, g, k, o) are differential interference contrast; images (d, h, l, p) are merged red and green channels. Image reproduced with permission.[289]

selectivity—only a very slight response to a large excess of hypochlorite was noted. The probe was shown to operate successfully in RAW264.7 macrophages when the cells were stimulated to produce $ONOO^-$ using a number of agents (LPS, IFN-γ and PMA). No response was observed when inhibitors of endogenous $ONOO^-$ production were introduced (TEMPO and aminoguanidine).

A multichannel probe $\mathbf{PN_{600}}$ (Fig. 73) that can clearly distinguish $ONOO^-$ from ClO^- has been developed by Yang (2012).[290] While both hypochlorite and peroxynitrite can oxidise the coumarin $\mathbf{PN_{600}}$ to the corresponding aminophenol **74**, only $ONOO^-$ is powerful enough to oxidise **74** to the red emitting iminoquinone **75**. Due to differing excitation yet similar emission wavelengths either of OCl^- or the $ONOO^-$ could be inferred by monitoring emission at 620 nm and selectively exciting at 355, 465 or 575 to identify which fluorophore had formed and hence which oxidant was present. In human glioma cell line U87 the probe was shown to quickly penetrate the cell membrane and was non-toxic (MTT assay). Using 3-morpholinosydnonimine (SIN-1), a compound known to decompose to $NO^\bullet$ which in turn forms $ONOO^-$,[291] a clear fluorescent response was observed.

Probes containing boron have recently emerged for the cellular sensing of peroxynitrite.[292] The nucleophilicity of $ONOO^-$ leads to initial formation of a C–O–B bond in place of the original C–B

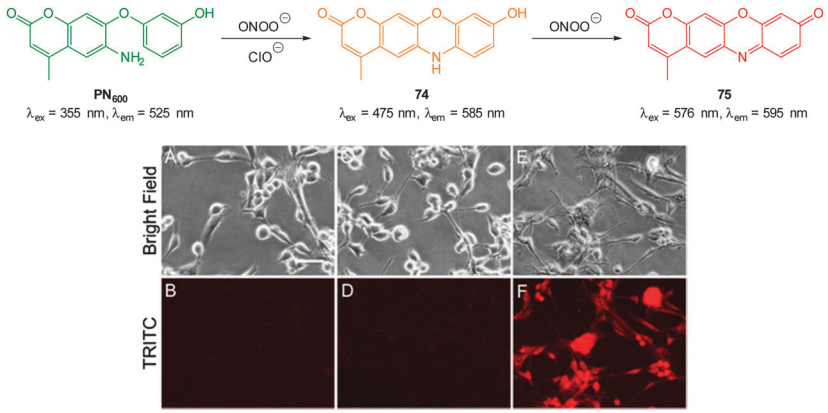

Fig. 73 Top: probe **PN$_{600}$** showing reaction with both $ONOO^-$ and ClO^- to form **74**, however only $ONOO^-$ can oxidise **74** to the red iminoquinone **75**. Bottom: live-cell imaging using **PN$_{600}$**. Phase contrast and fluorescence images of human glioma cells treated with (A, B) **PN$_{600}$**, (C, D) **PN$_{600}$** + ClO^-, and (E, F) **PN$_{600}$** + SIN-1. Scale = 50 μm. Image reproduced with permission.[290]

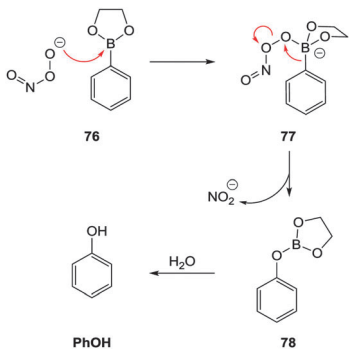

Scheme 2 Conversion of arylboronates to phenols using $ONOO^-$.

bond (Scheme 2). This insertion is followed by hydrolysis to afford C–O–H. The process is similar to the established hydroboration/oxidation using alkaline H_2O_2 however the reaction of boronates with $ONOO^-$ is nearly 1×10^7 times faster than the reaction with H_2O_2 and hence discrimination between these species is possible.[293]

The naphthalimide-based "switch off" probe **80** was reported by James in 2014 (Fig. 74).[294] The fluorescent D-fructose complex (λ_{em} = 525 nm) of **79** in which PET from the spacer N is prevented was "switched off" by $ONOO^-$ mediated oxidation to the corresponding phenol **81**. The product again has a free amine and PET quenches fluorescence. All other ROS except ClO^- did not elicit a significant response. In RAW264.7 macrophages $ONOO^-$ production was stimulated by a number of immunological factors (again including LPS) and the "switch off" was easily visualised. When TEMPO or aminoguanidine was added to the stressed cells prior to addition of the probe fluorescence was maintained due to a lack of endogenous $ONOO^-$.

In 2012 Han reported the "switch on" dioxaborolane pyrene probe **PyBor** (Fig. 75) which was synthesised in three steps from pyrene.[295] Reaction with $ONOO^-$ was complete in seconds (**PyBor** is converted to **PyOH**) and was accompanied by a significant increase in quantum yield from ϕ_F = 0.08 to 0.60 (**PyOH**, λ_{ex} = 347, λ_{em} = 410 nm). While slightly sensitive to

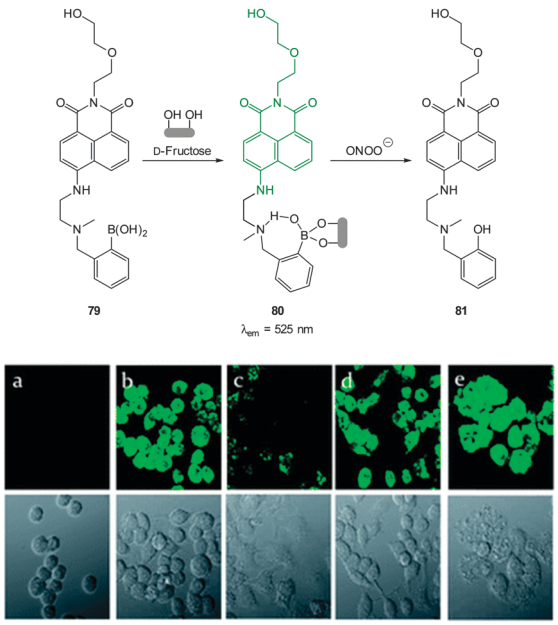

Fig. 74 Structure and three stage reaction of naphthalimide boronate **79** with D-fructose and $ONOO^-$. Bottom: fluorescent imaging for endogenous $ONOO^-$ in RAW264.7 cells. The probe **80** was formed by mixing **79** and D-fructose *in situ*. (a) Blank without probe; (b) probe **80** only; (c) probe **80** and LPS, IFN-γ, PMA; (d) c + aminoguanidine; (e) c + TEMPO. Image reproduced with permission.[294]

H_2O_2, ClO^- and BrO^- co-staining confirmed **PyBor** localised in the cytoplasm of RAW264.7 cells and intense intracellular fluorescence was observed when cells that had been incubated with **PyBor** were treated with LPS, IFN-γ and PMA. When the cells were pre-treated with aminoguanidine, only weak fluorescence was detected.

4.1.2 $ONOO^-$ mediated chalcogen oxidation. Fully reversible, NIR emissive, phenylselenylaniline probes **BzSe-Cy**, **Cy-PSe** and a related Te containing cyanine probe **Cy-NTe** have been developed by Tang and Han (Fig. 76). The first, benzylselenylcyanine **BzSe-Cy**,[296] is a "switch off" probe that can be recycled with ascorbic acid. In **BzSe-Cy** the selenium is an electron donating

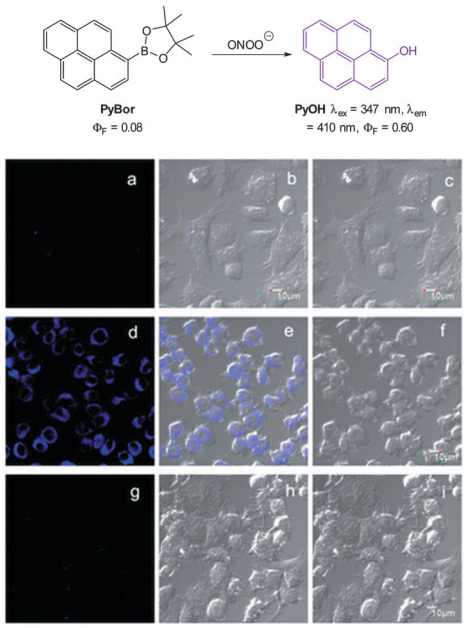

Fig. 75 Top: structure and reaction of **PyBor** with $ONOO^-$. Bottom: images of RAW264.7 macrophages treated with **PyBor** in the absence or presence of stimulants for 30 min. (a–c) Controls; (d–f) LPS and IFN-γ then PMA; (g–i) AG, LPS, IFN-γ and PMA. (a, d, g) fluorescence Images; (b, e, h) overlay images; (c, f, i) bright-field images. Image reproduced with permission.[295]

component of the cyanine system, however, in its oxidised Se=O form (readily accomplished by $ONOO^-$) electron donation is "switched off" and fluorescence is quenched. The second probe, **Cy-PSe**[297] is a "switch on" probe that uses PET from the dibenzylselenoether to quench BODIPY fluorescence. When oxidised to Se=O, electron transfer is inhibited and fluorescence is "switched on". The third, **Cy-NTe**[298] another "switch on" probe also operates using this principle. The Te component required six steps to construct prior to coupling with commercially available cyanine chloride. Both **Cy-PSe** and **Cy-NTe** are easily oxidised by $ONOO^-$ and also easily reduced by glutathione (GSH) which makes them mimics of the Se containing glutathione peroxidase enzymes (GPx). In the non-oxidised state the metals quench fluorescence by PET, however PET is not possible in the oxidised forms and strong fluorescence enhancement is observed (23-fold for **Cy-PSe** and 13-fold for **Cy-NTe**). The successful "switch on" oxidation, "switch off" reduction cycles for both **Cy-PSe** and **Cy-NTe** were demonstrated in RAW264.7 cells by successive treatment with LPS then an ROS scavenger glutathione S-transferase (GST) to "switch off" fluorescence. Mitochondrial localisation of **Cy-NTe** was reported as was a lack of toxicity (MTT assay) and the switching behaviour of the probe was sensitive enough to be visualised *in vivo* using BALB/c mice.

The selenium containing "switch off" BODIPY probe **BOD-Se** (Fig. 77) was reported by Han in 2012.[299] The authors proposed that, in light of the long time required to elicit a response, oxidation of the Se itself by $ONOO^-$ did not modulate fluorescence but that the product containing Se=O was hydrolysed

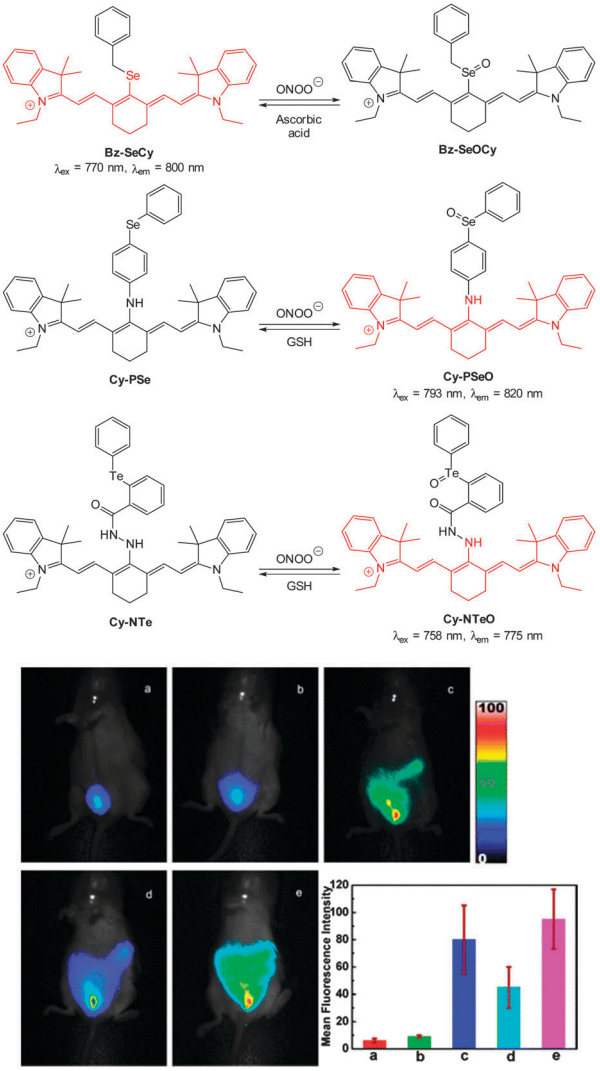

Fig. 76 Top: structure of **BzSe-Cy**, **Cy-PSe** and **Cy-NTe** probes and their oxidation products. Bottom: imaging of redox cycles between peroxynitrite and GSH in peritoneal cavity of BALB/c mice. (a) **Cy-NTe** and L-cysteine were injected in the i.p. cavity. (b) Mice injected i.p. with **Cy-NTe**. (c) Mice injected with LPS, IFN-γ then PMA followed by **Cy-NTe** (d) mice treated as described in (c), then injected i.p. with AG, GST and L-cysteine (e) mice treated as described in (d), then injected with SIN-1. Bar graph indicates total number of photons from the entire peritoneal cavity of the mice (a–e). Image reproduced with permission.[298]

(Fig. 78) to liberate a new selenium free florescent BODIPY **82**. The **BOD-Se** probe itself was highly fluorescent (λ_{em} = 572 nm, ϕ_F = 0.96) and a colour change from red to blue was noted upon exposure to $ONOO^-$ with an isosbestic point at 567 nm. Fluorescence intensity decreased more than 200-fold along with a shift of the emission maximum (λ_{em} = 680 nm, ϕ_F = 0.05). Again murine macrophage RAW264.7 cells were stressed using LPS/IFN-γ and PMA to induce endogenous production of $ONOO^-$ prior to imaging.

4.1.3 Peroxynitrite mediated nitration/nitrosylation. The **Ds-DAB** probe (Fig. 78) was described by Wang in 2013 and its synthesis was remarkably easy—one step from commercially available materials.[300] Fluorescence was initially quenched

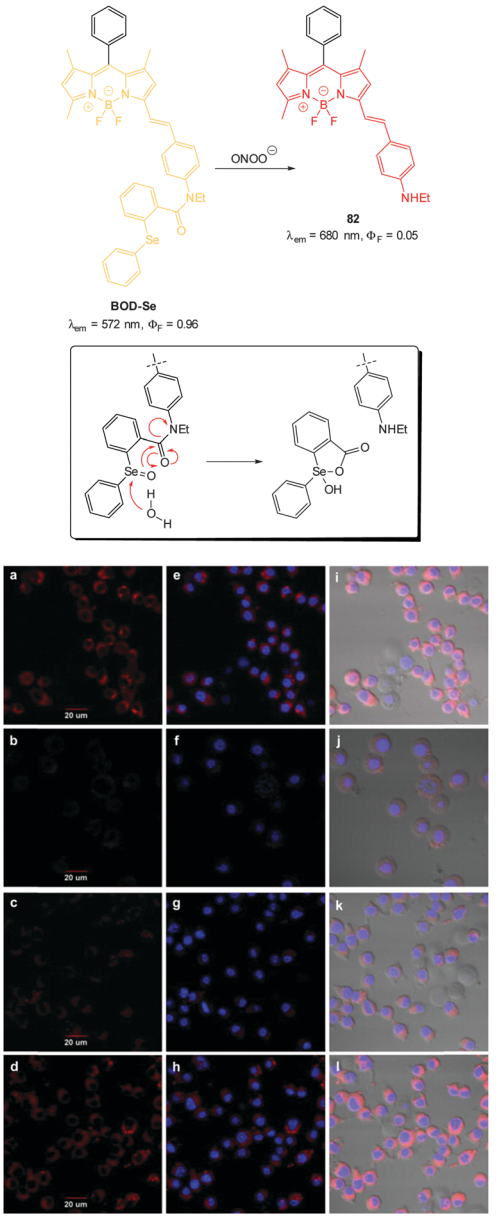

Fig. 77 Top: structure and reaction of **BOD-Se** with $ONOO^-$; inset: proposed tandem hydrolysis/cyclisation of oxidised **BOD-Se** leading to fragmentation. Bottom: images RAW264.7 cells incubated with **BOD-Se** then treated with (a, e, i) controls. (b, f, j) SIN-1 (c, g, k) LPS, IFN-γ then PMA. (d, h, l) AG, LPS and IFN-γ then PMA (e–h) overlay showing **BOD-Se** fluorescence and Hoechst dye; (i–l) bright-field overlay of **BOD-Se** and Hoechst dye. Image reproduced with permission.[299]

(presumably by PET) and the selective, ''switch on'' (6.5-fold enhancement) chemodosimeter reacts readily with $ONOO^-$ to form fluorescent dansyl acid (ϕ_F = 0.15, λ_{em} = 505 nm, λ_{ex} = 350 nm) and benzotriazole as indicated by ESMS, ^{1}H NMR spectroscopy and LC-MS. The proposed mechanism involves formation of a nitrosamine which subsequently fragments. Rapid uptake of the probe was reported as was no toxicity and again the probe was used to visualise production of endogenous $ONOO^-$ inside RAW264.7 macrophages when treated with LPS and PMA to induce cell stress.

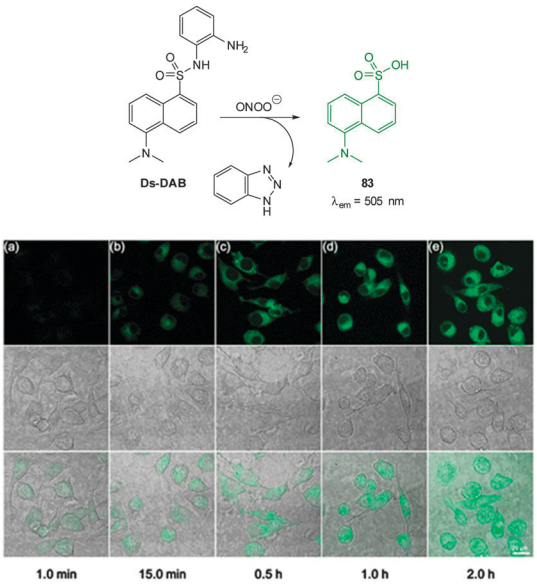

Fig. 78 Top: structure and reaction of **Ds-DAB** with peroxynitrite. Bottom: *in vitro* detection of $ONOO^-$ in RAW264.7 macrophages. Cells were treated with LPS then PMA and subsequently incubated with **Ds-DAB** for the time stated prior to imaging. Top = fluorescence, middle = bright-field, bottom = overlay; scale = 20 μm. Image reproduced with permission.[300]

A probe for nitrative stress (**NiSPY-3**, Fig. 79) was rationally designed by Nagano (2006)[301] and is an interesting example in which nitration leads to fluorescence ''switch on'' (λ_{ex} = 505 nm, λ_{em} = 520 nm) based on an a-PET process. The probe was selective for peroxynitrite and was successfully used to visualise exogenous $ONOO^-$ in live HeLa cells.

4.1.4 Miscellaneous. An interesting lanthanide-based probe for $ONOO^-$ bioimaging was reported by Guan in 2010 (see Section 3.2 for the general principles by which Ln emission is modulated).[93] The **DTTA** ligand (a combination of dimethoxyphenyl and terpyridinetetraacid, Fig. 80) was designed to be both a Ln chelator and also sensitive to a d-PET process. In practice the terbium complex $[$**(DTTA)Tb**$]^-$ (λ_{ex} = 335 nm, λ_{em} = 612 nm) was sensitive to $ONOO^-$ whereas the corresponding europium complex (λ_{ex} = 335 nm, λ_{em} = 541 nm) was not. The authors postulated that quenching by charge transfer, not PET, was responsible for the quenching, however, the electron rich dimethoxyphenyl substituent of **DTTA** is similar to that of **NiSPY-3** (shown in Fig. 79). Thus, with a ''cocktail'' of both lanthanides $[$**DTTA-Eu(III)**$]^-$ and $[$**DTTA-Tb(III)**$]^-$ ratiometric measuring was possible with only very slight interference noted from nitrate. The tetraacetoxymethyl ester form **AM-DTTA** readily entered HeLa cells esters along with solutions of both lanthanides. Ester hydrolysis inside cells was followed by assembly of the lanthanide complexes and their formation could be visualised using microscopy. Again using SIN-1 as a source of NO$^\bullet$ (reacts immediately with superoxide to form $ONOO^-$) a clear decrease in Tb emission in proportion to increasing SIN-1 concentration was observed.

An interesting example of a probe for the sensing of $ONOO^-$ by means of luciferin bioluminescence was reported in 2013 by

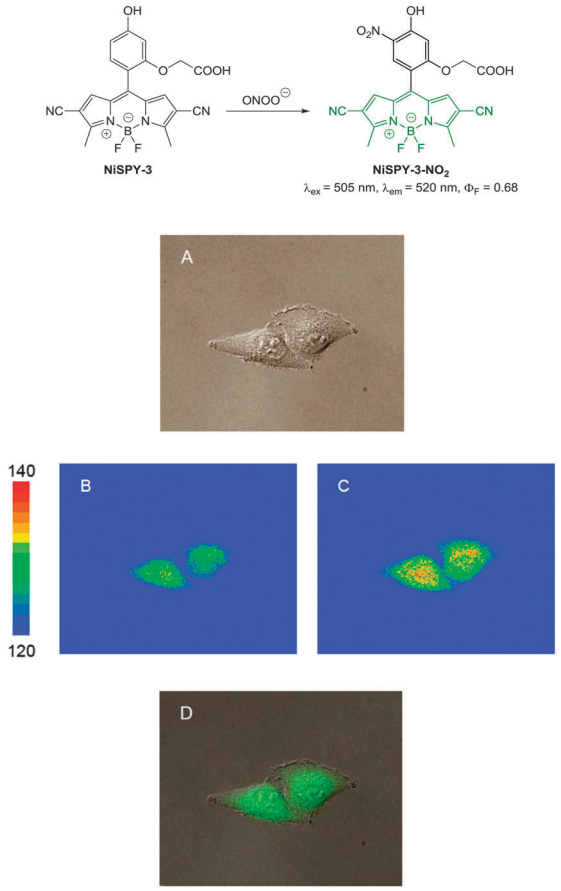

Fig. 79 Top: structure of **NiSPY-3** and its reaction with $ONOO^-$. Bottom: differential interference contrast (A), pseudo-colour fluorescence (B, C) and merged images (D) of HeLa cells loaded with **NiSPY-3**. Pseudo-colour images were obtained before (B) and after (C) addition of peroxynitrite. Image reproduced with permission.[301]

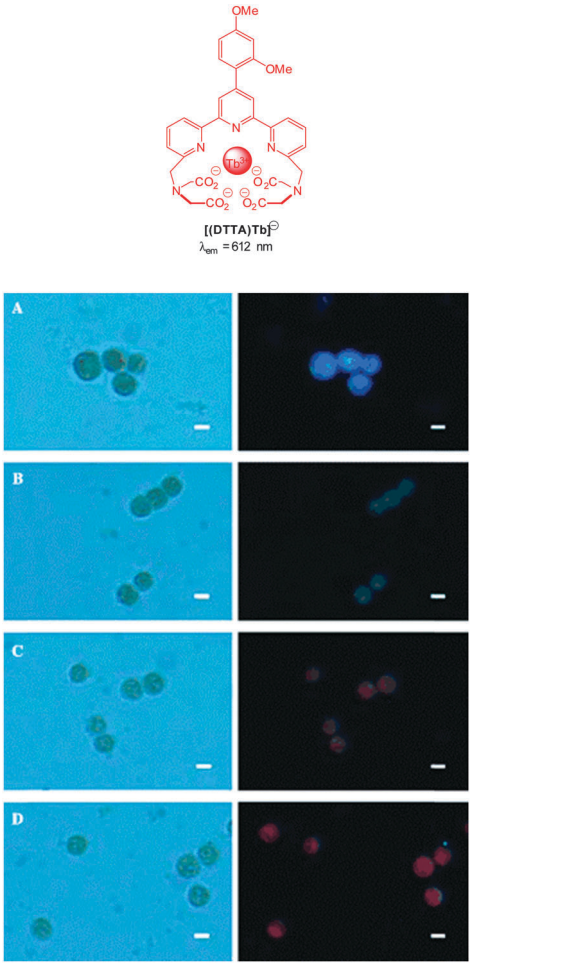

Fig. 80 Top: structure of the **DTTA-Tb(III)** complex. Bottom: bright-field (left) and normal luminescence (right) images of the [Eu(III)/Tb(III)(**DTTA**)]-loaded HeLa cells in the presence of $ONOO^-$ generated from SIN-1 (A: negative control; B: 100 μM; C: 200 μM; D: 500 μM of SIN-1). Scale = 10 μm. Image reproduced with permission.[93]

Bonini using the peroxy-caged luciferin **PCL-1** (Fig. 81).[302] Unfortunately, cell images were not shown in this instance. The boronic acid based chemodosimeter **PCL-1** (originally designed and used by Chang for the *in vivo* bioimaging of H_2O_2 in mice)[303] reacts far more rapidly with $ONOO^-$ than it does with H_2O_2 to form luciferin which in turn forms oxyluciferin with concomitant emission of light (λ_{em} = 560 nm).

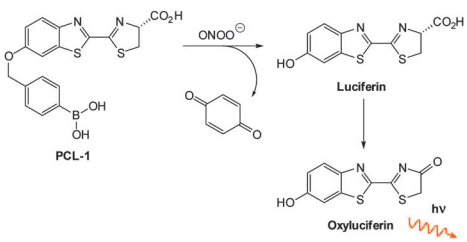

Fig. 81 Structure and reaction of luciferin based probe **PCL-1** with $ONOO^-$.

4.2 Hypochlorite

Hypochlorite plays an important physiological role defending against invading pathogens and endogenous hypochlorite is produced from the reaction of H_2O_2 with Cl^- and is catalysed by the heme enzyme myeloperoxidase (MPO). Over stimulation of the MPO immune response, and increased hypochlorite levels can lead to host tissue damage and inflammation that is associated with a number of serious disorders such as cancer, neurodegeneration, arthritis and cardiovascular disease.

$$H_2O_2 + Cl^{\ominus} \rightarrow H_2O + ClO^{\ominus} \quad (1)$$

Bioimaging agents must be selective for ClO^- over H_2O_2 if the MPO–H_2O_2–Cl^- enzymatic system is used to generate endogenous ClO^- otherwise the fluorescent signal may be due to exogenous H_2O_2. Another consideration is pH; the parent acid HOCl has a pK_a of 7.463 at 35 °C,[304] therefore at physiological pH approximately 50% of the acid is dissociated; so it possible that either the hypochlorite anion or the protonated form could be the detected species. Most researchers evaluate their probe over a pH range to identify whether hypochlorite or hypochlorous acid is being detected.

The majority of chemodosimeter for hypochlorite rely on *oxidation*; indeed ClO^- is well known, even at a household level, as a strong oxidising agent. The most common triggers include the oxidation of *p*-hydroxy and *p*-aminophenyl ethers to give quinones or iminoquinones (Section 4.2.1) although the *p*-aminophenyl ethers typically elicit a larger response to ClO^- and are more selective over $ONOO^-$ (*versus p*-hydroxy). Oximes provide a pathway for non-radiative decay and are also readily react with hypochlorite (Section 4.2.2). As for probes that target $ONOO^-$, the oxidation of S, Se, and Te has been employed in spirocyclic ring opening triggers for fluorescein and rhodamine dyes. This class of probe (notably the Se and Te based examples) are conveniently reversible as they can be reduced back to the parent structure by thiols (*e.g.* Cys, GSH) or hydrosulfide.

4.2.1 Hypochlorite mediated oxidation/fragmentation. An early example of a "switch on" probe for ClO^- was reported by Nagano in 2003.[305] Nagano's fluorescein system used hypochlorite to oxidise either a pendant *p*-hydroxyphenyl ether (**HPF**) or *p*-aminophenyl ether (**APF**) attached to the fluorescein fluorophore. Removal of the phenyl ethers (as the corresponding quinone or aminoquinone) restored ICT and gave rise to high fluorescence emission (λ_{em} = 514 nm, Φ_F = 0.81). Unfortunately, and confirming the challenging nature of selective ClO^- detection, **HPF** was more reactive towards $HO^\bullet$ and to a lesser extent $ONOO^-$. The second probe **APF** also gave a fluorescence response to $HO^\bullet$ and $ONOO^-$ which was greater than **HPF** but unlike **HPF**, **APF** gave a large response when treated with hypochlorite. While **HPF** and **APF** were not completely selective, the difference in reactivity was demonstrated in neutrophils which contain azurophilic granules that are abundant in the ClO^- generating MPO enzyme. Both **APF** and **HPF** loaded neutrophils were stimulated with PMA to stimulate endogenous ClO^- production and fluorescence images were collected after 10 minutes. Only the cells containing **APF** exhibited a significant increase in fluorescent emission.

An extension on the Nagano fluorescein system was reported in 2007 by Libby,[306] whereby the *p*-aminophenyl ether moiety was attached to a water soluble sulfonaphthofluorescein (**SNAPF**, Fig. 82). Oxidation with hypochlorite resulted in the expulsion of the aminoquinone moiety to reveal a fluorescein derivative with an extended π-system (λ_{em} = 676 nm). **SNAPF** was then used to detect hypochlorite produced by human neutrophils stimulated with PMA (Fig. 83). When a MPO inhibitor was co-administered in stimulated cells no fluorescence was observed, indicating that MPO produced hypochlorite was being detected. **SNAPF** was also used to detect hypochlorite in stimulated mouse macrophages transgenic for human MPO (h-MPOTg) and stimulated human MPO-containing macrophages. Using **SNAPF** the successful bioimaging of hypochlorite generated *in vivo* was also performed in h-MOPTg mice with thioglycollate induced peritonitis. The **SNAPF** probe was administered 24 hours after thioglycollate stimulation, and after a further hour a 1.4-fold increase in fluorescence was observed.

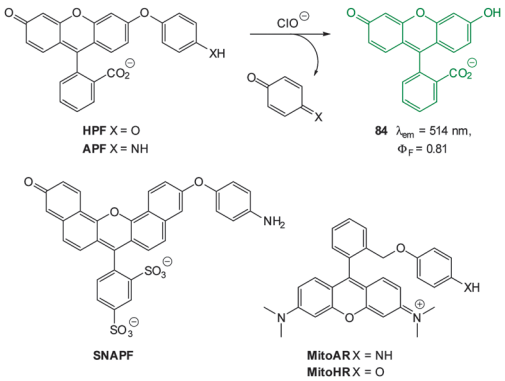

Fig. 82 Structures of "switch on" probes for ClO^- that function by oxidative cleavage.

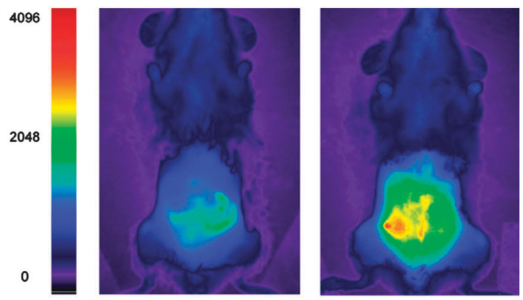

Fig. 83 *In vivo* demonstration of **SNAPF**: (left) h-MPOtg mouse with thioglycollate induced peritonitis pre-**SNAPF** injection; (right) the same animal post-injection of **SNAPF**. No visible fluorescence was observed when **SNAPF** was injected into mice that had been injected with saline solution as opposed to thioglycollate, nor was there any increase in fluorescence of a wavelength-matched control dye, **SNAPF**, when injected into mice with peritonitis compared to saline-injected animals (n = 4 per group). Image reproduced with permission.[306]

In conjunction with a rhodamine fluorophore the *p*-aminophenyl ether trigger (**MitoAR**, Fig. 82) was also exploited by Nagano (2007).[307] It was envisaged that the inherent positive charge of the ring open rhodamine would lead to accumulation of the probe within the mitochondria of living cells. In this instance the phenyl ether was located in the 2-position of the phenyl substituent in an effort to facilitate PET to the xanthene. Hypochlorite mediated oxidation of the *p*-aminophenyl ether correlated with a large increase in fluorescence response (λ_{em} = 574 nm) but only moderate selectivity over $HO^\bullet$ was noted. Nevertheless, **MitoAR** was used to monitor the MPO-catalysed production of mitochondrial ROS in HL-60 cells using H_2O_2 stimulation (Fig. 84).

Yuan *et al.* successfully employed the 4-amino-3-nitrophenyl moiety as a hypochlorite responsive PET trigger to modulate the luminescence of terpyridine polyacid lanthanide complexes, **ANMTTA-Tb(III)** and **ANMTTA-Eu(III)** (Fig. 85).[308] Oxidation of the 4-amino-3-nitrophenyl substituent gave the benzofurazan-1-oxide (BFO), which reacted with a further equivalent of ClO^- to restore the luminescent terbium and europium complexes **HTTA-Tb(III)** and **HTTA-Eu(III)**. Probe **ANMTTA-Eu(III)** was used for the time-gated spatiotemporal luminescence visualisation

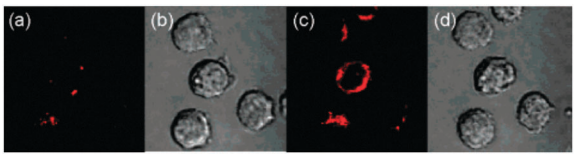

Fig. 84 Detection of endogenous ClO^- generation in mitochondria using **MitoAr**: (a, b) fluorescence and bright-field images of HL-60 cells loaded with **MitoAR** (c, d) 10 min after addition of H_2O_2. Image reproduced with permission.[307]

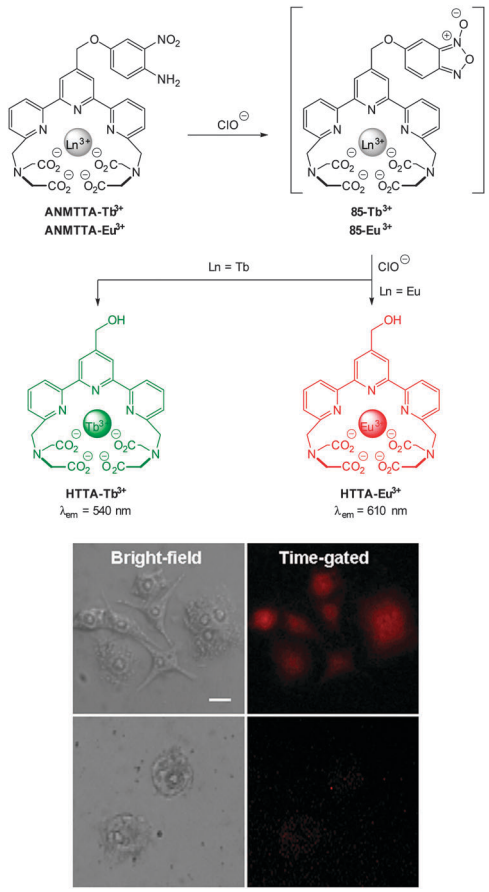

Fig. 85 Top: structures of **ANMTTA-Tb(III)**, **ANMTTA-Eu(III)** and their reaction with ClO^-. Bottom: time-gated luminescence images of the **ANMTTA-Eu(III)** loaded RAW264.7 macrophage cells after stimulation with LPS/IFN-γ/PMA (top) or stimulated with LPS/IFN-γ/PMA/4-aminobenzoic acid hydrazide (**ABAH**). Scale bar: 10 μm. Image reproduced with permission.[308]

of exogenous hypochlorite in HeLa and in LPS/IFN-γ/PMA-stimulated RAW264.7 macrophages. Addition of the MPO inhibitor, ABAH, to cells resulted in no fluorescence emission.

An elegantly designed system **HKOCl-1** (Fig. 86), related to the aforementioned probes, was reported by Yang in 2008.[309] This example used a BODIPY fluorophore which was suitably quenched ($\Phi_F < 0.01$) by a *p*-methoxyphenol substituent by means of PET. Oxidative demethylation of **HKOCl-1** to the quinone (**HKOCl**) was effected by hypochlorite; the greater oxidation potential of the quinone makes PET unfavourable and fluorescence is "switched on" (λ_{em} = 541 nm). This process

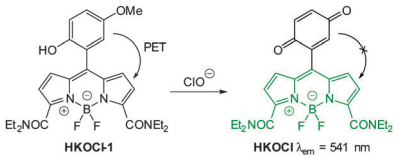

Fig. 86 Structure and reaction of **HKOCl-1** with ClO^-.

was selective for hypochlorite, with $ONOO^-$ eliciting a response only at a 10-fold higher concentration. The probe was used for the visualisation of live MPO producing RAW264.7 murine macrophages stimulated using lipopolysaccharide (LPS), interferon-γ (IFN-γ) and PMA. Stimulated cells showed an increase in the fluorescent output compared to the control. Additionally, when cells were stimulated in the presence of 2,2,6,6-tetramethylpiperidinooxy (TEMPO), much weaker fluorescent was observed. TEMPO is a known superoxide ($O_2^{\bullet -}$) scavenger which is an intermediate in hypochlorite synthesis from the MPO system.

In 2012 Yao reported the dihydrofluorescein based probe **FCN2** (Fig. 87) which, unlike preceding examples, is triggered by oxidation dealkylation rather than spirocycle ring opening.[310] Ether cleavage from **FCN2** restores the ICT of the dihydrofluorescein system (**86**) and results in a 1643-fold increase in fluorescent intensity (λ_{em} = 485 nm, Φ_F = 0.71). **FCN2** was completely soluble in aqueous solution and, although some autooxidation was noted (over 24 h), reacted rapidly enough (30 min) to be applicable for *in vitro* (NIH3T3 cells) and *in vivo* applications (larval and adult zebrafish). The fluorescent response generated from the treatment of 3 month old zebrafish with exogenous hypochlorite and **FCN2**, indicated the accumulation of hypochlorite in gall bladder, intestine, eye, liver and eggs.

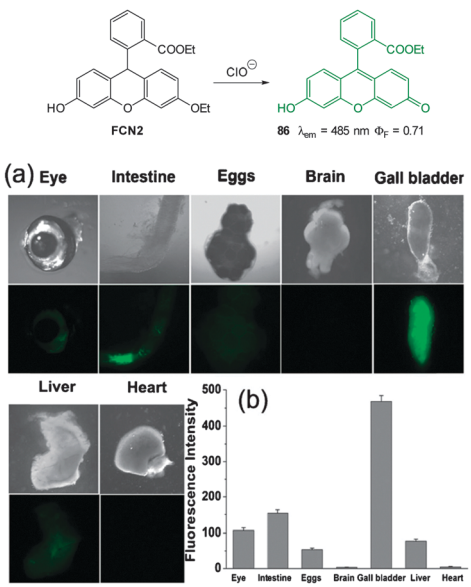

Fig. 87 Adult zebrafish were (a) exposed to ClO^- in E3 embryo media then incubated with **FCN2**. (b) The average emission intensities of isolated organs. Image reproduced with permission.[310]

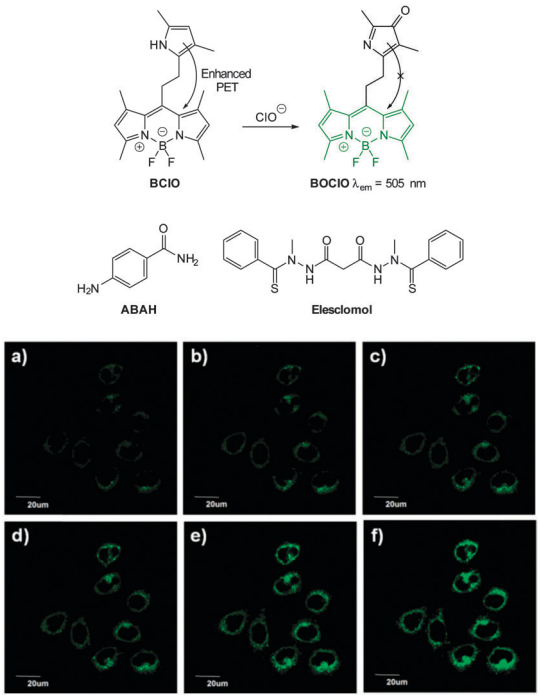

Fig. 88 Top: structure and reaction of **BClO** with hypochlorite. Middle: structures of **ABAH** and **elesclomol**. Bottom: live MCF-7 cells were cultured with **BClO** then confocal fluorescence images were recorded after the addition of **elesclomol** at different time points: (a) 0, (b) 30, (c) 60, (d) 90, (e) 120, and (f) 180 min. Image reproduced with permission.[311]

Peng and co-workers reported the oxidation-activated "enhanced PET" BODIPY-based probe **BClO** (Fig. 88) which was synthesised in an exquisite two step procedure from 2,4-dimethylpyrrole.[311] The PET quenching was mediated by a pendant pyrrole unit which was envisaged to provide "enhanced PET" compared to single electron donors (such as heavy metal containing probes). The resultant probe, **BClO** was essentially non-fluorescent at λ_{em} = 505 nm (Φ_F = 0.006), however, oxidation with hypochlorite afforded the pyrrol-3-one **BOClO** in which PET was restricted and a 56-fold "switch on" fluorescence response was observed (Φ_F = 0.347). In solution studies **BClO** was highly sensitive to hypochlorite with a limit of detection of 0.56 nM. Facilitated by the remarkable sensitivity of **BClO** the authors determined the basal hypochlorite levels in MCF-7 and HeLa cancer cell lines. When incubated with **BClO** (1 μM) for 20 min at 37 °C, both MCF-7 and HeLa displayed an increased fluorescence response (in relation to healthy COS-7 and RAW264.7 cells) corresponding to intracellular ClO^- concentrations of 9.45 nM and 8.23 nM respectively. In both of the cancer cell lines visualised, pre-treatment with the antioxidant GSH or 4-aminobenzoic acid hydrazide (ABAH, an MPO inhibitor) resulted in a significant drop in fluorescence response. The authors suggest that it may be possible to use **BClO** in a diagnostic capacity; differentiating healthy and cancer cells based on endogenous hypochlorite concentration. The utility of **BClO** was further demonstrated by the detection of hypochlorite produced in MCF-7 cells stimulated with elesclomol (an ROS generating anticancer agent).

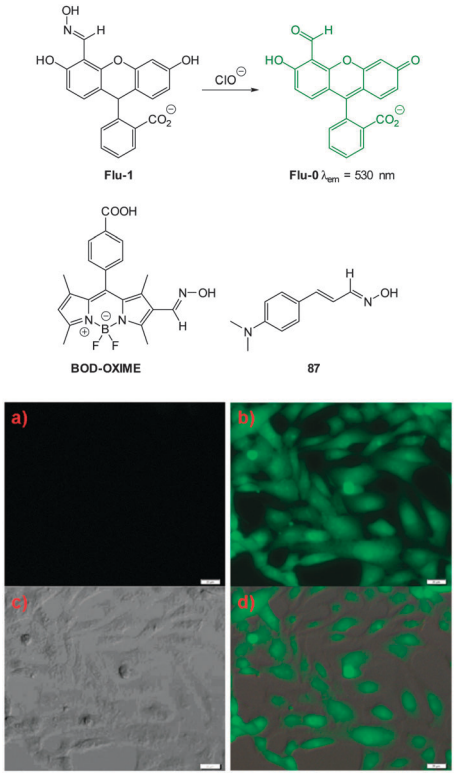

Fig. 89 Top: structure, and reaction of, **Flu-1** with ClO^-. Middle: structures of **BODOXIME** and **87**. Bottom: (a) image of HeLa cells incubated with **Flu-1** (20 μM) for 30 min. (b and c) Fluorescence and bright-field images of cells pre-treated with **Flu-1** then incubated with ClO^- for 30 min. (d) Overlay image of (b) and (c). Image reproduced with permission.[313]

4.2.2 Hypochlorite mediated oxime/imine oxidation. An early example of a probe that used the oxime oxidation approach (**Flu-1**, Fig. 89) was published by the Li group in 2011.[312] The emissive species (λ_{em} = 530 nm, Φ_F = 0.65) was an aldehyde containing fluorescein derivative (**Flu-0**) and when the aldehyde was protected as the oxime (**Flu-1**), fluorescence was effectively quenched (Φ_F = 0.01). Probe **Flu-1** displayed good selectivity against a suite of anionic species, however screening against ROS such as $ONOO^-$, $HO^•$, $O_2^{•-}$ *etc.* was not performed. Importantly, **Flu-1** failed to illicit a fluorescent response with H_2O_2 and bioimaging of exogenous hypochlorite was successfully demonstrated using HeLa cells incubated with **Flu-1**.

Wu, Zeng and Wu (2013) employed the same oxime/aldehyde strategy using a BODIPY fluorophore.[313] The water soluble **BOD-OXIME** (Fig. 89) was poorly fluorescent (Φ_F = 0.04) but reacted in a dose dependant "switch on" manner (LOD = 17.7 nm) with hypochlorite to give **BOD-CHO** which exhibited extraordinary fluorescence in aqueous solutions (Φ_F = 0.96, λ_{em} = 525 nm). The visualisation of both exogenous (ClO^-) and endogenous hypochlorite (PMA stimulation) in RAW264.7 macrophages was successfully demonstrated. Selectivity for ClO^- *in vitro* was excellent as no emission was observed when ABAH or taurine (a ClO^- scavenger) were added to the PMA stimulated cells.

A recent report from the Kumar group in 2014 identified 4-dimethylaminocinnimaldehyde oxime **87** (Φ_F = 0.008, Fig. 89)

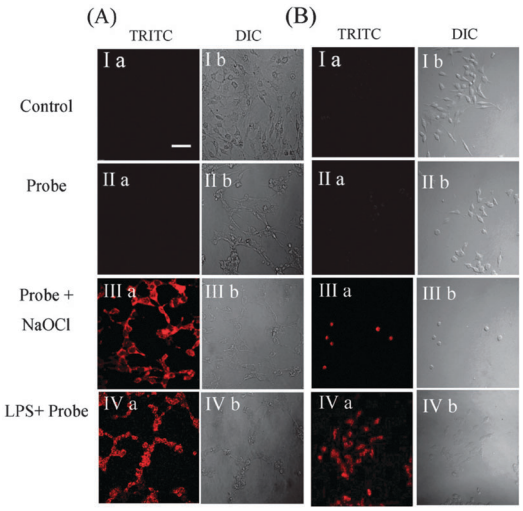

Fig. 90 Fluorescence and DIC images of C6 glial (A) and BV2 microglial (B) cell lines. (Ia) Control of C6 glial and BV2 microglial cell lines respectively. (Ib) DIC images of Ia. (IIa) Images of C6 glial and BV2 microglial cells with **87**. (IIb) DIC images of IIa. (IIIa) Red fluorescence images of C6 glial and BV2 microglial cells with **87** and NaOCl. (IIIb) DIC images of IIIa. (IVa) Red fluorescence images of C6 glial and BV2 microglial cells with **87** and LPS. (IVb) DIC images of IVa. Scale = 50 nm. Image reproduced with permission.[314]

as a selective ''switch on'' probe for hypochlorite.[314] Oxidation with hypochlorite gave the nitrile oxide and this group participates in an extended ICT system leading to strong emission at 556 nm (Φ_F = 0.51). The formation of the nitrile oxide was confirmed by spectroscopic means (^{1}H and ^{13}C NMR) and by *in situ* trapping using 2-butene to give the 4,5-dihydroisoxazole. The ability of probe **87** to visualise endogenous and exogenous hypochlorite was demonstrated using the brain resident murine macrophages (BV2 microglial) and C6 glial cell lines (Fig. 90). Addition of exogenous NaOCl and also LPS stimulated endogenous hypochlorite production led to increased fluorescence.

The first ratiometric fluorometric probe for hypochlorite was developed by Yuan using an analogous approach to those above.[315] The probe consists of a diaminomaleonitrile derived imine **88** of aminocoumarin aldehyde **89** (Fig. 91) The weakly fluorescent imine (λ_{em} = 585 nm, Φ_F = 0.02) reacted with hypochlorite to give the parent aldehyde and a bathochromic shift to an emission maximum centred at λ_{em} = 505 nm (Φ_F = 0.59) was observed. At physiological pH a marked increase in emission ratio (F_{505}/F_{585}) from 0.12 to 28.2 was observed after the probe was treated with hypochlorite. Probe **88** was successfully used to visualise exogenous hypochlorite in MCF-7 cells.

4.2.3 Hypochlorite mediated ring opening. A number of rhodamine based systems which react specifically with hypochlorite have been reported in recent years. Work in this area was pioneered by Nagano in 2007 with the rhodamine thioether spirocycle **HySOx**.[316] The thioether was critical for the stability of the closed form of the **HySOx** probe, particularly at higher pH. Hypochlorite oxidation of the thioether triggers ring opening and fluorescence ''switch on'' (λ_{em} = 575 nm, Φ_F = 0.34). Utilising this sensitivity to hypochlorite

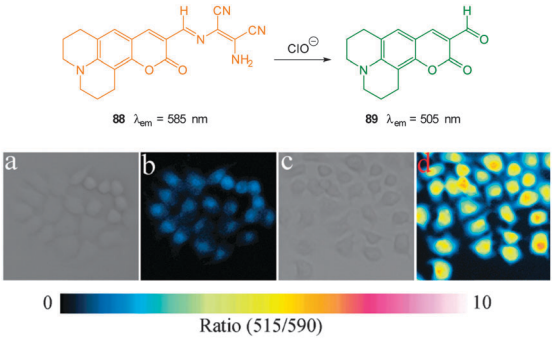

Fig. 91 Top: structure and reaction of aminocoumarinimine **88** with ClO^- (a) bright-field image of live MCF-7 cells incubated with only probe **88** (b) fluorescence ratio image (F_{505}/F_{585}) of (a); (c) bright-field image of live MCF-7 cells incubated with probe **88** then with ClO^-; (d) fluorescence ratio image (F_{505}/F_{585}) of (c). Image reproduced with permission.[315]

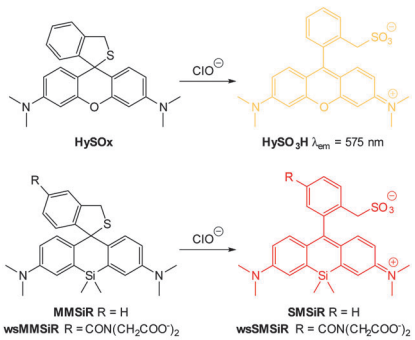

Fig. 92 Structure and spirocycle ring opening reactions of **HySOx** and **MMSiR** with hypochlorite.

the authors were able to image phagocytosis in porcine neutrophils.

In an extension of this work, Nagano (2011) reported the silylrhodamine analogue **MMSiR** (Fig. 92).[317] The isosteric replacement of oxygen with silicon resulted in a significant red-shift in the emission wavelength to the near-infrared (NIR) region (λ_{em} = 670 nm, ϕ_F = 0.31). Similar to **HySOx**, the **MMSiR** probe was also used in the imaging of phagocytosis. In addition the hydrophilic probe **wsMMSiR** was synthesised and applied to the *in vivo* imagining of hypochlorite in a mouse peritonitis model (Fig. 93). In this study C57BL/6 mice were treated with an intraperitoneal injection of zymosan to stimulate neutrophil invasion of the peritoneal cavity. Injection of **wsMMSiR** and PMA resulted in enhanced fluorescence emission in the abdomen.

Using a more traditional rhodamine fluorophore, Yoon (2007) developed both a thio- and selenoester trigger for selective ClO^- sensing.[318] Upon reaction with hypochlorite, the non-fluorescent **R19-S**, **R19-Se** and **R101-S** undergo ring opening and fluorescence is ''switched on'' at λ_{em} = 550 nm, 545 nm and 585 nm respectively (Fig. 94). Probe **R19-S** was used to visualise hypochlorite production in phagocytes and microbial hypochlorite generation in intestinal epithelia of *Drosophila melanogaster*.

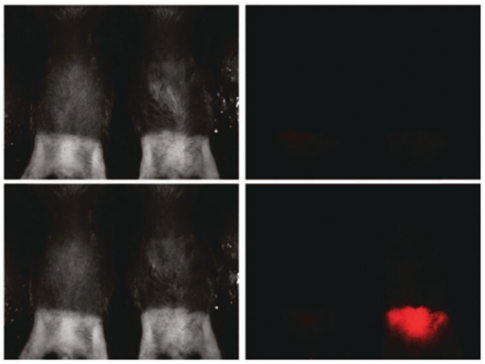

Fig. 93 Comparison of white light (left panels) and fluorescence (right panels) images of unstimulated mouse (left) and the peritonitis model mouse stimulated with zymosan and PMA (right). **wsMMSiR** and PMA were successively administered by intraperitoneal injection. Images were obtained just before (top) and 60 min after (bottom) PMA injection. Image reproduced with permission.[317]

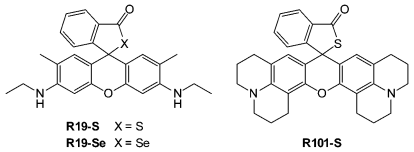

Fig. 94 Structure of the rhodamine probes developed by Yoon containing S and Se triggers.

In the last few years a number of diacylhydrazine–rhodamine probes have been reported. These probes rely on selective oxidation by hypochlorite to give a diacyl diimide, then subsequent hydrolysis reveals the fluorescent rhodamine. An early example of this approach was reported by Ma and co-workers although high pH was required (pH 12).[319] Modifications to the benzoyl substituent can be used to tailor probes which are more suited for imaging purposes. For example, by using a pendant alkoxyquinoline moiety (**RHQ**, Fig. 95) Goswami and co-workers were able to image endogenous hypochlorite in human peripheral blood mononuclear cells (PBMCs).[320] A similar fluorescein based system (**90** R=O and **91** R=S, Fig. 95) from the Li group was used to monitor hypochlorite in *Rhodobacter ferrooxidans* prokaryotes as a potential model for hypochlorite induced stress.[321]

In the last few years a number of diacylhydrazine–rhodamine probes have been reported. These probes rely on selective oxidation by hypochlorite to give a diacyl diimide, then subsequent hydrolysis reveals the fluorescent rhodamine. An early example of this approach was reported by Ma and co-workers although high pH was required (pH 12).[319] Modifications to the benzoyl substituent can be used to tailor probes which are more suited for imaging purposes. For example, by using a pendant alkoxyquinoline moiety (**RHQ**, Fig. 95) Goswami and co-workers were able to image endogenous hypochlorite in human peripheral blood mononuclear cells (PBMCs).[320] A similar fluorescein based system (**90** R=O and **91** R=S, Fig. 95) from the Li group was used to monitor hypochlorite in *Rhodobacter ferrooxidans* prokaryotes as a potential model for hypochlorite induced stress.[321]

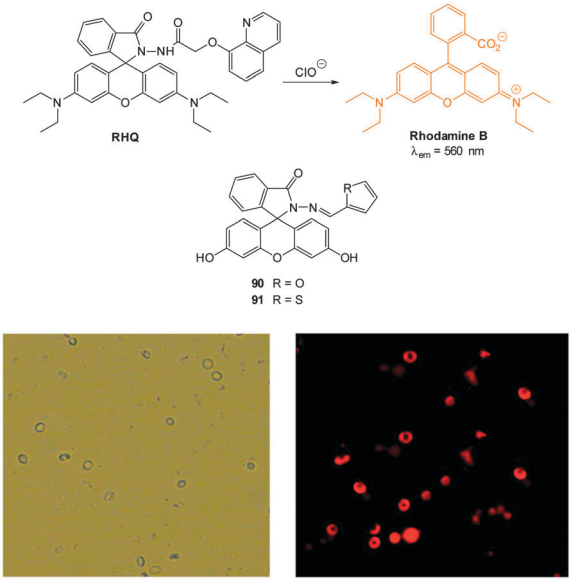

Fig. 95 Top: structure of **RHQ** probe and related probes **90** and **91**. Bottom: (left) bright field image of PBMCs (40×), (right) fluorescence image of PBMCs (40×) treated with **RHQ**. Image reproduced with permission.[320]

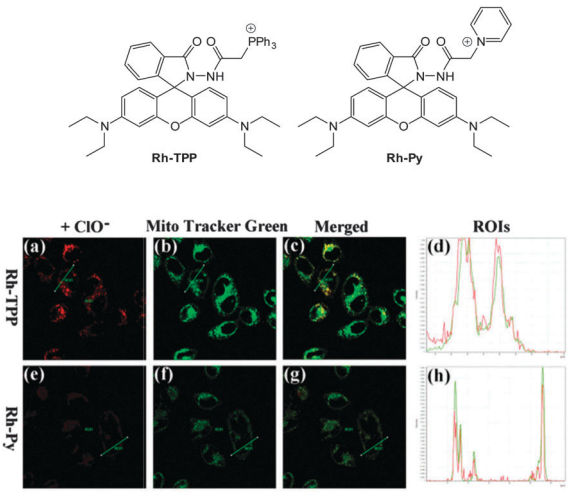

Fig. 96 Top: structure of mitochondria targeting probes **Rh-TPP** and **Rh-Py** Bottom: HeLa cells were stained with **Rh-TPP** or **Rh-Py**, incubated with ClO^-, then Mito Tracker Green was added. (a) and (e): Fluorescence images of **Rh-TPP** and **Rh-Py** with ClO^-; (b) and (f): the fluorescence images of Mito Tracker Green; (c) and (g): merged images; (d) and (h): intensity profile of ROIs across HeLa cells. Red lines represent the intensity of synthetic probes and green lines represent the intensity of Mito Tracker Green. Scale = 25 μm. Image reproduced with permission.[99]

In 2014 Hou *et al.* employed this trigger in the mitochondria targeting probes **Rh-TPP** and **Rh-Py** (Fig. 96).[99] The incorporation of a phosphonium (**Rh-TPP**) or pyridinium ion (**Rh-Py**) onto the probe facilitated the imaging of exogenous hypochlorite in the mitochondria of HeLa cells.

The ability of **Rh-TPP** and **Rh-Py** to visualise hypochlorite *in vivo* was also demonstrated (Fig. 97). Nude mice were injected with either probe followed by an injection with a ClO^-

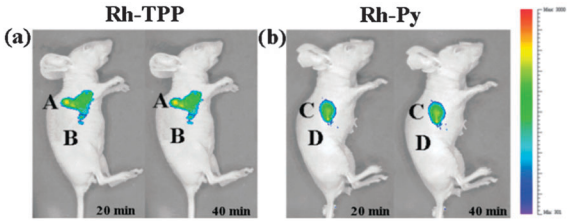

Fig. 97 Representative fluorescence images (pseudocolor) of nude mice given a skin-pop injection of (a) **Rh-TPP** and (b) **Rh-Py** (region A and C, respectively) and a subsequent skin-pop injection of ClO^-. Representative fluorescence images (pseudocolor) of nude mice given a skin-pop injection of (a) **Rh-TPP** and (b) **Rh-Py** region B and D, respectively). Images were taken after incubation for 20 and 40 min, respectively. Image reproduced with permission.[99]

solution. In each case a persistent fluorescent response was elicited from hypochlorite.

A hydroxamic acid variant of this approach was outlined by Shin and Tae in 2013.[322] In this case it was proposed that the hydroxamic acid was oxidised to the corresponding ring opened acyl nitroso group and it was anticipated that this product was rapidly hydrolysed to **rhodamine 19** (λ_{em} = 547 nm). Probe **92** (Fig. 98) could detect hypochlorite concentration at *ca.* 25 nM. Of interest, when the exocyclic amines had an additional ethyl substituent, or were replaced by hydroxyl groups (fluorescein) the probes did not respond to hypochlorite, even when a 20-fold excess was administered.

Probe **92** could be used to detect exogenous hypochlorite in A549 lung cancer cells with a clear dose responsive fluorescence "switch on" with increasing ClO^- concentration (Fig. 99). Furthermore **92** was successfully used for the *in vivo* detection of exogenous hypochlorite added to live zebrafish.

4.2.4 Hypochlorite mediated chalcogen oxidation. In 2013 Wu and Liu described the PET based BODIPY probe **HCSe** (Fig. 100) for hypochlorous acid.[323] In this instance the BODIPY fluorophore was functionalised with a 2-(phenylselenyl)phenyl substituent and the presence of the selenide quenches fluorescence by PET (Φ_F = 0.005). When oxidised by hypochlorite, the corresponding selenoxide (**HCSeO**) is formed and PET is unfavoured and BODIPY fluorescence is restored (λ_{em} = 526 nm, Φ_F = 0.690). Using RAW264.7 cells the utility of this probe *in vitro* was explored; cells were pre-treated with **HCSe**

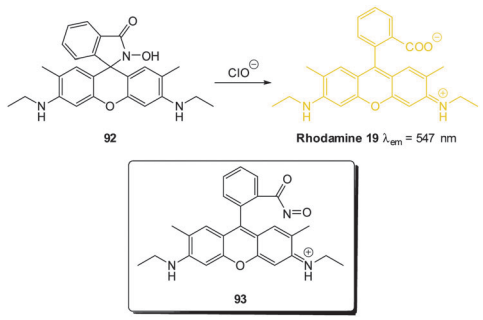

Fig. 98 Structure and reaction of **92** with hypochlorite. Inset shows proposed acylnitroso intermediate **93**.

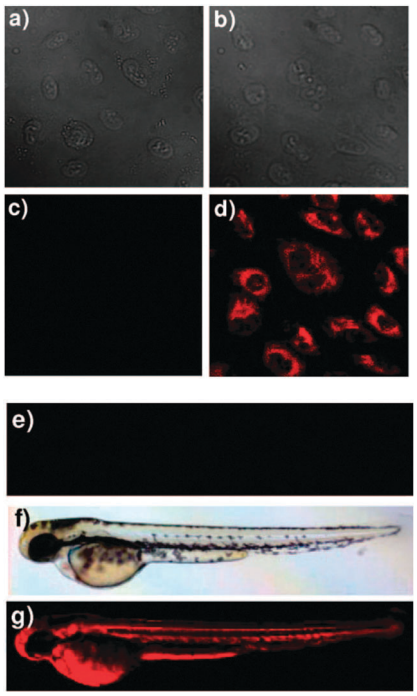

Fig. 99 Bright field image of A549 cells treated with (a) **92** in the absence of ClO^-. (b) With both ClO^- and **92**. Fluorescence image of A549 cells treated with (c) **92** in the absence of ClO^-. (d) Both ClO^- and **83**. Fluorescence images of zebrafish treated with (e) **92** in the absence of ClO^-. (f) Bright field image of zebrafish treated with **92** and ClO^- (g) fluorescence images of zebrafish treated both **92** and ClO^-. Image reproduced with permission.[322]

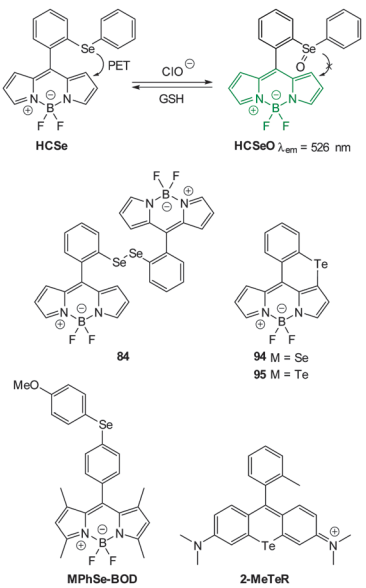

Fig. 100 Structures of Se and Te containing probes for ClO^-.

and upon addition of ClO^- enhanced fluorescence emission was detected. Subsequent treatment of these cells with glutathione (GSH) resulted in the loss of fluorescence intensity, indicating that the selenoxide (**HCSeO**) could be reduced back to its non-emissive precursor. Similarly, the endogenous

production of hypochlorite could be visualised in RAW264.7 cells that were stimulated using PMA.

Structurally similar annulated BODIPY chalcogenides (discovered somewhat serendipitously during the synthesis of dichalcogenides such as **93**) were reported by Churchill in 2013.[324] These unexpected annulated heterocycles were formed by base induced S_EAr reaction of the dipyrrole dichalcogenide (**93**) and their structure confirmed by means of an X-ray structure of the selenide derivative (**94**). It is of note that the diselenide **93** has been utilised as a reversible superoxide probe.[325] Despite not being applied to a living system, the annulated tellurium BODIPY (**95**) was shown to be at least 62-fold selective for ClO^- over other ROS ($O_2^{\bullet -}$, H_2O_2, ^{t}BuOOH, ClO^-, $HO^\bullet$, and ^{t}BuO$^\bullet$) under physiological conditions (0.1 M PBS/EtOH (99 : 1 v/v), pH 7.5). Following oxidation with hypochlorite, PET from the tellurium was blocked and fluorescence was "switched on" (λ_{em} = 597 nm, Φ_F increased from 0.06 to 0.23). Similar to **HCSe**, telluride oxidation could be reversed by treatment with GSH.

MPhSe-BOD is weakly fluorescent (Φ_F = 0.13, λ_{em} = 510 nm) due to a Se modulated PET process.[326] Hypochlorite oxidation interrupts the PET process and restores strong fluorescence (**MPhSeO-BOD**, Φ_F = 0.96). The reverse process (reduction) is selectively performed by HS^-. The probe was used to visualise endogenously produced hypochlorite in PMA stimulated RAW264.7 macrophages. The role of hypochlorite was confirmed by comparison to taurine and xanthine–xanthine oxidase controls. Imaging of the redox cycling between hypochlorite and HS^- was also demonstrated in RAW264.7 cells.

The tellurium containing rhodamine system (**2-MeTeR**, $\Phi_F < 0.001$) presented by Nagano in 2012 has the advantage that its oxidised form (**2-MeTeOR**) is red emissive (λ_{em} = 686 nm, Φ_F = 0.18).[327] However, this probe suffers from interference from other ROS such as $HO^\bullet$ and $ONOO^-$. Nevertheless the probe was used to visualise endogenously produced ROS in human promyelocytic leukemia (HL-60) cells following stimulation with H_2O_2. As the added H_2O_2 was consumed by MPO and/or the reaction was reversed by intracellular reductants, the increased fluorescent intensity was short lived. Fluorescence was restored following a second addition of H_2O_2 (Fig. 101). Fluorescence intensity was also reduced when the cells were treated with aminobenzoic acid hydrazide (ABAH).

In 2013 the Han group reported the 4-aminonaphthalimide-based hypochlorite sensor **NI-Se**, shown in Fig. 102.[328] While related to the aforementioned examples, the selenide was non-fluorescent (Φ_F = 0.04) and oxidation gave the fluorescent selenoxide **NI-SeO** (λ_{em} = 523 nm, Φ_F = 0.45). Unlike the previously described selenide–selenoxide systems fluorescence was not modulated by a PET mechanism. Instead, the 2-(phenylselenyl)benzyl moiety induced an excited state configurational twist which was not present in the oxidised **NI-SeO**. The reduction of the selenoxide could be reversed by the addition of HS^- to the system; this process was repeated up to six times with a decrease in fluorescence intensity of 50%. Cellular imagining of **NI-Se** was performed using mouse macrophage RAW264.7 cells stimulated with LPS and PMA and enhanced

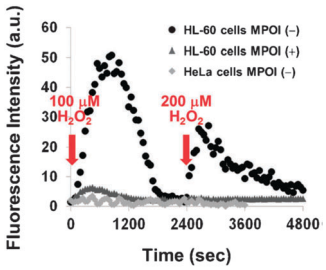

Fig. 101 Time courses of the change in fluorescence intensity observed with **2-MeTeR** for H_2O_2-stimulated or unstimulated HL-60 cells or H_2O_2-stimulated HeLa cells. H_2O_2 (100 μM and 200 μM final concentration) was added at 100 s and 2400 s, respectively. The myeloperoxidase inhibitor (MPOI) is aminobenzoic acid hydrazide (**ABAH**; 2 mM). The fluorescence intensity was measured at 690 nm with excitation at 660 nm. Image reproduced with permission.[327]

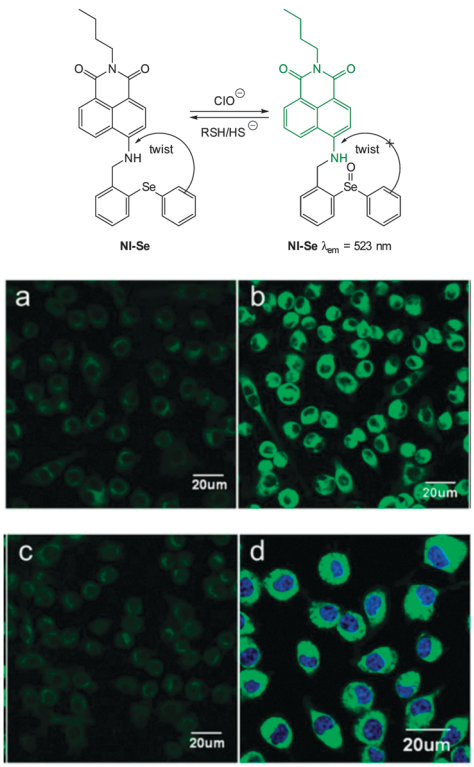

Fig. 102 Top: structure and reaction of **NI-Se** with hypochlorite. Bottom: fluorescence images of ClO^- in living RAW264.7 cells. (a–c) Cells were pretreated with LPS. (a) Incubated with **NI-Se**. (b) Incubated with **NI-Se** and then with PMA. (c) Incubated with **SHA** and co-incubated with PMA, then incubated with **NI-Se**. (d) RAW264.7 cells loaded with Hoechst 33342 and **NI-Se**. Image reproduced with permission.[328]

fluorescence was observed. Weak fluorescence was also observed when cells were pre-treated with salicylhydroxamic acid (SHA), a known inhibitor of MPO. A similar result was obtained with the use of a ROS scavenger glutathione S-transferase (GST, EC: 2.5.1.18). Co-staining with Hoechst 33342 revealed that probe was located mainly in the cytosol.

NI-Se was also used in living mice for the *in vivo* imaging of hypochlorite produced in a LPS model of acute inflammation (Fig. 103). Similar to the *in vitro* study, when LPS was injected,

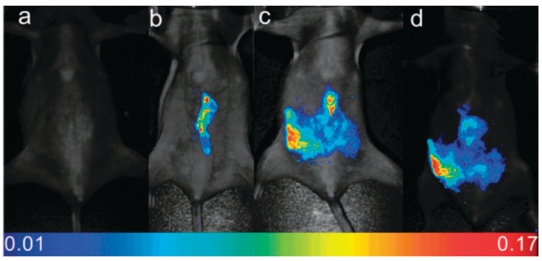

Fig. 103 Fluorescent images of ClO^- production and HS^- reduction in the peritoneal cavity of the mice with **NI-Se**. (a) Control, neither LPS nor **NI-Se** was injected; (b) saline was injected in the intraperitoneal (i.p.) cavity of mice, followed by i.p. injection of **NI-Se**; (c) LPS was injected into the peritoneal cavity of the mice, followed by i.p. injection of **NI-Se**. (d) An additional HS^- was injected in parallel to (c). Image reproduced with permission.[328]

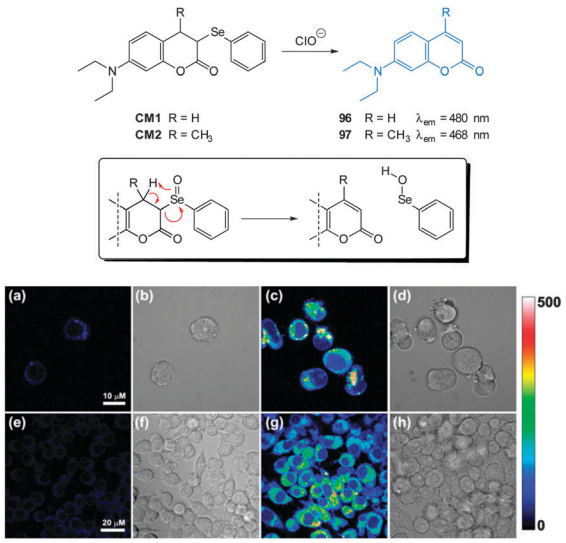

Fig. 104 Top: structure of **CM1** and **CM2** and the mechanism of their reaction with ClO^-. Bottom: (a) fluorescence images of HL-60 cells with **CM1** (b) bright-field images of cells in panel (a). (c) After addition of H_2O_2 (d) bright-field images of cells in panel (c). (e) Fluorescence images of RAW264.7 cells with **CM1** (f) bright-field images of cells in panel (e). (g) Cells loaded with **CM1** then LPS (h) bright-field images of cells in panel (g). Image reproduced with permission.[329]

followed by **NI-Se**, an enhanced signal was collected compared to the control (**NI-Se** only). Injection of HS^- resulted in a decrease in fluorescence emission.

A new strategy for the detection of hypochlorite involving a selenide containing probe was presented by Li *et al.* in 2013.[329] The partially reduced coumarin derivatives **CM1** and **CM2**, (Fig. 104) each bearing a 3-phenylselenyl moiety were synthesised and both were non-fluorescent ($\Phi_F < 0.001$). In this instance the selenoxide produced from hypochlorite oxidation underwent a cope-type elimination to give the corresponding fluorescent reporters **96** (λ_{em} = 480 nm, Φ_F = 0.036) and **97** (λ_{em} = 468 nm, Φ_F = 0.047). The utility of probe **CM1** was demonstrated *in vitro*, by the quantitative determination of exogenous hypochlorite in NIH3T3 cells. **CM1** was also used to indicate the endogenous formation of hypochlorite in H_2O_2 stimulated HL-60 human progranulocytic leukemia cell lines and RAW264.7 macrophages stimulated with lipopolysaccharide (LPS). In both of these instances there was a significant enhancement of the fluorescent response in relation to the controls.

A PET-based $Ru(bpy)_3^{2+}$ based probe for the monitoring of ClO^-/HS^- redox cycle was developed by the Sun group in 2014 (Fig. 105).[330] A pendent phenothiazine (PTZ) was attached to one of the 2,2′-bipyridine ligands, which suppressed fluorescence emission from the complex. Upon oxidation of the PTZ sulfur with ClO^- the fluorescence emission was restored (λ_{em} = 605 nm, λ_{ex} = 450 nm, Φ_F = 0.39). This process could be reversed with HS^- in a recyclable fashion (12 cycles). The authors were able to visualise this ClO^-/HS^- redox cycle in live mice; weak fluorescence was observed after administration of probe **98** and this response was modulated during alternating additions of ClO^- and HS^-.

The groups of Wang and Peng reported a cyanine–phenothiazine hybrid probe, **PTZ-Cy2** which was sensitive to both hypochlorite and $HO^•$.[331] The sulphur atom of the non-fluorescent probe was initially oxidised by OCl^- and/or $HO^•$ to give the fluorescent sulfoxide **OPTZ-Cy2** which gave a pink emission (λ_{em} = 595 nm). Continued addition of OCl^- to **OPTZ-Cy2** led to a blue shifted emission (λ_{em} = 470 nm) resulting from the degradation of the conjugated cyanine alkene to the aldehyde **OPTA**. This blue shifted emission was not seen during $HO^•$ addition, rather, excessive $HO^•$ lead to a decrease in the total emission indicating decomposition. **PTZ-Cy2** was used to visualise the ROS in PMA stimulated HeLa cells (Fig. 106). Co-staining with MitoTracker Deep Red FM indicates that fluorescence resulting from **PTZ-Cy2** and **OPTZ-Cy2** was localised in the mitochondria. Non-mitochondrial fluorescence was ascribed to the non-charged **OPTA** diffusing away from the mitochondria.

4.2.5 Miscellaneous. Lin and co-workers developed a series of rhodamine–merocyanine hybrid probes which absorb and

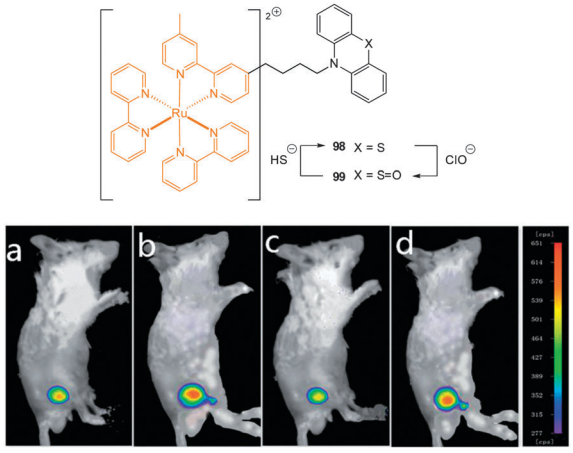

Fig. 105 The luminescence imaging of the redox cycle between ClO^- and HS^- in live mice: (a) **98** was loaded into the leg cortex of the mice; (b) ClO^- was loaded in the same position; (c) HS^- was loaded in the same position; and (d) another ClO^- was loaded in the same position. Image reproduced with permission.[330]

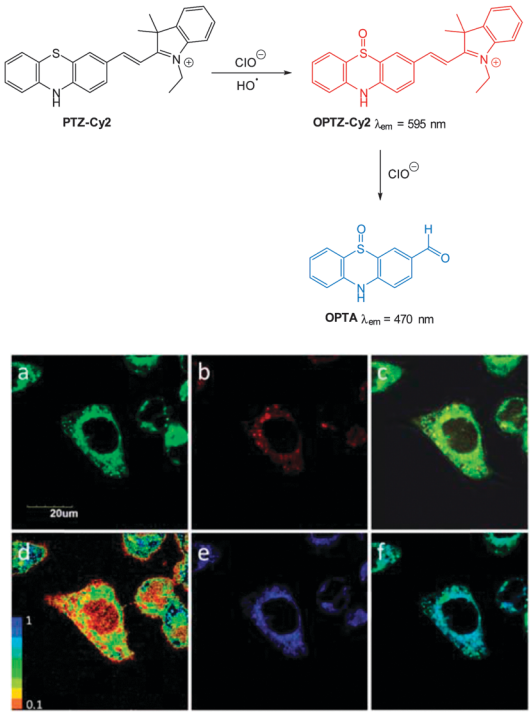

Fig. 106 Top: structure and reaction of **PTZ-Cy2** with ClO^-. Bottom: HeLa cells pre-treated with PMA then **PTZ-Cy2** plus MitoTracker Deep Red FM. (a) Emission of **PTZ-Cy2** at 470 nm; (b) emission of **PTZ-Cy2** at 590 nm; (c) merged image of (a) and (b) with bright-field image; (d) pseudocolour ratiometric images (F_{470}/F_{590}); (e) fluorescence image of MitoTracker Deep Red FM (λ_{em} = 690 nm); (f) overlay of (a) and (e). Image reproduced with permission.[331]

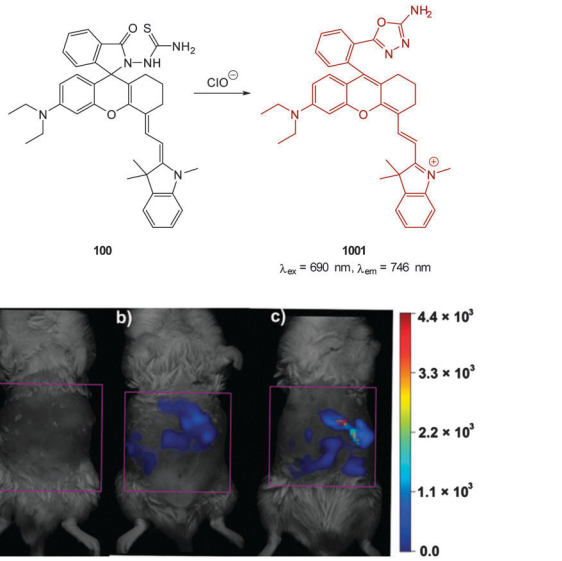

Fig. 107 Representative fluorescent images (pseudocolour) of *in vivo* ClO^- production from the peritoneal cavity of the mice with **100** during an LPS-mediated inflammatory response: (a) negative control, neither LPS nor **100** was injected; (b) saline was injected in the intraperitoneal (i.p.) cavity of mice, followed by i.p. injection of **100**; (c) LPS was injected into the peritoneal cavity of the mice, followed by i.p. injection of **100**. Image reproduced with permission.[332]

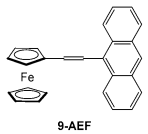

Fig. 108 Structure of hypochlorite sensitive probe **9-AEF** as described by Ma.[333]

emit in the NIR range.[332] The non-fluorescent spirocyclic benzoyl thiosemicarbazide **100** (Fig. 107), in the presence of hypochlorite undergoes oxidative cyclisation to give the 2-amino-1,3,4-oxadiazole (**101**) which simultaneously opens the spirocycle and restores ICT (λ_{ex} = 690 nm, λ_{em} = 746 nm). Imaging of hypochlorite in LPS and PMA stimulated RAW264.7 macrophages established the viability of probe **100** *in vitro* and also revealed mitochondrial localisation. Probe **100** was applicable as a hypochlorite responsive probe in imprinting control region (ICR) mice treated with LPS; higher fluorescent emission was recorded when compared with the control or **100** alone.

Ma (2010) described the PET system **9-AEF** consisting of an anthracene linked by an alkene to ferrocene (Fig. 108).[333] The electron rich ferrocene instigates PET to the anthracene and fluorescence is quenched ($\Phi_F < 0.001$). Hypochlorite could oxidise the alkene, and in the product (not characterised) PET is unfavoured and anthracene-like emission was observed (λ_{em} = 441 nm, Φ_F = 0.12). It should be noted that no single product was identified, nevertheless, the response to hypochlorite was dose dependant and the probe was successfully used to image hypochlorite in HeLa cells. No fluorescence was observed in cells containing **9-AEF** unless they were pre- or post-treated with hypochlorite.

4.3 Hypobromite

In an analogous manner to hypochlorite, hypobromous acid/hypobromite can be produced endogenously by macrophages and eosinophils from the reaction between H_2O_2 and bromide which is catalysed by eosinophil peroxidase (EPO) in response to invading pathogens. Overproduction of HOBr can lead to diseases such as cancer, arthritis, cardiovascular disease and asthma. There is a demonstrated correlation between clinical severity in asthma patients and serum EPO levels. While the fraction of HOBr/BrO^- is likely to be high (the pK_a for HOBr is 8.7–8.8 at 25 °C) a small percentage of the anionic species is likely to exist at physiological pH and in certain compartments such as mitochondria a considerable percentage of BrO^- is likely. The design of fluorescent probes for *in vitro* of detection of this species has recently received attention.

4.3.1 Recent developments. In 2012, the Han group reported two reversible fluorescent probes for the *in vitro* imagining of redox stress caused by HOBr.[334] Both probes, **mCyTem-OH** and **CyTem-OH** (Fig. 109), respond through the HOBr mediated oxidation of a 2,2,6,6-tetramethylpiperidine-*N*-oxyl moiety to the corresponding oxyammonium cation which leads to a donor-excited PET (d-PET) quenching mechanism (Φ_F decrease from 0.11 to 0.02 for **mCy-TemOH**). Oxidation of **mCyTemOH** (λ_{em} = 550 nm) results in a red-shifted emission centred at 632 nm. *In vitro* investigations used **mCy-TeOH** to monitor changes in endogenous HOBr concentration in

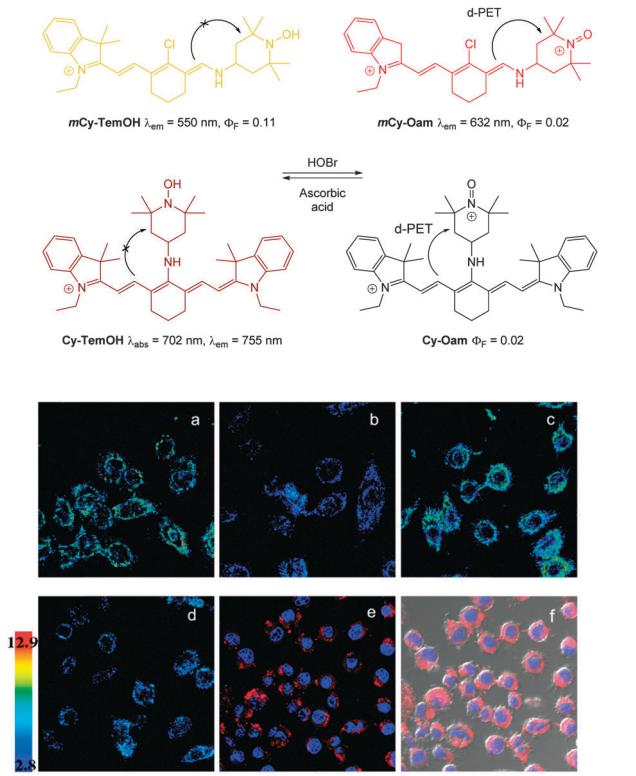

Fig. 109 Top: structure of **mCy-TemOH** and **Cy-TemOH** and their reaction with BrO^-. Bottom: ratiometric fluorescence images (F_{632}/F_{550}) of living RAW264.7 cells with **mCy-TemOH** (a)–(d). pseudo color images represent the ratio of emission intensities. (a) Control. (b) **mCy-TemOH**-loaded cells incubated with H_2O_2, EPO and KBr. (c) **mCy-TemOH** loaded, EPO, and H_2O_2 treated cells incubated with glutathione S-transferase, then ascorbic acid. (d) Cells exposed to a second dose of EPO, KBr and H_2O_2. (e) and (f) Confocal microscopy imaging for subcellular locations of **mCy-TemOH** in living RAW264.7 cells. (e) Cells incubated with **mCy-TemOH** (red) and co-staining with Hoechst dye (blue). (f) Overlay of (e) and its bright-field image. Image reproduced with permission.[334]

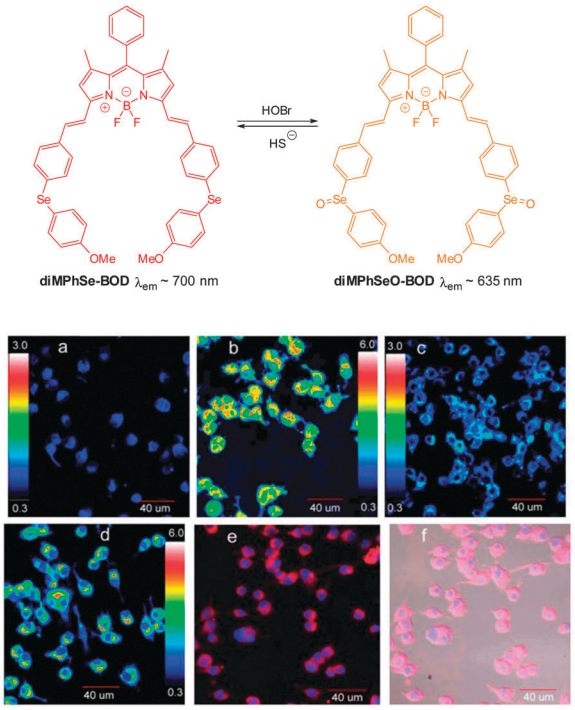

Fig. 110 Confocal fluorescence images of the redox cycles between HOBr and H_2S in RAW264.7 cells. Macrophage cells. (a) Control; (b) **diMPhSe-BOD**-loaded cells with H_2O_2, EPO, and KBr; (c) cells in (b) after addition of HS^-; (d) (c) was treated with a second dose of H_2O_2, EPO and KBr; (e) overlay of images showing fluorescence from **diMPhSe-BOD** and Hoechst dye; (f) overlay of bright-field, **diMPhSe-BOD**, and Hoechst dye images. Image reproduced with permission.[335]

RAW264.7 macrophages; treatment with EPO, H_2O_2 and KBr resulted in an increased in the F_{632}/F_{550} ratio from 2.8 to 12.9. Addition of ascorbic acid to the system resulted in reduction of the oxyammonium cation and a decrease in the F_{632}/F_{550} ratio.

The full cyanine probe, **Cy-TemOH**, exhibited NIR absorption (λ_{abs} = 702 nm) and emission (λ_{em} = 755 nm). **Cy-TemOH** also responded to the HOBr/ascorbic acid redox cycle but suffered from severe bleaching after three cycles. Nevertheless, **Cy-TemOH** was successfully used to visualise the redox cycle in RAW264.7 cells. Both **Cy-TemOH** and **mCy-TemOH** localised in the cytoplasm and cells remained viable (MTT assay).

The same group then developed a NIR-reversible BODIPY-based probe which could monitor the redox cycle between HOBr and HS^-.[335] The probe, **diMPhSe-BOD** (Fig. 110) absorbs strongly (ε_{672} = 22 770 M^{-1} cm^{-1}) but was weakly fluorescent (λ_{em} = 711 nm, Φ_F = 0.00083) due to the electron transfer (PET) from the diarylselenides. Oxidation with HOBr leads to a blue-shifted emission (λ_{em} = 635 nm) and 118-fold increase in the F_{635}/F_{711} ratio. The reverse reaction is accomplished by HS^- (selectively over other RSS such as Cys, Hcys and GSH). It is also notable that the emission ratio generated from the reaction with HOBr was *ca.* 6-fold greater than with ClO^-. The HOBr/HS^- redox cycle could be visualised in RAW264.7 cells and using **diMPhSe-BOD** HOBr and H_2S could be detected at concentrations as low as 50 and 100 nM respectively.

5. Conclusion and future work

One of the key purposes of this review was to highlight that the strategies employed for the design of small fluorescent anion sensors can be applied to *in vitro* and *in vivo* bioimaging.

As such further developments in fluorophore design and strategies for signal modulation[336] are likely to have immediate imaging applications. The emerging use of multiphoton excitation is already having an impact. Developments in the use of fluorescence lifetime[337] will also broaden the range of approaches that can be used. Probes that are compatible with a super-resolution approach would also be beneficial for the ultimate aim of pinpointing the origin and/or fate of the species of interest.

Despite some impressive examples, many of the probes described herein do not meet the highly demanding criteria set out for an ''ideal probe'' in Section 1.2. Complete selectivity for the analyte of interest is not always realised and probes that are not dependent on a chemical transformation are currently the most prone to interference. Indeed it is a truly formidable

challenge to design a selective, *reversible*, recognition process that operates by means of non-covalent forces in an exceptionally competitive media! Further refinement of fundamental recognition principles and the ability to readily synthesise (or assemble) sophisticated structures is required to overcome this hurdle. While the selectivity of chemodosimeters is often excellent the reactions are typically *irreversible* and hence they are incapable of mapping in a truly spatiotemporal manner.

Furthermore, despite the obvious potential that these probes offer, many are destined to be research tools only; the widespread use of fluorescent probes in clinical settings is hampered by expensive operational set-up and sample by sample analysis. Nevertheless, several of the probes included herein have been successfully used in flow systems[147,171,281] and with the current rapid progress in the field of micro-fluidics and micro-optics the goal of cost effective, "smartphone style", point of care diagnostics using selective fluorescent probes is sure to be realised.[338–342]

It is also interesting to note that for many small anions (Cl^-, I^-, HCO_3^-, and BrO^-) the complete list of probes is very short and hence any progress would be welcome. Nevertheless, the field of anion sensing is rapidly advancing, and for the researchers involved in this field these challenges should be seen as nothing more than an excellent opportunity to further the fundamental understanding of our natural world.

Glossary of cell lines

RAW264.7	Murine/mouse macrophages
PC3	Prostate cancer
HUVEC	Human umbilical vein endothelial cell
NIH3T3	Murine/mouse fibroblast
HeLa	Epithelial cervical cancer
MCF-7	Breast cancer
HEK-293	Human embryonic kidney cells
L929	Murine/mouse fibroblast
A549	Adenocarcinomic human alveolar basal epithelial cells
COS-7	Fibroblast-like
B16-F10	Murine/mouse skin melanoma
U266	Human myeloma
HepG2	Hepatocellular carcinoma
PMN	Human polymorphonuclear neutrophils
BV2 microglial	Brain resident murine macrophages
MDA-MB-231	Human breast adenocarcinoma
SH-SY5Y	Human neuronal neuroblasts
HL-60	Human promyelocytic leukemia
GES	Human breast cancer cells

Acknowledgements

The authors TDA, KJ and FP would like to thank the Australian Research Council (ARC DP140100227) and TDA and FP also thank the Strategic Research Centre for Chemistry and Biotechnology (Deakin University) for financial support.

References

1 *Supramolecular Chemistry: From Molecules to Nanomaterials*, ed. P. A. Gale and J. W. Steed, John Wiley and Sons, Chichester, 2012.
2 *Recognition of Anions*, ed. R. Vilar, Springer-Verlag, Berlin, 2008.
3 *Anion Receptor Chemistry*, ed. J. L. Sessler, P. A. Gale and W.-S. Cho, The Royal Society of Chemistry, Cambridge, 2006.
4 *Encyclopedia of Supramolecular Chemistry*, ed. J. L. Atwood and J. W. Steed, Marcel Dekker, New York, 2004.
5 *Supramolecular Chemistry of Anions*, ed. A. Bianchi, K. Bowman-James and E. García-España, Wiley-VCH, New York, 1997.
6 M. M. G. Antonisse and D. N. Reinhoudt, *Chem. Commun.*, 1998, 443–448.
7 S. Kubik, C. Reyheller and S. Stuwe, *J. Inclusion Phenom. Macrocyclic Chem.*, 2005, **52**, 137–187.
8 E. A. Katayev, Y. A. Ustynyuk and J. L. Sessler, *Coord. Chem. Rev.*, 2006, **250**, 3004–3037.
9 F. P. Schmidtchen, *Coord. Chem. Rev.*, 2006, **250**, 2918–2928.
10 P. Blondeau, M. Segura, R. Perez-Fernandez and J. de Mendoza, *Chem. Soc. Rev.*, 2007, **36**, 198–210.
11 J. W. Steed, *Chem. Soc. Rev.*, 2009, **38**, 506–519.
12 S. Kubik, *Chem. Soc. Rev.*, 2010, **39**, 3648–3663.
13 F. P. Schmidtchen, *Chem. Soc. Rev.*, 2010, **39**, 3916–3935.
14 A. E. Hargrove, S. Nieto, T. Zhang, J. L. Sessler and E. V. Anslyn, *Chem. Rev.*, 2011, **111**, 6603–6782.
15 M. Wenzel, J. R. Hiscock and P. A. Gale, *Chem. Soc. Rev.*, 2012, **41**, 480–520.
16 P. A. Gale, N. Busschaert, C. J. E. Haynes, L. E. Karagiannidis and I. L. Kirby, *Chem. Soc. Rev.*, 2014, **43**, 205–241.
17 M. J. Langton and P. D. Beer, *Acc. Chem. Res.*, 2014, **47**, 1935–1949.
18 H. D. P. Ali, P. E. Kruger and T. Gunnlaugsson, *New J. Chem.*, 2008, **32**, 1153–1161.
19 T. Gunnlaugsson, A. P. Davis and M. Glynn, *Chem. Commun.*, 2001, 2556–2557.
20 H. Miyaji and J. L. Sessler, *Angew. Chem., Int. Ed.*, 2001, **40**, 154–157.
21 T. Gunnlaugsson, A. P. Davis, J. E. O'Brien and M. Glynn, *Org. Lett.*, 2002, **4**, 2449–2452.
22 R. Martinez-Manez and F. Sancenon, *Chem. Rev.*, 2003, **103**, 4419–4476.
23 C. Suksai and T. Tuntulani, *Chem. Soc. Rev.*, 2003, **32**, 192–202.
24 F. P. Schmidtchen, in *Anion Sensing*, ed. I. Stibor, 2005, pp. 1–29.
25 C. Suksai and T. Tuntulani, in *Anion Sensing*, ed. I. Stibor, 2005, pp. 163–198.
26 T. Gunnlaugsson, M. Glynn, G. M. Tocci, P. E. Kruger and F. M. Pfeffer, *Coord. Chem. Rev.*, 2006, **250**, 3094–3117.
27 B. T. Nguyen and E. V. Anslyn, *Coord. Chem. Rev.*, 2006, **250**, 3118–3127.
28 R. M. Duke, E. B. Veale, F. M. Pfeffer, P. E. Kruger and T. Gunnlaugsson, *Chem. Soc. Rev.*, 2010, **39**, 3936–3953.

29 M. E. Moragues, R. Martinez-Manez and F. Sancenon, *Chem. Soc. Rev.*, 2011, **40**, 2593–2643.
30 J. Du, M. Hu, J. Fan and X. Peng, *Chem. Soc. Rev.*, 2012, **41**, 4511–4535.
31 L. E. Santos-Figueroa, M. E. Moragues, E. Climent, A. Agostini, R. Martinez-Manez and F. Sancenon, *Chem. Soc. Rev.*, 2013, **42**, 3489–3613.
32 H. T. Ngo, X. J. Liu and K. A. Jolliffe, *Chem. Soc. Rev.*, 2012, **41**, 4928–4965.
33 P. A. Gale and C. Caltagirone, *Chem. Soc. Rev.*, 2015, DOI: 10.1039/C4CS00179F.
34 X. Li, X. Gao, W. Shi and H. Ma, *Chem. Rev.*, 2014, **114**, 590–659.
35 K. Kaur, R. Saini, A. Kumar, V. Luxami, N. Kaur, P. Singh and S. Kumar, *Coord. Chem. Rev.*, 2012, **256**, 1992–2028.
36 S. K. Kim, D. H. Lee, J.-I. Hong and J. Yoon, *Acc. Chem. Res.*, 2009, **42**, 23–31.
37 M. Cametti and K. Rissanen, *Chem. Commun.*, 2009, 2809–2829.
38 T. W. Hudnall, C.-W. Chiu and F. P. Gabbai, *Acc. Chem. Res.*, 2009, **42**, 388–397.
39 C. R. Wade, A. E. J. Broomsgrove, S. Aldridge and F. P. Gabbaï, *Chem. Rev.*, 2010, **110**, 3958–3984.
40 F. Wang, L. Wang, X. Chen and J. Yoon, *Chem. Soc. Rev.*, 2014, **43**, 4312–4324.
41 Q. Xu, C. Jin, X. Zhu and G. Xing, *Chin. J. Org. Chem.*, 2014, **34**, 647–661.
42 D. Zhang, J. R. Cochrane, A. Martinez and G. Gao, *RSC Adv.*, 2014, **4**, 29735–29749.
43 M. H. Lee, J. S. Kim and J. L. Sessler, *Chem. Soc. Rev.*, 2015, DOI: 10.1039/C4CS00280F.
44 Y. Zhou and J. Yoon, *Chem. Soc. Rev.*, 2012, **41**, 52–67.
45 E. J. New, D. Parker, D. G. Smith and J. W. Walton, *Curr. Opin. Chem. Biol.*, 2010, **14**, 238–246.
46 X. J. Liu, H. T. Ngo, Z. J. Ge, S. J. Butler and K. A. Jolliffe, *Chem. Sci.*, 2013, **4**, 1680–1686.
47 J. L. Sessler, P. A. Gale and W.-S. Cho, in *Anion Receptor Chemistry*, ed. J. L. Sessler, P. A. Gale and W. -S. Cho, The Royal Society of Chemistry, 2006, pp. 1–26.
48 J. Chan, S. C. Dodani and C. J. Chang, *Nat. Chem.*, 2012, **4**, 973–984.
49 Y. Yang, Q. Zhao, W. Feng and F. Li, *Chem. Rev.*, 2012, **113**, 192–270.
50 L. M. Hyman and K. J. Franz, *Coord. Chem. Rev.*, 2012, **256**, 2333–2356.
51 Y. Urano, *Curr. Opin. Chem. Biol.*, 2012, **16**, 602–608.
52 N. Kumar, V. Bhalla and M. Kumar, *Coord. Chem. Rev.*, 2013, **257**, 2335–2347.
53 J. Wang, L. Long, D. Xie and Y. Zhan, *J. Lumin.*, 2013, **139**, 40–46.
54 L. Yuan, W. Lin, K. Zheng, L. He and W. Huang, *Chem. Soc. Rev.*, 2013, **42**, 622–661.
55 Z. Guo, S. Park, J. Yoon and I. Shin, *Chem. Soc. Rev.*, 2014, **43**, 16–29.
56 E. Pershagen and K. E. Borbas, *Coord. Chem. Rev.*, 2014, **273–274**, 30–46.
57 S. F. Peteu, R. Boukherroub and S. Szunerits, *Biosens. Bioelectron.*, 2014, **58**, 359–373.
58 K. Wang, H. Peng and B. Wang, *J. Cell. Biochem.*, 2014, **115**, 1007–1022.
59 X. Wu and W. Zhu, *Chem. Soc. Rev.*, 2015, DOI: 10.1039/C4CS00152D.
60 S. Wang, N. Li, W. Pan and B. Tang, *TrAC, Trends Anal. Chem.*, 2012, **39**, 3–37.
61 K. P. Carter, A. M. Young and A. E. Palmer, *Chem. Rev.*, 2014, **114**, 4564–4601.
62 R. Y. Tsien, *Annu. Rev. Neurosci.*, 1989, **12**, 227–253.
63 R. Y. Tsien, in *Methods in Cell Biology*, ed. D. Lansing Taylor and Y.-L. Wang, Academic Press, 1989, pp. 127–156.
64 S. A. Hilderbrand, *Live Cell Imaging*, 2009, pp. 17–45.
65 S. A. Hilderbrand and R. Weissleder, *Curr. Opin. Chem. Biol.*, 2010, **14**, 71–79.
66 R. Weissleder and V. Ntziachristos, *Nat. Med.*, 2003, **9**, 123–128.
67 J. O. Escobedo, O. Rusin, S. Lim and R. M. Strongin, *Curr. Opin. Chem. Biol.*, 2010, **14**, 64–70.
68 W. R. Zipfel, R. M. Williams and W. W. Webb, *Nat. Biotechnol.*, 2003, **21**, 1369–1377.
69 F. Helmchen and W. Denk, *Nat. Methods*, 2005, **2**, 932–940.
70 P. Klán and J. Wirz, *Photochemistry of Organic Compounds*, John Wiley & Sons, Ltd, 2009, pp. 25–72.
71 K. Baathulaa, Y. Xu and X. Qian, *J. Photochem. Photobiol., A*, 2010, **216**, 24–34.
72 P. Abbyad, W. Childs, X. Shi and S. G. Boxer, *Proc. Natl. Acad. Sci. U. S. A.*, 2007, **104**, 20189–20194.
73 P. Horváth, P. Šebej, T. Šolomek and P. Klán, *J. Org. Chem.*, 2015, DOI: 10.1021/jo502213t.
74 N. Boens, V. Leen and W. Dehaen, *Chem. Soc. Rev.*, 2012, **41**, 1130–1172.
75 H. Lu, J. Mack, Y. Yang and Z. Shen, *Chem. Soc. Rev.*, 2014, **43**, 4778–4823.
76 X. Chen, T. Pradhan, F. Wang, J. S. Kim and J. Yoon, *Chem. Rev.*, 2011, **112**, 1910–1956.
77 H. Zheng, X.-Q. Zhan, Q.-N. Bian and X.-J. Zhang, *Chem. Commun.*, 2013, **49**, 429–447.
78 Y. Q. Sun, J. Liu, X. Lv, Y. Liu, Y. Zhao and W. Guo, *Angew. Chem., Int. Ed.*, 2012, **51**, 7634–7636.
79 S. T. Manjare, Y. Kim and D. G. Churchill, *Acc. Chem. Res.*, 2014, **47**, 2985–2998.
80 X. Wang, H. Chang, J. Xie, B. Zhao, B. Liu, S. Xu, W. Pei, N. Ren, L. Huang and W. Huang, *Coord. Chem. Rev.*, 2014, **273–274**, 201–212.
81 C. P. Montgomery, B. S. Murray, E. J. New, R. Pal and D. Parker, *Acc. Chem. Res.*, 2009, **42**, 925–937.
82 M. C. Heffern, L. M. Matosziuk and T. J. Meade, *Chem. Rev.*, 2013, **114**, 4496–4539.
83 S. J. Butler and D. Parker, *Chem. Soc. Rev.*, 2013, **42**, 1652–1666.
84 A. Demchenko, *J. Fluoresc.*, 2010, **20**, 1099–1128.
85 J. Fan, M. Hu, P. Zhan and X. Peng, *Chem. Soc. Rev.*, 2013, **42**, 29–43.
86 D.-G. Cho and J. L. Sessler, *Chem. Soc. Rev.*, 2009, **38**, 1647–1662.

87 X. Lou, D. Ou, Q. Li and Z. Li, *Chem. Commun.*, 2012, **48**, 8462–8477.
88 F. Zheng, F. Zeng, C. Yu, X. Hou and S. Wu, *Chem. – Eur. J.*, 2013, **19**, 936–942.
89 B. Ke, W. Chen, N. Ni, Y. Cheng, C. Dai, H. Dinh and B. Wang, *Chem. Commun.*, 2013, **49**, 2494–2496.
90 R. Y. Tsien, *Nature*, 1981, **290**, 527–528.
91 J. P. Crow, *Nitric oxide*, 1997, **1**, 145–157.
92 T. Peng and D. Yang, *Org. Lett.*, 2010, **12**, 4932–4935.
93 C. Song, Z. Ye, G. Wang, J. Yuan and Y. Guan, *Chem. – Eur. J.*, 2010, **16**, 6464–6472.
94 F. Di Virgilio, T. H. Steinberg, J. A. Swanson and S. C. Silverstein, *J. Immunol.*, 1988, **140**, 915–920.
95 R. Horobin, J. Stockert and F. Rashid-Doubell, *Histochem. Cell Biol.*, 2013, **139**, 623–637.
96 F. Rashid and R. W. Horobin, *Histochemistry*, 1990, **94**, 303–308.
97 S. Trapp and R. Horobin, *Eur. Biophys. J.*, 2005, **34**, 959–966.
98 S. Trapp, G. Rosania, R. Horobin and J. Kornhuber, *Eur. Biophys. J.*, 2008, **37**, 1317–1328.
99 J. T. Hou, M. Y. Wu, K. Li, J. Yang, K. K. Yu, Y. M. Xie and X. Q. Yu, *Chem. Commun.*, 2014, **50**, 8640–8643.
100 T. Liu, Z. Xu, D. R. Spring and J. Cui, *Org. Lett.*, 2013, **15**, 2310–2313.
101 Y. Zhou, J. F. Zhang and J. Yoon, *Chem. Rev.*, 2014, **114**, 5511–5571.
102 C. D. Geddes, K. Apperson, J. Karolin and D. J. S. Birch, *Anal. Biochem.*, 2001, **293**, 60–66.
103 H. S. Horowitz, *J. Public Health Dent.*, 2003, **63**, 3–8.
104 S. Ayoob and A. K. Gupta, *Crit. Rev. Environ. Sci. Technol.*, 2006, **36**, 433–487.
105 E. Bassin, D. Wypij, R. Davis and M. Mittleman, *Cancer Causes Control*, 2006, **17**, 421–428.
106 A. L. Choi, G. Sun, Y. Zhang and P. Grandjean, *Environ. Health Perspect.*, 2012, **120**, 1362–1368.
107 E. Galbraith and T. D. James, *Chem. Soc. Rev.*, 2010, **39**, 3831–3842.
108 Z. Guo, I. Shin and J. Yoon, *Chem. Commun.*, 2012, **48**, 5956–5967.
109 T. Gunnlaugsson, P. E. Kruger, T. C. Lee, R. Parkesh, F. M. Pfeffer and G. M. Hussey, *Tetrahedron Lett.*, 2003, **44**, 6575–6578.
110 T. Gunnlaugsson, P. E. Kruger, P. Jensen, F. M. Pfeffer and G. M. Hussey, *Tetrahedron Lett.*, 2003, **44**, 8909–8913.
111 L. S. Evans, P. A. Gale, M. E. Light and R. Quesada, *Chem. Commun.*, 2006, 965–967.
112 S. Camiolo, P. A. Gale, M. B. Hursthouse and M. E. Light, *Org. Biomol. Chem.*, 2003, **1**, 741–744.
113 X. Zheng, W. Zhu, D. Liu, H. Ai, Y. Huang and Z. Lu, *ACS Appl. Mater. Interfaces*, 2014, **6**, 7996–8000.
114 R. Liu, Y. Gao, Q. Zhang, X. Yang, X. Lu, Z. Ke, W. Zhou and J. Qu, *New J. Chem.*, 2014, **38**, 2941–2945.
115 A. K. Mahapatra, R. Maji, K. Maiti, S. S. Adhikari, C. Das Mukhopadhyay and D. Mandal, *Analyst*, 2014, **139**, 309–317.
116 F. M. Pfeffer, K. F. Lim and K. J. Sedgwick, *Org. Biomol. Chem.*, 2007, **5**, 1795–1799.
117 J. L. Sessler, D.-G. Cho and V. Lynch, *J. Am. Chem. Soc.*, 2006, **128**, 16518–16519.
118 G. Sivaraman and D. Chellappa, *J. Mater. Chem. B*, 2013, **1**, 5768–5772.
119 P. G. M. Wuts and T. W. Greene, *Greene's Protective Groups in Organic Synthesis*, John Wiley & Sons, Inc., 2006, pp. 16–366.
120 S. Y. Kim, J. Park, M. Koh, S. B. Park and J.-I. Hong, *Chem. Commun.*, 2009, 4735–4737.
121 B. Zhu, H. Kan, J. Liu, H. Liu, Q. Wei and B. Du, *Biosens. Bioelectron.*, 2014, **52**, 298–303.
122 B. Zhu, F. Yuan, R. Li, Y. Li, Q. Wei, Z. Ma, B. Du and X. Zhang, *Chem. Commun.*, 2011, **47**, 7098–7100.
123 Z. Luo, B. Yang, C. Zhong, F. Tang, M. Yuan, Y. Xue, G. Yao, J. Zhang and Y. Zhang, *Dyes Pigm.*, 2013, **97**, 52–57.
124 G. Wei, J. Yin, X. Ma, S. Yu, D. Wei and Y. Du, *Anal. Chim. Acta*, 2011, **703**, 219–225.
125 L. Gai, H. Chen, B. Zou, H. Lu, G. Lai, Z. Li and Z. Shen, *Chem. Commun.*, 2012, **48**, 10721–10723.
126 D. Kim, S. Singha, T. Wang, E. Seo, J. H. Lee, S.-J. Lee, K. H. Kim and K. H. Ahn, *Chem. Commun.*, 2012, **48**, 10243–10245.
127 P. Hou, S. Chen, H. Wang, J. Wang, K. Voitchovsky and X. Song, *Chem. Commun.*, 2014, **50**, 320–322.
128 S. Zhang, J. Fan, S. Zhang, J. Wang, X. Wang, J. Du and X. Peng, *Chem. Commun.*, 2014, **50**, 14021–14024.
129 W. Gong, R. Su, L. Li, K. Xu and B. Tang, *Chin. Sci. Bull.*, 2011, **56**, 3260–3265.
130 T.-Y. Chen and T.-C. Hwang, *Physiol. Rev.*, 2008, **88**, 351–387.
131 P. A. Gale, *Acc. Chem. Res.*, 2011, **44**, 216–226.
132 N. Busschaert, I. L. Kirby, S. Young, S. J. Coles, P. N. Horton, M. E. Light and P. A. Gale, *Angew. Chem., Int. Ed.*, 2012, **51**, 4426–4430.
133 C. J. E. Haynes and P. A. Gale, *Chem. Commun.*, 2011, **47**, 8203–8209.
134 P. R. Brotherhood and A. P. Davis, *Chem. Soc. Rev.*, 2010, **39**, 3633–3647.
135 A. P. Davis, D. N. Sheppard and B. D. Smith, *Chem. Soc. Rev.*, 2007, **36**, 348–357.
136 J. T. Davis, O. Okunola and R. Quesada, *Chem. Soc. Rev.*, 2010, **39**, 3843–3862.
137 G. W. Gokel and N. Barkey, *New J. Chem.*, 2009, **33**, 947–963.
138 B. A. McNally, W. M. Leevy and B. D. Smith, *Supramol. Chem.*, 2007, **19**, 29–37.
139 A. S. Verkman, *Am. J. Physiol.*, 1990, **259**, C375–C388.
140 S. Jayaraman, L. Teitler, B. Skalski and A. S. Verkman, *Am. J. Physiol.*, 1999, **277**, C1008–C1018.
141 C. D. Geddes, K. Apperson, J. Karolin and D. J. S. Birch, *Dyes Pigm.*, 2001, **48**, 227–231.
142 *Molecular Probes Handbook, A Guide to Fluorescent Probes and Labeling Technologies*, ed. I. Johnson, Life Technologies Corporation, 2010.
143 A. S. Verkman, in *Physiology and Pathology of Chloride Transporters and Channels in the Nervous System*, ed.

F. J. Alvarez-Leefmans and E. Delpire, Academic Press, San Diego, 2010, pp. 109–123.
144 D. Arosio and G. M. Ratto, *Front. Cell. Neurosci.*, 2014, **8**, 258, DOI: 10.3389/fncel.2014.00258.
145 J. Biwersi and A. S. Verkman, *Biochemistry*, 1991, **30**, 7879–7883.
146 J. R. Inglefield and R. D. Schwartz-Bloom, *J. Neurosci. Methods*, 1997, **75**, 127–135.
147 B. Pilas and G. Durack, *Cytometry*, 1997, **28**, 316–322.
148 Y. Kovalchuk and O. Garaschuk, *Cold Spring Harb. Protoc.*, 2012, DOI: 10.1101/pdb.prot070037.
149 J. Biwersi, B. Tulk and A. S. Verkman, *Anal. Biochem.*, 1994, **219**, 139–143.
150 B. A. McNally, A. V. Koulov, B. D. Smith, J.-B. Joos and A. P. Davis, *Chem. Commun.*, 2005, 1087–1089.
151 S. B. J. V. A. S. Jayaraman, *Am. J. Physiol.*, 1999, **276**, C747–C757.
152 N. D. Sonawane, J. R. Thiagarajah and A. S. Verkman, *J. Biol. Chem.*, 2002, **277**, 5506–5513.
153 P. Li, T. Xie, N. Fan, K. Li and B. Tang, *Chem. Commun.*, 2012, **48**, 2077–2079.
154 P. Li, S. Zhang, N. Fan, H. Xiao, W. Zhang, W. Zhang, H. Wang and B. Tang, *Chem. – Eur. J.*, 2014, **20**, 11760–11767.
155 S. Amatori, G. Ambrosi, M. Fanelli, M. Formica, V. Fusi, L. Giorgi, E. Macedi, M. Micheloni, P. Paoli, R. Pontellini, P. Rossi and M. A. Varrese, *Chem. – Eur. J.*, 2012, **18**, 4274–4284.
156 S. Amatori, G. Ambrosi, E. Borgogelli, M. Fanelli, M. Formica, V. Fusi, L. Giorgi, E. Macedi, M. Micheloni, P. Paoli, P. Rossi and A. Tassoni, *Inorg. Chem.*, 2014, **53**, 4560–4569.
157 J. J. Gassensmith, S. Matthys, J.-J. Lee, A. Wojcik, P. V. Kamat and B. D. Smith, *Chem. – Eur. J.*, 2010, **16**, 2916–2921.
158 C. G. Collins, E. M. Peck, P. J. Kramer and B. D. Smith, *Chem. Sci.*, 2013, **4**, 2557–2563.
159 P. J. DeMott, *Atmos. Res.*, 1995, **38**, 63–99.
160 C. D. Geddes, *Meas. Sci. Technol.*, 2001, **12**, R53.
161 G. Dai, O. Levy and N. Carrasco, *Nature*, 1996, **379**, 458–460.
162 A. K. Mahapatra, J. Roy, P. Sahoo, S. K. Mukhopadhyay and A. Chattopadhyay, *Org. Biomol. Chem.*, 2012, **10**, 2231–2236.
163 P. Castric, *Curr. Microbiol.*, 1994, **29**, 19–21.
164 J. L. Way, *Annu. Rev. Pharmacol. Toxicol.*, 1984, **24**, 451–481.
165 J. R. Govan and V. Deretic, *Microbiol. Rev.*, 1996, **60**, 539–574.
166 B. Ryall, X. Lee, J. Zlosnik, S. Hoshino and H. Williams, *BMC Microbiol.*, 2008, **8**, 108.
167 *Cyanide in Water and Soil: Chemistry, Risk, and Management*, ed. D. A. Dzombak, R. S. Ghosh and G. M. Wong-Chong, CRC Press, Boca Raton, Florida, 2005.
168 Z. Xu, X. Chen, H. N. Kim and J. Yoon, *Chem. Soc. Rev.*, 2010, **39**, 127–137.
169 K.-S. Lee, H.-J. Kim, G.-H. Kim, I. Shin and J.-I. Hong, *Org. Lett.*, 2007, **10**, 49–51.
170 J. Zhao, S. Ji, Y. Chen, H. Guo and P. Yang, *Phys. Chem. Chem. Phys.*, 2012, **14**, 8803–8817.
171 S. K. Kwon, S. Kou, H. N. Kim, X. Chen, H. Hwang, S.-W. Nam, S. H. Kim, K. M. K. Swamy, S. Park and J. Yoon, *Tetrahedron Lett.*, 2008, **49**, 4102–4105.
172 S. W. Nam, X. Chen, J. Lim, S. H. Kim, S. T. Kim, Y. H. Cho, J. Yoon and S. Park, *PLoS One*, 2011, **6**, e21387.
173 M. K. Bera, C. Chakraborty, P. K. Singh, C. Sahu, K. Sen, S. Maji, A. K. Das and S. Malik, *J. Mater. Chem. B*, 2014, **2**, 4733.
174 S. Madhu, S. K. Basu, S. Jadhav and M. Ravikanth, *Analyst*, 2013, **138**, 299–306.
175 X. Cheng, R. Tang, H. Jia, J. Feng, J. Qin and Z. Li, *ACS Appl. Mater. Interfaces*, 2012, **4**, 4387–4392.
176 C.-H. Lee, H.-J. Yoon, J.-S. Shim and W.-D. Jang, *Chem. – Eur. J.*, 2012, **18**, 4513–4516.
177 M. Sun, S. Wang, Q. Yang, X. Fei, Y. Li and Y. Li, *RSC Adv.*, 2014, **4**, 8295–8299.
178 L. Yang, X. Li, Y. Qu, W. Qu, X. Zhang, Y. Hang, H. Ågren and J. Hua, *Sens. Actuators, B*, 2014, **203**, 833–847.
179 S. Y. Chung, S. W. Nam, J. Lim, S. Park and J. Yoon, *Chem. Commun.*, 2009, 2866–2868.
180 C. D. Sifri, J. Begun and F. M. Ausubel, *Trends Microbiol.*, 2005, **13**, 119–127.
181 X. Chen, S. W. Nam, G. H. Kim, N. Song, Y. Jeong, I. Shin, S. K. Kim, J. Kim, S. Park and J. Yoon, *Chem. Commun.*, 2010, **46**, 8953–8955.
182 U. Reddy G, P. Das, S. Saha, M. Baidya, S. K. Ghosh and A. Das, *Chem. Commun.*, 2013, **49**, 255–257.
183 H. S. Jung, J. H. Han, Z. H. Kim, C. Kang and J. S. Kim, *Org. Lett.*, 2011, **13**, 5056–5059.
184 W. Cao, X.-J. Zheng, D.-C. Fang and L.-P. Jin, *Dalton Trans.*, 2014, **43**, 7298–7303.
185 Y.-Y. Guo, X.-L. Tang, F.-P. Hou, J. Wu, W. Dou, W.-W. Qin, J.-X. Ru, G.-L. Zhang, W.-S. Liu and X.-J. Yao, *Sens. Actuators, B*, 2013, **181**, 202–208.
186 M. Lee, J. H. Moon, K. M. K. Swamy, Y. Jeong, G. Kim, J. Choi, J. Y. Lee and J. Yoon, *Sens. Actuators, B*, 2014, **199**, 369–376.
187 S. Xu, M. He, H. Yu, X. Cai, X. Tan, B. Lu and B. Shu, *Anal. Biochem.*, 2001, **299**, 188–193.
188 A. E. Timms, Y. Zhang, R. G. G. Russell and M. A. Brown, *Rheumatology*, 2002, **41**, 725–729.
189 S. Lee, K. K. Y. Yuen, K. A. Jolliffe and J. Yoon, *Chem. Soc. Rev.*, 2015, DOI: 10.1039/c1034cs00353e.
190 J. F. Zhang, S. Kim, J. H. Han, S.-J. Lee, T. Pradhan, Q. Y. Cao, S. J. Lee, C. Kang and J. S. Kim, *Org. Lett.*, 2011, **13**, 5294–5297.
191 D.-N. Lee, A. Jo, S. B. Park and J.-I. Hong, *Tetrahedron Lett.*, 2012, **53**, 5528–5530.
192 W. Zhu, X. Huang, Z. Guo, X. Wu, H. Yu and H. Tian, *Chem. Commun.*, 2012, **48**, 1784–1786.
193 R. K. Pathak, K. Tabbasum, A. Rai, D. Panda and C. P. Rao, *Anal. Chem.*, 2012, **84**, 5117–5123.
194 S. Goswami, A. K. Das, B. Pakhira, S. Basu Roy, A. K. Maity, P. Saha and S. Sarkar, *Dalton Trans.*, 2014, **43**, 12689–12697.

195 S. Bhowmik, B. N. Ghosh, V. Marjomaki and K. Rissanen, *J. Am. Chem. Soc.*, 2014, **136**, 5543–5546.
196 M. Leppilampi, P. Koistinen, E.-R. Savolainen, J. Hannuksela, A.-K. Parkkila, O. Niemelä, S. Pastoreková, J. Pastorek, A. Waheed, W. S. Sly, S. Parkkila and H. Rajaniemi, *Clin. Cancer Res.*, 2002, **8**, 2240–2245.
197 W. S. Sly and P. Y. Hu, *Annu. Rev. Biochem.*, 1995, **64**, 375–401.
198 W. Wu, H.-K. Kong, H. Li, Y.-M. Ho, Y. Gao, J. Hao, M. B. Murphy, M. H.-W. Lam, K.-L. Wong and C.-S. Lee, *Eur. J. Org. Chem.*, 2011, 5054–5060.
199 D. Parker, *Aust. J. Chem.*, 2011, **64**, 239–243.
200 B. S. Murray, E. J. New, R. Pal and D. Parker, *Org. Biomol. Chem.*, 2008, **6**, 2085–2094.
201 E. J. New and D. Parker, *Org. Biomol. Chem.*, 2009, **7**, 851–855.
202 S. J. Butler, L. Lamarque, R. Pal and D. Parker, *Chem. Sci.*, 2014, **5**, 1750–1756.
203 A. Thibon and V. Pierre, *Anal. Bioanal. Chem.*, 2009, **394**, 107–120.
204 M. S. Tremblay, M. Halim and D. Sames, *J. Am. Chem. Soc.*, 2007, **129**, 7570–7577.
205 D. G. Smith, G. L. Law, B. S. Murray, R. Pal, D. Parker and K. L. Wong, *Chem. Commun.*, 2011, **47**, 7347–7349.
206 D. G. Smith, R. Pal and D. Parker, *Chem. – Eur. J.*, 2012, **18**, 11604–11613.
207 P. Nagy, Z. Palinkas, A. Nagy, B. Budai, I. Toth and A. Vasas, *Biochim. Biophys. Acta*, 2014, **1840**, 876–891.
208 K. R. Olson, J. A. Donald, R. A. Dombkowski and S. F. Perry, *Respir. Physiol. Neurobiol.*, 2012, **184**, 117–129.
209 A. Stein and S. M. Bailey, *Redox Biol.*, 2013, **1**, 32–39.
210 J. L. Wallace, *Trends Pharmacol. Sci.*, 2007, **28**, 501–505.
211 P. Kamoun, *Amino Acids*, 2004, **26**, 243–254.
212 J. I. Toohey, *Anal. Biochem.*, 2011, **413**, 1–7.
213 R. E. Hansen and J. R. Winther, *Anal. Biochem.*, 2009, **394**, 147–158.
214 M. Vendrell, D. Zhai, J. C. Er and Y. T. Chang, *Chem. Rev.*, 2012, **112**, 4391–4420.
215 V. S. Lin and C. J. Chang, *Curr. Opin. Chem. Biol.*, 2012, **16**, 595–601.
216 B. Peng and M. Xian, *Asian J. Org. Chem.*, 2014, **3**, 914–924.
217 X. Cao, W. Lin, K. Zheng and L. He, *Chem. Commun.*, 2012, **48**, 10529–10531.
218 C. Tang, Q. Zheng, S. Zong, Z. Wang and Y. Cui, *Sens. Actuators, B*, 2014, **202**, 99–104.
219 D. Maity, A. Raj, P. K. Samanta, D. Karthigeyan, T. K. Kundu, S. K. Pati and T. Govindaraju, *RSC Adv.*, 2014, **4**, 11147.
220 Z. Huang, S. Ding, D. Yu, F. Huang and G. Feng, *Chem. Commun.*, 2014, **50**, 9185–9187.
221 Z. Xu, L. Xu, J. Zhou, Y. Xu, W. Zhu and X. Qian, *Chem. Commun.*, 2012, **48**, 10871–10873.
222 X. Wang, J. Sun, W. Zhang, X. Ma, J. Lv and B. Tang, *Chem. Sci.*, 2013, **4**, 2551.
223 J. Liu, Y. Q. Sun, J. Zhang, T. Yang, J. Cao, L. Zhang and W. Guo, *Chem. – Eur. J.*, 2013, **19**, 4717–4722.
224 Y. Chen, C. Zhu, Z. Yang, J. Chen, Y. He, Y. Jiao, W. He, L. Qiu, J. Cen and Z. Guo, *Angew. Chem., Int. Ed.*, 2013, **52**, 1688–1691.
225 S. K. Das, C. S. Lim, S. Y. Yang, J. H. Han and B. R. Cho, *Chem. Commun.*, 2012, **48**, 8395–8397.
226 A. R. Lippert, E. J. New and C. J. Chang, *J. Am. Chem. Soc.*, 2011, **133**, 10078–10080.
227 F. Yu, P. Li, P. Song, B. Wang, J. Zhao and K. Han, *Chem. Commun.*, 2012, **48**, 2852–2854.
228 Y. Zheng, M. Zhao, Q. Qiao, H. Liu, H. Lang and Z. Xu, *Dyes Pigm.*, 2013, **98**, 367–371.
229 W. Sun, J. Fan, C. Hu, J. Cao, H. Zhang, X. Xiong, J. Wang, S. Cui, S. Sun and X. Peng, *Chem. Commun.*, 2013, **49**, 3890–3892.
230 Q. Wan, Y. Song, Z. Li, X. Gao and H. Ma, *Chem. Commun.*, 2013, **49**, 502–504.
231 V. S. Lin, A. R. Lippert and C. J. Chang, *Proc. Natl. Acad. Sci. U. S. A.*, 2013, **110**, 7131–7135.
232 Q. Qiao, M. Zhao, H. Lang, D. Mao, J. Cui and Z. Xu, *RSC Adv.*, 2014, **4**, 25790.
233 S. Yang, Y. Qi, C. Liu, Y. Wang, Y. Zhao, L. Wang, J. Li, W. Tan and R. Yang, *Anal. Chem.*, 2014, **86**, 7508–7515.
234 S. K. Bae, C. H. Heo, D. J. Choi, D. Sen, E. H. Joe, B. R. Cho and H. M. Kim, *J. Am. Chem. Soc.*, 2013, **135**, 9915–9923.
235 L. Zhang, S. Li, M. Hong, Y. Xu, S. Wang, Y. Liu, Y. Qian and J. Zhao, *Org. Biomol. Chem.*, 2014, **12**, 5115–5125.
236 X. L. Liu, X. J. Du, C. G. Dai and Q. H. Song, *J. Org. Chem.*, 2014, **79**, 9481–9489.
237 R. Wang, F. Yu, L. Chen, H. Chen, L. Wang and W. Zhang, *Chem. Commun.*, 2012, **48**, 11757–11759.
238 H. Wu, S. Krishnakumar, J. Yu, D. Liang, H. Qi, Z. W. Lee, L. W. Deng and D. Huang, *Chem. – Asian J.*, 2014, **9**, 3604–3611.
239 W. Sun, W. Li, J. Li, J. Zhang, L. Du and M. Li, *Tetrahedron*, 2012, **68**, 5363–5367.
240 W. Chen, S. Chen, B. Zhou, H. Wang, X. Song and H. Zhang, *Dyes Pigm.*, 2015, **113**, 596–601.
241 H. Chen, W. Lin, H. Cui and W. Jiang, *Chem. – Eur. J.*, 2015, **21**, 733–745.
242 B. Peng, W. Chen, C. Liu, E. W. Rosser, A. Pacheco, Y. Zhao, H. C. Aguilar and M. Xian, *Chem. – Eur. J.*, 2014, **20**, 1010–1016.
243 L. Yuan and Q. P. Zuo, *Chem. – Asian J.*, 2014, **9**, 1544–1549.
244 T. Liu, X. Zhang, Q. Qiao, C. Zou, L. Feng, J. Cui and Z. Xu, *Dyes Pigm.*, 2013, **99**, 537–542.
245 X. Pei, H. Tian, W. Zhang, A. M. Brouwer and J. Qian, *Analyst*, 2014, **139**, 5290–5296.
246 F. Zheng, M. Wen, F. Zeng and S. Wu, *Polymer*, 2013, **54**, 5691–5697.
247 S. El Sayed, C. d. l. Torre, L. E. Santos-Figueroa, E. Pérez-Payá, R. Martínez-Máñez, F. Sancenón, A. M. Costero, M. Parra and S. Gil, *RSC Adv.*, 2013, **3**, 25690.
248 B. Chen, C. Lv and X. Tang, *Anal. Bioanal. Chem.*, 2012, **404**, 1919–1923.
249 C. S. Lim, S. K. Das, S. Y. Yang, E. S. Kim, H. J. Chun and B. R. Cho, *Anal. Chem.*, 2013, **85**, 9288–9295.

250 G. J. Mao, T. T. Wei, X. X. Wang, S. Y. Huan, D. Q. Lu, J. Zhang, X. B. Zhang, W. Tan, G. L. Shen and R. Q. Yu, *Anal. Chem.*, 2013, **85**, 7875–7881.
251 B. Chen, W. Li, C. Lv, M. Zhao, H. Jin, H. Jin, J. Du, L. Zhang and X. Tang, *Analyst*, 2013, **138**, 946–951.
252 C. Yu, X. Li, F. Zeng, F. Zheng and S. Wu, *Chem. Commun.*, 2013, **49**, 403–405.
253 K. Zheng, W. Lin and L. Tan, *Org. Biomol. Chem.*, 2012, **10**, 9683–9688.
254 G. Zhou, H. Wang, Y. Ma and X. Chen, *Tetrahedron*, 2013, **69**, 867–870.
255 T. Chen, Y. Zheng, Z. Xu, M. Zhao, Y. Xu and J. Cui, *Tetrahedron Lett.*, 2013, **54**, 2980–2982.
256 J. Zhang and W. Guo, *Chem. Commun.*, 2014, **50**, 4214–4217.
257 J. Zhou, Y. Luo, Q. Li, J. Shen, R. Wang, Y. Xu and X. Qian, *New J. Chem.*, 2014, **38**, 2770.
258 K. Liu and S. Zhang, *Tetrahedron Lett.*, 2014, **55**, 5566–5569.
259 L. E. Santos-Figueroa, C. de laTorre, S. El Sayed, F. Sancenón, R. Martínez-Máñez, A. M. Costero, S. Gil and M. Parra, *Eur. J. Org. Chem.*, 2014, 1848–1854.
260 K. Wang, H. Peng, N. Ni, C. Dai and B. Wang, *J. Fluoresc.*, 2014, **24**, 1–5.
261 K. Sun, X. Liu, Y. Wang and Z. Wu, *RSC Adv.*, 2013, **3**, 14543–14548.
262 S. I. Reja, N. Kumar, R. Sachdeva, V. Bhalla and M. Kumar, *RSC Adv.*, 2013, **3**, 17770–17774.
263 D. Zhu, L. Xue, G. Li, Y. Che and H. Jiang, *Org. Chem. Front.*, 2014, **1**, 501.
264 W. Xuan, R. Pan, Y. Cao, K. Liu and W. Wang, *Chem. Commun.*, 2012, **48**, 10669–10671.
265 Z. Wu, Y. Feng, B. Geng, J. Liua and X. Tang, *RSC Adv.*, 2014, **4**, 30398–30401.
266 S. Chen, P. Hou, J. W. Foley and X. Song, *RSC Adv.*, 2013, **3**, 5591.
267 X. Li, Y. Gong, K. Wu, S. H. Liang, J. Cao, B. Yang, Y. Hu and Y. Han, *RSC Adv.*, 2014, **4**, 36106.
268 Z. Dong, X. Le, P. Zhou, C. Dong and J. Ma, *New J. Chem.*, 2014, **38**, 1802–1808.
269 A. Zhu, Z. Luo, C. Ding, B. Li, S. Zhou, R. Wang and Y. Tian, *Analyst*, 2014, **139**, 1945–1952.
270 B. C. Dickinson and C. J. Chang, *Nat. Chem. Biol.*, 2011, **7**, 504–511.
271 X. Chen, X. Tian, I. Shin and J. Yoon, *Chem. Soc. Rev.*, 2011, **40**, 4783–4804.
272 B. Kalyanaraman, V. Darley-Usmar, K. J. A. Davies, P. A. Dennery, H. J. Forman, M. B. Grisham, G. E. Mann, K. Moore, L. J. Roberts Ii and H. Ischiropoulos, *Free Radical Biol. Med.*, 2012, **52**, 1–6.
273 R. Radi, *J. Biol. Chem.*, 2013, **288**, 26464–26472.
274 J.-H. M. Tsai, J. G. Harrison, J. C. Martin, T. P. Hamilton, M. van der Woerd, M. J. Jablonsky and J. S. Beckman, *J. Am. Chem. Soc.*, 1994, **116**, 4115–4116.
275 C. Szabo, H. Ischiropoulos and R. Radi, *Nat. Rev. Drug Discovery*, 2007, **6**, 662–680.
276 P. B. J. S. L. L. Pacher, *Physiol. Rev.*, 2007, **87**, 315–424.
277 M. G. Bonini, R. Radi, G. Ferrer-Sueta, A. M. D. C. Ferreira and O. Augusto, *J. Biol. Chem.*, 1999, **274**, 10802–10806.
278 S. L. Hempel, G. R. Buettner, Y. Q. O'Malley, D. A. Wessels and D. M. Flaherty, *Free Radical Biol. Med.*, 1999, **27**, 146–159.
279 H. Possel, H. Noack, W. Augustin, G. Keilhoff and G. Wolf, *FEBS Lett.*, 1997, **416**, 175–178.
280 N. W. Kooy, J. A. Royall, H. Ischiropoulos and J. S. Beckman, *Free Radical Biol. Med.*, 1994, **16**, 149–156.
281 A. Negre-Salvayre, N. Augé, C. Duval, F. Robbesyn, J.-C. Thiers, D. Nazzal, H. Benoist and R. Salvayre, *Methods Enzymology*, Academic Press, 2002, pp. 62–71.
282 G. Ambikapathi, S. Kempahanumakkagari, B. Ramappa Lamani, D. Kuramkote Shivanna, H. Bodagur Maregowda, A. Gupta and P. Malingappa, *J. Fluoresc.*, 2013, **23**, 705–712.
283 D. Yang, Y.-C. Tang, J. Chen, X.-C. Wang, M. D. Bartberger, K. N. Houk and L. Olson, *J. Am. Chem. Soc.*, 1999, **121**, 11976–11983.
284 D. Yang, H.-L. Wang, Z.-N. Sun, N.-W. Chung and J.-G. Shen, *J. Am. Chem. Soc.*, 2006, **128**, 6004–6005.
285 Z.-N. Sun, H.-L. Wang, F.-Q. Liu, Y. Chen, P. Kwong, H. Tam and D. Yang, *Org. Lett.*, 2009, **11**, 1887–1890.
286 R. B. R. Muijsers, E. van den Worm, G. Folkerts, C. J. Beukelman, A. S. Koster, D. S. Postma and F. P. Nijkamp, *Br. J. Pharmacol.*, 2000, **130**, 932–936.
287 T. Peng, N. K. Wong, X. Chen, Y. K. Chan, D. H. Ho, Z. Sun, J. J. Hu, J. Shen, H. El-Nezami and D. Yang, *J. Am. Chem. Soc.*, 2014, **136**, 11728–11734.
288 J. T. Hou, J. Yang, K. Li, Y. X. Liao, K. K. Yu, Y. M. Xie and X. Q. Yu, *Chem. Commun.*, 2014, **50**, 9947–9950.
289 X. Zhou, Y. Kwon, G. Kim, J.-H. Ryu and J. Yoon, *Biosens. Bioelectron.*, 2015, **64**, 285–291.
290 Q. Zhang, Z. Zhu, Y. Zheng, J. Cheng, N. Zhang, Y. T. Long, J. Zheng, X. Qian and Y. Yang, *J. Am. Chem. Soc.*, 2012, **134**, 18479–18482.
291 F. Martin-Romero, Y. Gutiérrez-Martin, F. Henao and C. Gutiérrez-Merino, *J. Fluoresc.*, 2004, **14**, 17–23.
292 J. Zielonka, A. Sikora, M. Hardy, J. Joseph, B. P. Dranka and B. Kalyanaraman, *Chem. Res. Toxicol.*, 2012, **25**, 1793–1799.
293 A. Sikora, J. Zielonka, M. Lopez, J. Joseph and B. Kalyanaraman, *Free Radical Biol. Med.*, 2009, **47**, 1401–1407.
294 X. Sun, Q. Xu, G. Kim, S. E. Flower, J. P. Lowe, J. Yoon, J. S. Fossey, X. Qian, S. D. Bull and T. D. James, *Chem. Sci.*, 2014, **5**, 3368.
295 F. Yu, P. Song, P. Li, B. Wang and K. Han, *Analyst*, 2012, **137**, 3740–3749.
296 K. Xu, H. Chen, J. Tian, B. Ding, Y. Xie, M. Qiang and B. Tang, *Chem. Commun.*, 2011, **47**, 9468–9470.
297 F. Yu, P. Li, G. Li, G. Zhao, T. Chu and K. Han, *J. Am. Chem. Soc.*, 2011, **133**, 11030–11033.
298 F. Yu, P. Li, B. Wang and K. Han, *J. Am. Chem. Soc.*, 2013, **135**, 7674–7680.
299 B. Wang, F. Yu, P. Li, X. Sun and K. Han, *Dyes Pigm.*, 2013, **96**, 383–390.
300 K.-K. Lin, S.-C. Wu, K.-M. Hsu, C.-H. Hung, W.-F. Liaw and Y.-M. Wang, *Org. Lett.*, 2013, **15**, 4242–4245.

301 T. Ueno, Y. Urano, H. Kojima and T. Nagano, *J. Am. Chem. Soc.*, 2006, **128**, 10640–10641.
302 N. A. Sieracki, B. N. Gantner, M. Mao, J. H. Horner, R. D. Ye, A. B. Malik, M. E. Newcomb and M. G. Bonini, *Free Radical Biol. Med.*, 2013, **61**, 40–50.
303 G. C. Van de Bittner, E. A. Dubikovskaya, C. R. Bertozzi and C. J. Chang, *Proc. Natl. Acad. Sci. U. S. A.*, 2010, **107**, 21316–21321.
304 J. C. Morris, *J. Phys. Chem.*, 1966, **70**, 3798–3805.
305 K. Setsukinai, Y. Urano, K. Kakinuma, H. J. Majima and T. Nagano, *J. Biol. Chem.*, 2003, **278**, 3170–3175.
306 J. Shepherd, S. A. Hilderbrand, P. Waterman, J. W. Heinecke, R. Weissleder and P. Libby, *Chem. Biol.*, 2007, **14**, 1221–1231.
307 Y. Koide, Y. Urano, S. Kenmoku, H. Kojima and T. Nagano, *J. Am. Chem. Soc.*, 2007, **129**, 10324–10325.
308 Y. Xiao, R. Zhang, Z. Ye, Z. Dai, H. An and J. Yuan, *Anal. Chem.*, 2012, **84**, 10785–10792.
309 Z.-N. Sun, F.-Q. Liu, Y. Chen, P. K. H. Tam and D. Yang, *Org. Lett.*, 2008, **10**, 2171–2174.
310 Y. Zhou, J. Y. Li, K. H. Chu, K. Liu, C. Yao and J. Y. Li, *Chem. Commun.*, 2012, **48**, 4677–4679.
311 H. Zhu, J. Fan, J. Wang, H. Mu and X. Peng, *J. Am. Chem. Soc.*, 2014, **136**, 12820–12823.
312 X. Cheng, H. Jia, T. Long, J. Feng, J. Qin and Z. Li, *Chem. Commun.*, 2011, **47**, 11978–11980.
313 G. Wu, F. Zeng and S. Wu, *Anal. Methods*, 2013, **5**, 5589–5596.
314 S. I. Reja, V. Bhalla, A. Sharma, G. Kaur and M. Kumar, *Chem. Commun.*, 2014, **50**, 11911–11914.
315 L. Yuan, W. Lin, J. Song and Y. Yang, *Chem. Commun.*, 2011, **47**, 12691–12693.
316 S. Kenmoku, Y. Urano, H. Kojima and T. Nagano, *J. Am. Chem. Soc.*, 2007, **129**, 7313–7318.
317 Y. Koide, Y. Urano, K. Hanaoka, T. Terai and T. Nagano, *J. Am. Chem. Soc.*, 2011, **133**, 5680–5682.
318 X. Chen, K. A. Lee, E. M. Ha, K. M. Lee, Y. Y. Seo, H. K. Choi, H. N. Kim, M. J. Kim, C. S. Cho, S. Y. Lee, W. J. Lee and J. Yoon, *Chem. Commun.*, 2011, **47**, 4373–4375.
319 X. Chen, X. Wang, S. Wang, W. Shi, K. Wang and H. Ma, *Chem. – Eur. J.*, 2008, **14**, 4719–4724.
320 S. Goswami, S. Das, K. Aich, P. K. Nandi, K. Ghoshal, C. K. Quah, M. Bhattacharyya, H.-K. Fun and H. A. Abdel-Aziz, *RSC Adv.*, 2014, **4**, 24881–24886.
321 X. Jin, L. Hao, Y. Hu, M. She, Y. Shi, M. Obst, J. Li and Z. Shi, *Sens. Actuators, B*, 2013, **186**, 56–60.
322 Y.-K. Yang, H. J. Cho, J. Lee, I. Shin and J. Tae, *Org. Lett.*, 2009, **11**, 859–861.
323 S.-R. Liu and S.-P. Wu, *Org. Lett.*, 2013, **15**, 878–881.
324 S. T. Manjare, J. Kim, Y. Lee and D. G. Churchill, *Org. Lett.*, 2014, **16**, 520–523.
325 S. T. Manjare, S. Kim, W. D. Heo and D. G. Churchill, *Org. Lett.*, 2014, **16**, 410–412.
326 B. Wang, P. Li, F. Yu, P. Song, X. Sun, S. Yang, Z. Lou and K. Han, *Chem. Commun.*, 2013, **49**, 1014–1016.
327 Y. Koide, M. Kawaguchi, Y. Urano, K. Hanaoka, T. Komatsu, M. Abo, T. Terai and T. Nagano, *Chem. Commun.*, 2012, **48**, 3091–3093.
328 Z. Lou, P. Li, Q. Pan and K. Han, *Chem. Commun.*, 2013, **49**, 2445–2447.
329 G. Li, D. Zhu, Q. Liu, L. Xue and H. Jiang, *Org. Lett.*, 2013, **15**, 2002–2005.
330 F. Liu, Y. Gao, J. Wang and S. Sun, *Analyst*, 2014, **139**, 3324–3329.
331 F. Liu, T. Wu, J. Cao, H. Zhang, M. Hu, S. Sun, F. Song, J. Fan, J. Wang and X. Peng, *Analyst*, 2013, **138**, 775–778.
332 L. Yuan, W. Lin, Y. Yang and H. Chen, *J. Am. Chem. Soc.*, 2012, **134**, 1200–1211.
333 S. Chen, J. Lu, C. Sun and H. Ma, *Analyst*, 2010, **135**, 577–582.
334 F. Yu, P. Song, P. Li, B. Wang and K. Han, *Chem. Commun.*, 2012, **48**, 7735–7737.
335 B. Wang, P. Li, F. Yu, J. Chen, Z. Qu and K. Han, *Chem. Commun.*, 2013, **49**, 5790–5792.
336 E. M. Stennett, M. A. Ciuba and M. Levitus, *Chem. Soc. Rev.*, 2014, **43**, 1057–1075.
337 M. K. Kuimova, *Phys. Chem. Chem. Phys.*, 2012, **14**, 12671–12686.
338 A. F. Coskun and A. Ozcan, *Curr. Opin. Biotechnol.*, 2014, **25**, 8–16.
339 X. Fan and I. M. White, *Nat. Photonics*, 2011, **5**, 591–597.
340 D. A. Basiji, W. E. Ortyn, L. Liang, V. Venkatachalam and P. Morrissey, *Clin. Lab. Med.*, 2007, **27**, 653–670.
341 A. Ozcan, *Lab Chip*, 2014, **14**, 3187–3194.
342 H. Zhu, S. Mavandadi, A. F. Coskun, O. Yaglidere and A. Ozcan, *Anal. Chem.*, 2011, **83**, 6641–6647.